ADHESION WITH SLENDER STRUCTURES: TAPE LOOPS, CRUMPLES, AND ORIGAMI

A Dissertation
Submitted to the Graduate Faculty
of the
North Dakota State University
of Agriculture and Applied Science

By

Theresa Marie Elder

In Partial Fulfillment of the Requirements
for the Degree of
DOCTOR OF PHILOSOPHY

Major Program:
Materials and Nanotechnology

June 2021

Fargo, North Dakota

North Dakota State University
Graduate School

Title

Adhesion with Slender Structures: Tape Loops, Crumples, and Origami

By

Theresa Marie Elder

The Supervisory Committee certifies that this ***disquisition*** complies with North Dakota State University's regulations and meets the accepted standards for the degree of

DOCTOR OF PHILOSOPHY

SUPERVISORY COMMITTEE:

Andrew B. Croll
Chair

Erik Hobbie

Yechun Wang

Yongki Choi

Approved:

July 5, 2021
Date

Erik Hobbie
Department Chair

ABSTRACT

The desire for improved adhesive systems led us to examine three geometries: tape loops, crumples, and origami shapes. The tape loop is mechanically interesting because it is stable in more than one configuration. For example, the first configuration is a circular loop. The second is an elongated oval shape that occurs after the loop is pushed into a surface. In this work we examined this cycle and derive a simple mathematical model. We found a solution to the model that only needs one input measurement, that of the loop radius, to determine a tape loop's adhesion. We explored how a sticky but crumpled film adhered to smooth and rough surfaces. To do this we crumpled inextensible sheets because crumples have been shown to maintain a high compliance while increasing contact area through deforming around obstacles. We found that there was no significant difference in the adhesive behavior of the crumples on rough surfaces compared to flat surfaces. Finally, we designed a switchable adhesive based on thin film origami. We examined a unit cell of the Ron Resch pattern which had two different configurations (open and closed) aided by a 3-D printed device In the closed state the device had a high pull off force, and in the open state a different style of peel off occurred, lowering the peak force. We present promising results that show this to be the case.

ACKNOWLEDGMENTS

This work was supported by my research mentor Dr. Andrew B. Croll and fellow team members, especially Timothy Twohig and Damith Rosairo. Funding was provided by the Graduate College of Interdisciplinary Studies at NDSU and Materials and Nanotechnology Program. Funding was also provided by the National Science Foundation through grant number CMMI 2011681.

DEDICATION

I dedicate this dissertation to my family and friends. To my mom, Bessie Elletson who supported me the entire way, but unfortunately is no longer here to see the completed work. To my remaining parents, grandparents, and older generation relatives for their support and encouragement, Tony and Chantal Elder, Beverly Elder, Tim and Amy Carr, Chris Moss, Corey Elletson, and others not named. This also would not have been possible without the love from my siblings Craig and Megan Elder, Cassandra Romans and her family, Ginette Castaneda and her family, and my brothers and sisters in spirit although not biologically related and their families. To my best friend Lydia Kelley and her mom Lodema Weathers who was also a mother figure to me. All of my friends and loved ones who have hearts of gold and helped me keep my confidence. To my cats Morgan and Prince who comfort me and put up with me every day which deserves some credit. To everyone in my acknowledgements my research group, professors and mentors, and fellow student peers. Lastly I would like to thank my other family and friends, both human and animal, unnamed here due to time and space considerations. All the people that helped me along the journey and through the struggles and hardships that accompanied it, I dedicate this thesis to you.

TABLE OF CONTENTS

LIST OF TABLES

LIST OF FIGURES

LIST OF ABBREVIATIONS

PC	Polycarbonate.
GPa	Giga pascal.
2-D	Two dimensional.
3-D	Three dimensional.
PDMS	Polydimethylsiloxane.
kPa	Kilo pascal.
MPa	Mega pascal.
PE	Polyethylene.
PS	Polystyrene.
ASTM	American Standard Test Method.
D-cone	Developable cone.
cos	Cosine.
JKR	Johnson-Kendall-Roberts.
M.S.	Master of Science.
ASTM D412	American Standard Test Method specifying a specific tension test.
s	Second(s).
rpm	Rotations per minute.
G	Gram(s).
PAA	Polyacrylic acid.
DI	Deionized water.
in	Inch(es).
mm	Millimeters.
N	Newtons.

°C ....Degrees Celsius.

LIST OF SYMBOLS

C.....Carbon.

Si .....Silicon.

Hg.....Mercury.

n_{gauche} .....Number of gauche bonds in a polymer.

n_{trans} .....Number of trans bonds in a polymer.

ΔE.....Energy difference between the minima of the trans and gauche configurations.

k .....Boltzmann constant.

T .....Temperature.

T_G .....Glass transition temperature.

F .....Force.

σ .....Stress.

A .....Area, proportionality constant.

ε.....Strain.

L .....Length.

ΔL.....Change in length.

E .....Young's modulus.

ν .....Poisson's ratio.

ε_t .....Strain perpendicular to the force direction.

ε_l.....Strain in the same direction as applied force.

σ_x.....Stress along the x axis.

ε_y.....Strain along the y axis.

C .....Constitutive equation.

C_{xy}.....Constitutive equation for the x and y axes that includes modulus and Poisson ratio.

ε_{xx} .....Strain tensor along the xx plane.

ε_{yy} .....Strain tensor along the yy plane.

ε_{zz}.....Strain tensor along the zz plane.

γ_{xy} .....Strain tensor along the xy plane.

γ_{yx} .....Strain tensor along the yx plane.

σ_{xx} .....Stress along the xx plane.

σ_{yy}.....Stress along the yy plane.

σ_{yx} .....Stress along the yx plane.

σ_{xy}.....Stress along the xy plane.

σ_{zz} .....Stress along the zz plane.

σ_{xz} .....Stress along the xz plane.

σ_{zx} .....Stress along the zx plane.

σ_{yz} .....Stress along the yz plane.

σ_{zx} .....Stress along the zy plane.

ρ .....Density.

R .....Gas constant.

M_c.....Molecular weight between crosslinks.

λ .....Deformation.

$\left(\frac{f-2}{f}\right)$ .....Crosslink chain density.

$\varepsilon(t)$.....Strain as a function of time.

σ_0.....Initial stress.

$G(t)$.....Material compliance.

$\sigma(t)$ .....Stress as a function of time.

ε_0 .....Initial strain.

$J(t)$ ..... Stiffness.

U ..... Energy of a system.

r ..... Radius of curvature.

t ..... Thickness, time.

M_{tot} ..... Total moment.

b ..... Width.

bx ..... Incremental distance moved along the beam width.

dx ..... Incremental distance moved along the beam thickness.

M ..... Moment.

Ú ..... Elastic energy of the sheet which is in contact with the rough frame it is being pushed through.

B ..... Bending stiffness, bending modulus.

R ..... Radius of a frame (D-cone)., radius of a sphere.

R_* ..... Parameter of the size of the core region.

R_p ..... Radius of region outside of D-cone.

θ_c ..... Angle of D-cone curve.

R_c ..... Radius of D-cone.

E_s ..... Stretching modulus.

F_0 ..... Initial force.

H ..... Height.

α ..... Experimentally determined exponent, Legrangian multiplier.

P ..... Force, initial load.

dF ..... Change in free energy.

U_T ..... Total energy.

dU_T .....Change in total energy.

U_E .....Elastic energy.

dU_E .....Change in elastic energy.

U_P .....Potential energy.

dU_P .....Change in potential energy.

U_S .....Stored energy.

dU_S .....Change in stored energy.

γ .....Surface energy.

γ_1 .....Surface energy of surface 1.

γ_2 .....Surface energy of surface 2.

γ_{12} .....Interfacial energy.

dA .....Change in area.

w .....Thermodynamic work of adhesion, Dupré's energy of adhesion.

G .....Energy release rate, energy of adhesion.

G_C .....Critical energy release rate.

U_M .....Mechanical energy.

a .....Radius of circle, . length along a side of the hexagon as well as from a corner to the center, length of a side of a square.

a_1^2 .....Radius of circular area of contact between two solids.

θ .....Angle.

K .....Combination of elastic constants with respect to geometry.

k_1 .....Elastic constant of a sphere over a certain volume.

k_2 .....Elastic constant of a sphere over a certain volume.

C_0 .....JKR compliance.

E^* .....Effective modulus.

h .....Hertzian contact.

P' .....Final load.

δ .....Initial displacement, incremental displacement.

δ' .....Final displacement.

E_{PDMS} .....Young's Modulus of PDMS.

E_{PS} .....Young's Modulus of PS.

E_{PC} .....Young's Modulus of PC.

τ .....Relaxation time.

β .....Proportionality constant.

F_t .....Force at a point in time.

F_{40} .....Force at 40 s into the experiment.

ℓ_{ec} .....Elastocapillary length.

$\Delta\gamma$ .....Work of adhesion.

δL .....Change of length.

ℓ .....Free length.

$\theta(s)$ .....Shape function.

$\theta(\ell/2)$ .....Function of free length of the boundary condition at point $\ell/2$.

$\theta(-\ell/2)$ .....Function of free length of the boundary condition at point $-\ell/2$.

$\theta(0)$ .....Shape function at length 0.

θ' .....Change in angle of a segment.

s .....Position along a curve.

c_1 .....Integration constant.

$\theta'(\ell/2)$ .....Curve shape at $\ell/2$.

am .....Jacobi Amplitude Function.

F .....Elliptic integral of the first kind.

H_0 .....Equilibrium plate separation.

C .....Compliance or stiffness.

c .....Constant.

F_{on} .....Force in the ‘on’ position.

F_{off} .....Force in the ‘off’ position.

1. INTRODUCTION

Polymers are present in numerous capacities in modern life in products ranging from medical devices[1] and pharmaceuticals[2] to clothing[3] and cosmetics[4] to automobiles[5] and coatings[6]. As polymers become increasingly prevalent in all aspects of daily life it is important to know their stress-strain relations, how they interact with external forces such as adhesion, and how geometric effects can improve their ability to satisfy engineering design requirements. In this work we investigate thin polymer films in different geometries in order to make functional adhesive structures. Specifically we show that the tape loop geometry can be modeled such that an adhesion measurement can be conducted using only the height of the loop, that sticky crumples adhere equally well to rough surfaces as they do to flat surfaces, and that origami structures with two configurations can be used as switchable adhesives.

Polymers are long chains of molecules bonded in a chain like beads on a necklace[7]. Polymers have a range of properties that differ from those of the individual molecular components due to the length of each molecular strand. Modifying the length and compositions of these strands can therefore change material properties, allowing polymers to be tailored to suit specific needs. Polymer properties can be further tailored to solve engineering problems through changing the chemical components, bonding, crystallization, thicknesses[8], arrangements, and states.

1.1. Polymers

Polymers are macromolecules composed of multiple units of smaller molecules referred to as monomers. Monomers are covalently or physically bonded together with the same backbone element, often C or Si, forming a chain. Most polymer molecules have organic side groups such as hydrocarbons, nitrogen, and halides[9]. The number of molecules in close

proximity in polymer chains, contributes to weaker bonds than monoatomic crystalline solids. The higher number of bonds in longer polymers cause higher fracture toughness as more energy is required to break both the covalent bonds and inter-chain bonds[10]. The amount of force necessary to break covalent bonds is an order of magnitude greater than that of weaker inter-chain bonds; therefore polymers have a unidirectional strength along the backbone chain that is higher than in other directions. Longer polymers in a melt or molten state also have entanglements, where long strands wind around each other restricting movement. The entangled chains can become stuck for long time periods in areas where they are surrounded by other chains, much like a pile of tangled cords.

The arrangement of a polymer in space, is dictated by a balance between free energy and entropy. Constrained conformations have higher enthalpy and lower entropy, while more open configurations have higher entropy and lower enthalpy. The arrangement of a monomer in the polymer backbone chain is largely restricted by the place of its nearest neighbor due to the covalent bonding[11]. The spatial arrangement of each monomer along the polymer backbone, as well as the entropy and free energy of the system, are dictated by physical and chemical interactions. These interactions will determine a polymers mobility.

The chemical properties of each monomer and their arrangement along the polymer chain affect the properties of the polymer. Monomers can be identical, creating what is called a homopolymer, or monomers can be a mixture of different molecules forming what is called a copolymer. Copolymers are categorized based on the sequence of monomers in the chain as alternating, random, or block[9,10]. Alternating polymers are copolymers that have monomer sequences that alternate in a regular pattern. Random copolymers have no discernable pattern in

monomer bonding. Block copolymers have two or more types of homopolymer bonded together[11,12].

The chemical properties of monomers affect their interactions with solvent and other monomers. Monomers with different chemical behavior can produce polymers with unique properties. For example, hydrophobic molecules (that do not disperse in water) can be bonded to hydrophilic molecules (that disperse well in aqueous and polar solvents) to form polymer which disperses well in both water and non-polar solvents. If the hydrophilic and hydrophobic monomers are joined as blocks an amphiphilic polymer will result[13]. Amphiphilic polymers have segments that will minimize contact with certain solvents resulting in aggregation and may have different phase and crystallization behavior across segments[7,8,14].

Polymers have diverse structures due to the numerous bonding sites along the chains. More than one chain can join, creating nonlinear polymers such as terpolymers, branched, star, and dendrimers. Terpolymers are four polymer chains that originate from a single C in the chain. Dendrimers are terpolymers that have additional chains on each base chain resulting in a structure resembling neurons or tree branching. Branched polymers have shorter polymer chains bonded to a longer polymer chain. Star polymers like terpolymers have multiple branches from a single central backbone monomer[8,11].

The diversity of possible monomers that can compose a polymer mean diverse chemical synthesis methods for producing polymers. Polymer synthesis methods depend on the desired monomers; some of the most common monomer precursors are multi-bonded C-C molecules, cyclic molecules, or molecules with functional end groups. Multi-bonded C molecules, double bonds and triple bonds, form reactive free radicals when a bond is broken. The free radicals react with other multi-bonded Cs to form new bonds and radicals, continuing to form a chain

until the reaction is terminated by the addition of a radicalized end group. Cyclic monomers are synthesized in a similar process of radical formation, chain perpetuation, and chain termination to that of the multi-bonded C monomer precursor[8]. In cyclic monomer precursors the free radical results from the breaking of a bond in the cyclic monomer, one of the atoms will have the free electron while the other is generally stabilized through some form of rearrangement or addition of an acidic hydride. Monomer precursors with functional end groups form bonds which create small molecules, such as water in hydrolysis, that leave allowing the two monomers to bond to each other.

Monomers can attach in different conformations where the side groups will occupy different regions in space relative to that of the two neighboring monomers at points of rotation around the bond. Side groups in the same plane as those of neighbors are trans. Side groups in one of the other two possible planes of attachment are in a more energetic gauche configuration. Gauche chains coil as each bond moves the others out of plane[15].

The distribution of trans and gauche configurations are related to the energy difference between the two configurations and the thermodynamics of the polymer with a relationship:

$$\frac{n_{gauche}}{n_{trans}} = 2^{\frac{-\Delta E}{kT}} \quad (1)$$

where n_{gauche} is the number of gauche bonds, n_{trans} is the number of trans bonds, ΔE is the energy difference between the minima of the trans and gauche configurations, k is Boltzmann constant, and T is the temperature. At room temperature all configurations are equally likely which contributes to the random shape of polymer chains[15]. The energy barrier dictates the rate of change between the two configurations. The configuration and steric hindrance of side groups and crosslinking effect the energy of the polymer system with higher potential energies for trans

and lower for gauche[15]. The more easily the chain can go back and forth the more flexible it is. Stiffer chains have less rotation at room temperature.

Tacticity is permanent isomerism that specifies the placement and alignment of side groups. The isomerism of a polymer chain with alternating gauche side groups is syndiotactic. Isotactic polymer chains have the same side groups all aligning in the same plane. The organized alignment of isotactic or syndiotactic polymer groups makes crystallization more likely as side by side chains can fit more neatly together. Atactic polymer chains have no regular pattern of alignment. If sections of polymer line up, the gaps create an amorphous region rather than a crystalline region[11]. Tacticity affects crystallization as it determines if planar alignments with neighboring monomers are possible to either facilitate parallel alignment such as with bricks, interspersed alignments such as puzzle pieces, or no alignments that lead to close proximity and order.

Further classification of polymers is based on how they can be processed and arranged at various temperatures. Polymers that can be melted and shaped through industrial processes are thermoplastic. Thermoplastic polymers are mostly long linear polymer systems that are aligned during processing into shapes or fibers. Crosslinked polymers that connect into 3-D networks cannot be melted as their shape is fixed by the bonding network. Crosslinked polymers are referred to as thermoset polymers due to set shape[16]. Polymers that arrange in an orderly configuration where segments align in rows forming other hierarchal shapes are crystalline polymers. Polymers are so long the neat arrangement needed for complete crystallization is often incomplete or entropically difficult resulting in amorphous regions, the exception being polyethylene[8,14]. Semicrystalline polymers can have almost equal amounts of crystalline and

amorphous regions. Polymers are called glassy when they assort randomly into a shape that has no order over long ranges[17, 18].

The molecular weight of a polymer effects flow and failure in polymer melts and solids. Shorter polymers will flow like Newtonian fluids in melts while longer chains entangle which restricts flow, flow becomes viscoelastic[7]. Solids composed of shorter chains experience more brittle failure as the chains remain separate[19]. Solids composed of longer chains have different failure mechanisms as the chains need to pull and separate before fracture, necking and crazing. Necking is where a section of the length stretches and elongates growing thinner before fracture occurs[20]. Crazing occurs when fracture is incomplete and polymer strands remain connecting the two sides of the crack[21].

1.1.1. Glassy Polymers

A glassy polymer is a polymer that stops flowing below a certain temperature, the glass transition temperature T_G, arresting the molecules in an arrangement lacking long range order[7,17,18]. This occurs when a polymer does not have time to properly organize or side groups are too bulky for monomers to arrange in an orderly way. The monomers will not assume a regular pattern of crystallization[7]. Glassy polymers have different optical and failure properties than crystallized polymers as a result of the lack of order. Above the glass transition temperature entropy determines mechanical properties[7, 11].

In this work we use polycarbonate (PC) as a representative glassy thermoset polymer. Typically PC has a glass transition temperature of 145°C[22] and a modulus of 2.0-2.6 GPa[23]. However, physical properties of polymers often change depending on the polymer's molecular weight. The molecular weight of PC, for example, affects thermal properties such as T_G. In thermogravimetric experiments the decomposition of the samples were greater at lower

molecular weights[24]. Lower molecular weight PC is more brittle experiencing failure at lower loads[25] and aging more rapidly than corresponding higher molecular weight PC[26]. Craze stress and the width of a craze opening are also dependent on molecular weight although yield stress does not show significant dependence[25]. Lower molecular weight PC also has lower tensile strength[27] and lower T_G[28]. Enthalpy relaxation time differs for different molecular weights with higher relaxation times at higher weights[26].

1.1.2. Crosslinked Polymers

Crosslinking is covalent bonding between two neighboring strands of polymer. Numerous amounts of crosslinks create 3-D networks that form highly extensible polymer solids. The modulus and elasticity of the formed solid depends on the chemical nature of the monomers and the crosslink density which determines the average molecular weight between crosslinks. Crosslinks between longer chains have lower modulus values and flexibility. polydimethylsiloxane, PDMS, is a good example of an easily crosslinked polymer which can easily be crosslinked to different degrees, forming soft solids with modulus of kPa to MPa range. Alternatively, epoxies, which typically have closer and more numerous crosslinks, result in a higher modulus solid, typically in the GPa range similar to many glassy polymers. Crosslinked polymer networks that remain flexible, such as PDMS, are known as elastomers[7,11].

Crosslinked polymers differ from thermosets in other important ways. For example, crosslinked polymers do not often dissolve in good solvents the way that linear polymers do, instead they absorb the surrounding solvent forming a state known as a gel. The solvent enters the network and causes expansion of the solid on macroscopic scales. Polymer networks do not flow when melted (raised above T_G); degradation at higher temperatures leads to the breakage of

backbone bonds and flow rather than the weakening of inter chain bonds leading to a solid to liquid transition in a glassy material[11].

1.1.3. Crystalline Polymers

Polymer crystallization differs from molecular crystallization. In molecular crystallization, the ordered structure forms bonds based on closest packing between individual atoms or molecules. In polymers it is based on the closest packing of each polymer, meaning each chain has to completely extend and align parallel to its neighbor. Polymers have an entropic barrier to complete alignment with their neighbors because of a dramatic reduction of entropy incurred by straightening a long chain molecule. Furthermore, long polymer chains aligning completely in parallel to each other is difficult to achieve due to entanglements between strands[7].

The endpoint of crystallization in polymers is kinetic rather than based on achieving an equilibrium state. Polymers can partially crystalize if they have high symmetry in their backbones such as isotactic or syndiotactic polymer as these arrangements allow straightened areas to fit side by side like bricks or interlock like puzzle pieces, respectively. Polymer crystallization is more of a separation process of regions of the polymer, those that can freely move and stretch from those entangled, end groups, and bulky regions. This separation creates two regions or phases in the form of crystallite layers and amorphous regions. The crystallite layer is the layer where the mobile segments have been organized via folding into a crystalline structure. The amorphous region is the remainder of polymer and elements not incorporated into the crystallite layer[9]. Few polymers have 100% crystallization, most notably polyethylene (PE).

Crystallites often grow from nucleation sites. These nuclei grow in radial patterns that produce somewhat circular crystals called spherulites[7]. Crystallization can also be achieved

from methods which orient the polymer in a specific direction followed by quenching. Spinning or cold drawing of fibers is one example of an induced crystallization. Here the polymer is crystallized from an amorphous glassy state continuously rather than at discrete nucleation sites[29]. This creates fibers of high strength such as Kevlar, a polymer oriented into fibers, used to make bullet proof vests[30].

1.2. Mechanics

Mechanics, simply put, is the response of a material to stress or strain. Stress is defined as the force exerted by a load on an object over its given area:

$$\sigma = \frac{F}{A} \tag{2}$$

where σ is the stress and A is the cross-sectional area the force, F, is applied to. Strain is a directional displacement defined as:

$$\varepsilon = \frac{\Delta L}{L} \tag{3}$$

where ε is the directional strain along the axis, L is the original length, and ΔL is the change in length.

A material stress-strain response is in the Hookean regime when the stress, σ, and strain, ε, are proportional in a linear relationship:

$$\sigma = E\varepsilon \tag{4}$$

where E is a proportionality constant, Young's modulus. This equation does not specify axes as the relationship applies to any strain and stress combination. Materials that do not have a linear relationship between stress and strain or which are only Hookean under low stress or low strain are referred to as non-Hookean. Materials might also have different modulus for different

directions of stress-strain, or different temperatures and each may be linear or non-linear at any given strain.

As a material is deformed in one dimension, say length, conservation of mass leads to a decrease or increase in another dimension such as width. The amount of this increase or decrease is a material property. The ratio of change in the cross-sectional area of the material is Poisson's ratio, ν:

$$\nu = -\frac{\varepsilon_t}{\varepsilon_l} \tag{5}$$

where ε_t is strain perpendicular to the force direction, and ε_l is the strain in the direction of applied force and stretching[31, 32].

Most of the basic equations apply easily to a one dimensional material, where one dimension is significantly larger than both of the other two dimensions, such as a thin polymer fiber. However, when we deal with materials that are 2-D or 3-D Poisson's ratio becomes a more important factor as materials with high Poisson's ratio and low Poisson's ratio will differ in stress-strain behavior. A material with a high Poisson's ratio will have a greater change in cross-sectional area, meaning that the area the force is spread over is changing. High change in cross-sectional area also means that there is a higher stress in one direction as it deforms more to a longer length.

For a material with a 3-D geometry we use:

$$\sigma_x = C_{xy}\varepsilon_y \tag{6}$$

where σ_x is the stress along the x axis, ε_y is the strain along the y axis, and C_{xy} is a constitutive equation that includes the modulus and Poisson ratio values for the x and y axes. The Hookean constitutive equation, C, for a 3-D isotropic material is:

$$C = \frac{E}{(1-\nu)(1-2\nu)}\begin{bmatrix} 1-\nu & \nu & \nu & 0 & 0 & 0 \\ \nu & 1-\nu & \nu & 0 & 0 & 0 \\ \nu & \nu & 1-\nu & 0 & 0 & 0 \\ 0 & 0 & 0 & (1-2\nu)/2 & 0 & 0 \\ 0 & 0 & 0 & 0 & (1-2\nu)/2 & 0 \\ 0 & 0 & 0 & 0 & 0 & (1-2\nu)/2 \end{bmatrix} \quad (7)$$

The equations for stress and strain of 3-D and 2-D materials are matrices in order to represent every possible direction of stress tensor or strain that can occur along the axes[33] shown in Figure 1.

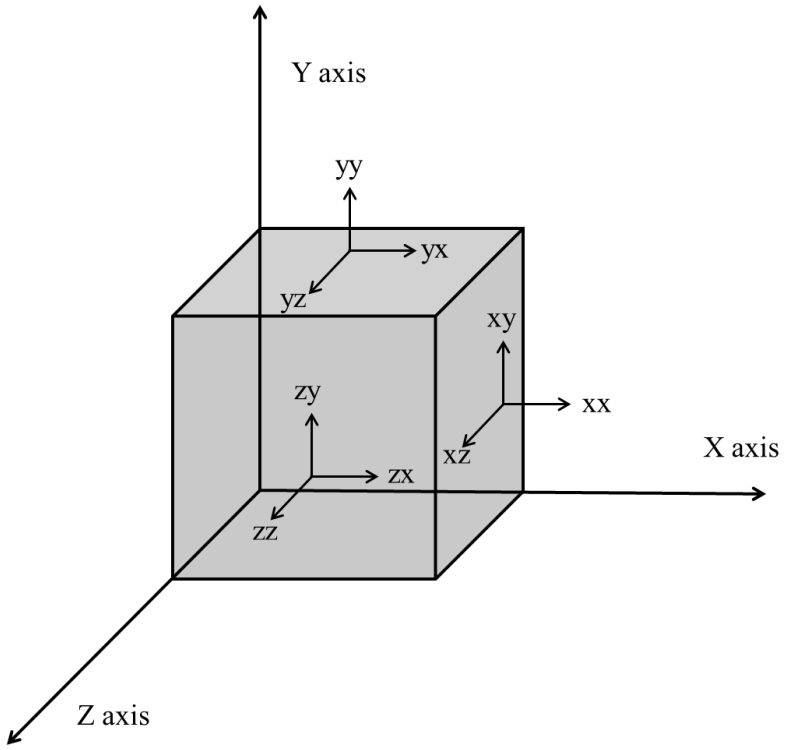

Figure 1. A visual representation of the all xyz axis designations for stress and strain.

In the case of a geometry that is a sheet, much wider in two dimensions and thin in the third (a 2-D structure) the sheet is commonly referred to as being in a state of plane stress. The plane stress state is dependent on the stress and strain in the directions of the wider dimensions as the stress acting in the thin direction is negligible. Matrices of all the coordinate strains can then be simplified as the strain along the third axis is considered negligible.

To calculate the stress for a 2-D material we can use the simplified equation:

$$\begin{Bmatrix}\sigma_{xx}\\ \sigma_{yy}\\ \sigma_{yx}\end{Bmatrix} = \frac{E}{(1+\nu^2)}\begin{bmatrix}1-\nu & \nu & 0\\ \nu & 1-\nu & 0\\ 0 & 0 & (1-\nu)/2\end{bmatrix}\begin{Bmatrix}\varepsilon_{xx}\\ \varepsilon_{yy}\\ \gamma_{xy}\end{Bmatrix} \tag{8}$$

where γ_{xy} is the strain tensor in the xy direction which is often a shear strain. We assume that $\sigma_{zx} = \sigma_{xz} = \sigma_{zy} = \sigma_{yz} = 0$, $\sigma_{yx} = \sigma_{xy}$, and $\gamma_{xy} = \gamma_{yx}$ for an isotropic material. Solving this equation gives the plane stress:

$$\sigma_{xx} = \left(\frac{E}{(1-\nu^2)}\right)\left(\varepsilon_{xx} + \nu\varepsilon_{yy}\right),^{34} \tag{9}$$

and corresponding strain of:

$$\varepsilon_{xx} = -\frac{1}{E}\left(\sigma_{xx} + \nu\sigma_{yy}\right). \tag{10}$$

Plane strain is where one of the dimensions along a plane is so large that the displacement (deformation) along that axis is effectively zero. The stress components are also independent of the large axis. For example, if z axis is the long axis than it is assumed that strain along ε_{zz}, ε_{xz}, and ε_{yz} are zero, which reduces the strain tensor to:

$$\varepsilon = \begin{bmatrix}\varepsilon_{xx} & \gamma_{xy}\\ \gamma_{yx} & \varepsilon_{yy}\end{bmatrix} \tag{11}$$

where γ_{xy} and γ_{yx} are the strain tensors in indicated planes. Calculating the plane strain:

$$\begin{Bmatrix}\sigma_{xx}\\ \sigma_{yy}\\ \sigma_{yx}\end{Bmatrix} = \frac{E}{(1+\nu)(1-2\nu)}\begin{bmatrix}1-\nu & \nu & 0\\ \nu & 1-\nu & 0\\ 0 & 0 & (1-2\nu)/2\end{bmatrix}\begin{Bmatrix}\varepsilon_{xx}\\ \varepsilon_{yy}\\ \gamma_{xy}\end{Bmatrix} \tag{12}$$

the solutions along x-axis is:

$$\sigma_{xx} = \frac{E}{(1+\nu)(1-2\nu)}\left((1-\nu)\varepsilon_{xx} + \nu\varepsilon_{yy}\right). \tag{13}$$

A similar solution is found for the y-axis interchanging x and y accordingly, while:

$$\sigma_{xy} = \frac{E}{2(1+\nu)}\varepsilon_{xy} \tag{14}$$

is a solution along the xy-axis[35].

1.2.1. Crosslinked Systems

Crosslinked systems are used extensively in this thesis therefore, it is necessary to briefly cover the mechanics of crosslinked systems, especially as it pertains to crosslink density. Crosslink density effects the modulus, viscosity, and overall mechanics of a crosslinked system as it is the measure of the degree of interconnection of the component polymers, much as the stiffness of a fabric depends on how tightly and intricately it is woven together. Real systems can vary in length of polymer between crosslinks or incomplete crosslinking, however, for the sake of simplicity and approximation we will assume an idealized network.

The modulus of a crosslinked system can be calculated based on the crosslink density and the molecular weight between crosslinks. The force distribution of a crosslinked system is:

$$F = \frac{\rho RT}{M_c} \tag{15}$$

where F is the applied force, ρ is the density of the polymer crosslinking, R is the gas constant, T is temperature, and M_c is the molecular weight between crosslinks[36]. The stress equation then becomes:

$$\sigma = \left(\frac{f-2}{f}\right)\frac{\rho RT}{M_c}\left(\lambda^2 - \frac{1}{\lambda}\right) \tag{16}$$

where λ is deformation, and $\left(\frac{f-2}{f}\right)$ is the crosslink chain density that is often omitted for simplification and will be omitted in our modulus equation[11]. Substituting $E/2(1+\nu)$ in place of the deformation term[37] and solving for E gives:

$$E = \frac{\rho RT}{M_c 2(1+\nu)} \tag{17}$$

the modulus of a crosslinked polymer network with respect to the crosslink density.

1.2.2. Dynamic Tests

Mechanical testing for stress-strain behavior is varied depending on material, amount of material, and material property of interest. Among some of the more common tests are tensile test and compression tests. Tensile and compression tests can both be run in ways to do creep, stress relaxation, or recovery tests.

Creep tests the response of a material at a constant stress, that is a constant force is applied and maintained, over time. The material will then respond accordingly over certain timescales[9]. The response is generally molecular movement of the material to spread out the area the force affects in order to lower the pressure[38]. This molecular movement creates macroscopic deformation. Creep deformation leads to a constant strain after an initial fast elastic response. Creep as a function of time is:

$$\varepsilon(t) = \sigma_0 J(t) \tag{18}$$

where $\varepsilon(t)$ is strain as a function of time, σ_0 is initial stress, and $J(t)$ is material compliance.

Tests done for stress relaxation are run to determine the stress response of a material at a constant strain over time. In order to equilibrate in a constrained position, the material will need to rearrange to reduce stress, changing the load force. At the beginning of stress relaxation as at the beginning of creep there is a fast elastic response lowering stress followed by a constant stress or a slower decrease in stress[7]. Stress relaxation as a function of time is:

$$\sigma(t) = \varepsilon_0 G(t) \tag{19}$$

where $\sigma(t)$ is the stress as a function of time, ε_0 is the initial strain, and $G(t)$ is the stiffness. In glassy polymers such as polystyrene (PS) and PC this relaxation can be on large time scales due to the long times needed for molecular rearrangement[39].

Recovery is another way to test dynamic polymer mechanics. This is the application of a force that is then removed to determine the material's ability to restore itself to initial dimensions[9]. The recovery process of a material depends largely on applied stress and time over which the stress was maintained. These two factors will determine if the recovery lies in the elastic or plastic regimes of the material.

1.2.3. Simplified Terminology

Using the following umbrella terms we can simplify our discussion of mechanics. Below are listed definitions for elastic, viscoelastic, and plastic. These definitions describe regimes of material stress-strain behavior.

1.2.3.1. Elastic

A material is considered elastic if a mechanical cycle sees no energy lost. In elastic materials there is a full recovery to original dimensions after a stress or strain cycle. Most materials have a region where they exhibit elastic behavior; however, past a certain critical stress or strain they will exhibit non-elastic behavior. This elastic region is often considered Hookean for simplicity. In this case stress and strain are linearly proportional with a slope proportional to the material's Young's modulus.

1.2.3.2. Viscoelastic

The stress-strain behavior of fluid-like soft-condensed matter systems are often dependent on the speed of the experiment. If an experiment is run quickly, response is often elastic. However, if the system is observed over a longer timescale, there can be viscous flow and stress and/or strain can continue to evolve. This can cause energy loss which creates a different force curve for the compression and extension stages of an experiment. Force-

displacement hysteresis is in general an indicator of an energy loss (in this case to viscoelasticity).

1.2.3.3. Plastic

The plastic regime of a material is where the material undergoes deformation in response to a stress or strain beyond that which is recoverable by elastic responses. This deformation causes a permanent energy loss. Plastic energy loss differs from viscoelastic energy loss in that it does not restore to the original state prior to the next cycle, it is not hysteretic.

1.2.4. Tensile Tests

Tensile or pull testing often involves a fixed grip and a movable grip that hold the test specimen on opposite ends. The sample is generally of a high aspect ratio shape such as a tube, rod, plate, or dumbbell shape. The dumbbell or dog-bone shape has wider areas on the ends for placing the grips and a narrower central region. The length of the central region and the slope from central region to wide end region is dependent on desired test parameters: sample thickness, sample treatment, and sample rigidity. Grip attachment is positioned for pull force to be along the longest axis of the sample. The mobile grip is then moved at a constant velocity away from the fixed grip until a certain distance or tensile force is reached or fracture occurs in the narrow cross sectional region. The Young's modulus is then determined from the linear region of the resulting stress-strain curve[40].

The initial dimensions of the sample are measured prior to it being placed securely in the grips with the sample as aligned along the axis of pull as possible. Speed is then determined by sample shape and rigidity. Measurements are taken of force and distance as the sample is pulled producing a load-extension curve. This curve provides information on modulus, tensile strength, tensile stress, and toughness, while the change in dimensions give elongation, deformation, and

Poisson ratio. The specifics of each test are set and can be referenced by American Standard Test Methods (ASTM) numerical designations. Plastic samples tested by appropriate ASTM methods are smoothed and marked with gage marks to determine dimensional changes such as elongation[40].

1.2.5. Compression Tests

Compression tests are those where the sample is confined between two plates. As in the tensile test one plate is usually mobile while the other is fixed. The distance between the plates is decreased at a set speed to a set distance. The plates can then be held at this fixed point for creep or stress relaxation tests. The cycle can be continued with the plates separating again for tests such as force recovery.

1.3. Thin Films

The ability of a thin system to dynamically fold, stretch, or bend into different shapes is a useful advantage over rigid 3-D structures. The benefits of thin film properties are actively being exploited in emerging technology. For example: folding systems, such as origami batteries in the shape of ninja stars that run on water impurities[41], foldable biosensors for pregnancy, HIV, and Malaria[42, 43, 44, 45], ingestible origami robots[46], bendable phones[47, 48], and satellites with solar panels that expand outward to deploy when they are in space[49] have been demonstrated. The benefits of 2-D systems that enable an expanding list of functions include designs that bend and stretch without sustaining damage, the enormous versatility of final shape, increased portability, and potentially lower cost. The versatility and large number of desirable traits achieved with thin systems makes understanding the underlying mechanics and engineering challenges very important.

The process of configuring a 2-D material into a predetermined 3-D shape can be accomplished in numerous ways. One common method of shaping a -2D material is origami. Origami is traditionally known as the art of paper folding[50, 51, 52, 53], but origami design is now used to describe any 2-D material that is bent or folded out of plane. Interestingly, all 3-D origami geometries are constructed from only a few structural components: bends, folds, ridges, and D-cones. Bends are out of plane deformations that give curvature to an area of the material. The radius of this curvature is greater than the material's thickness[54]. Folds and ridges are sharper bends in a material. In a fold, the material is deformed out of plane at a smaller radius of curvature, on the order of the film thickness, that brings the two sections of material on either side into close proximity. The small size of the fold radius typically causes material failure along the bend line that holds the material in that position even without additional external forces. A ridge is used to denote the bent region between two developable cones. D-cones, or developable cones, are localized points of stretching in a system[55]. These localized structures form because of the high energetic cost of stretching compared to bending in thin systems[56].

1.3.1. Bends

Bends, Figure 2, are the result of a point moving out of plane creating a curved global deformation in a sheet. As the point moves further out of plane the bend assumes a higher curvature[50]. Bends can be components of larger more complex 3-D structures or the entire system could assume a bend such as a tear drop. As bends do not induce damage barring the presence of adhesion or confining forces they are generally reversible.

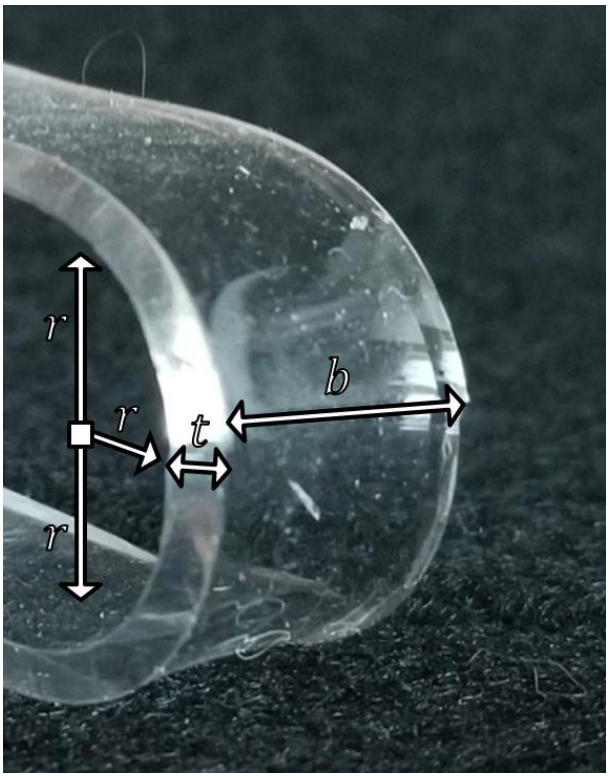

Figure 2. A bend in a sheet of 10:1 PDMS film showing the thickness, t, the width, b, and the radius of the bend, r.

The curvature of a bend is largely dependent on three things: the material, the sheet thickness, and the force acting on the sheet. Curvature has an energetic cost, U, of:

$$U \sim \left(\frac{1}{r}\right)^2 \tag{20}$$

where the value of $1/r$ is the curvature of the bent region, which is reciprocal of the radius ,r. Stretching a film requires more energy:

$$U \sim \varepsilon t, \tag{21}$$

where t is film thickness. The lower energetic cost of a bend is why they are so common in thin films.

A simple way to see this is to look at the bending of a beam. Bending stress is shown in terms of moments, rates of change of each point mass, acting on the section(s) moving to form

the bend. The rate of change of each point mass is equal to the force on that point mass with total moment being the sum of the total rate of change both internally and on the outer surface of the system. The total moment, M_{tot}, can be expressed as:

$$M_{tot} = \int_0^b \int_0^t \frac{B}{r} bx dx^2 \tag{22}$$

where b is the width of the beam, t is beam thickness, B is the bending modulus, and r is the radius of the bend, bx is the incremental distance moved along the beam width, and dx is the incremental distance moved along the beam thickness. Integrating gives the moment, M:

$$M = \frac{E}{r} \frac{bt^3}{12(1-v^2)} \tag{23}$$

which gives us the force of bending through a summation of forces in relation to rotation and curvature[57], showing a large dependence on film thickness.

A higher curvature bend, curvature below $\sim 1/t$ is a fold. Folds hold their shape as the higher curvature generally deforms the sheet. The strain on the sheet of this deformation generally causes lasting damage.

1.3.2. D-cones

A D-cone is also a common structure found in origami shapes. A D-cone is a shape formed when a 2-D material such as paper is folded in such a way that a sharp point is created towards a central area, for example, this occurs when a sheet is forced through a circular opening that is smaller than the sheet's lateral dimensions[55, 56]. D-cones can result from several different folding methods in addition to being pressed through a cylinder such as doubly folding a sheet.

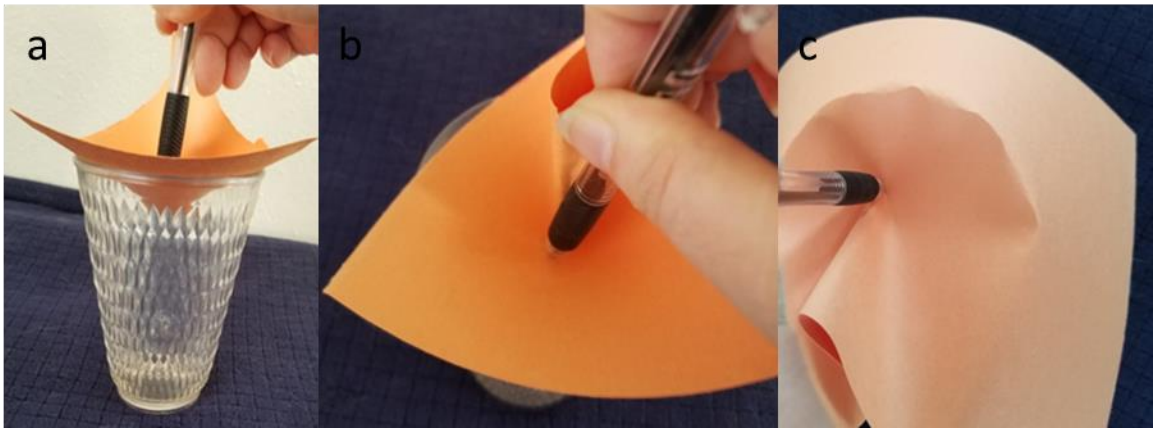

Figure 3. In figure a. and b. show the formation of a D-cone by applying a force in a small area on a sheet. This sheet is then pressed through a round opening forming the D-cone. In c. a heavy sheet is used, as the force pushes the sheet through the round opening D-cones are also formed along the edges of the opening; the sharp points seen in the picture.

The total energy of a D-cone is composed of the bending energy and the stretching energy. The averaged force of the D-cone tip is:

$$F = \frac{1}{R}\frac{\partial Ú}{\partial \varepsilon} = \frac{B_s}{R} ln \frac{R_C}{R_*} \frac{2\varepsilon\left(a^2 + \frac{1}{2}\varepsilon^2\right)}{(1+\varepsilon^2)^{3/2}} (\pi - \theta_c + \tan\theta_c) \tag{24}$$

Where Ú is the elastic energy of the sheet which is in contact with the rough frame it is being pushed through, R is the radius of the frame, B_s is the bending stiffness, R_c is the radius of the cone, R_* is a parameter of the size of the core region[58], and θ_c is the angle of the cone (Figure 4). The core is the only region experiencing stretching, energy outside of this D-cone core is the product of just bending. The radius of this stretched core is:

$$R_c \approx \left(\frac{B}{E_s}\right)^{1/6} \varepsilon^{-F} R^{2/3} \tag{25}$$

where B is the bending modulus, E_s is the stretching modulus, and F is the force. The strain is force dependent with it being close to zero when the force exceeds a certain value due to the change in geometry response, additional stretching that eliminates the excess strain[55].

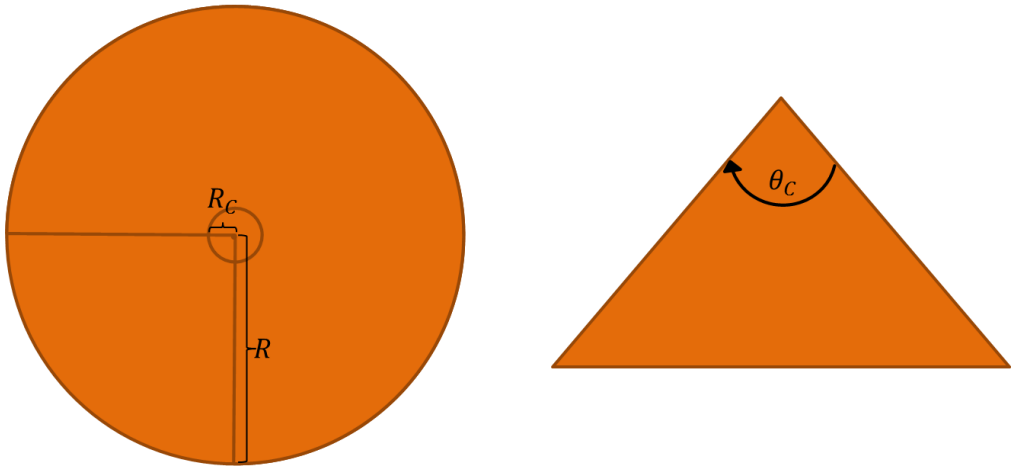

Figure 4. D-cone schematic showing the area surrounding the D-cone with radius of R_C and angle of θ_C, and the radius of the sheet from the D-cone to the edges touching a circular frame, R.

1.3.3. Crumples

Crumpled matter is a complex, random system made up of folds, bends, ridges, and D-cones, which we refer to as origami component shapes. Crumples form when a sheet undergoes compressive stress or applied forces and is confined in a small spherical region of space where it compacts[59]. The result, a roughly spherical shape, can be seen when balling up a sheet of paper as in Figure 5. Crumples can be compressed further if more force is applied, however, at some point they resist further compression due to the inner structures. Whereas an origami structure designed with a thin sheet might require a complex assembly process, making a crumple of equal complexity does not follow or require any instruction. Therefore, a crumple is a much quicker building solution for thin sheet construction.

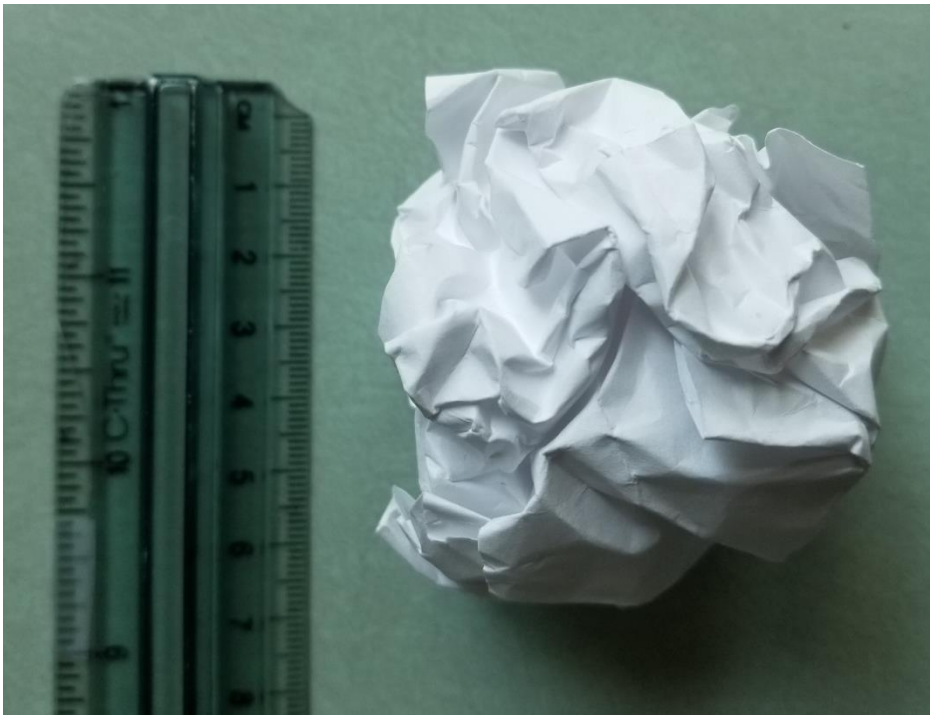

Figure 5. A sheet of paper with length of 27.5 cm and width of 21.5 cm crumpled into a ball with a radius of 5.3 cm.

Crumples in compression tests have force distance curves well fit by a power law:

$$F = F_0 H^{-\alpha} \tag{26}$$

where F_0 is the initial force, H is the height of the cylinder determined by the compressing parallel plates, and α is an experimentally determined exponent. The average indentation α value for 10:1 PDMS crumple to be 2.8±0.5[60].

1.4. Adhesion

Holding an object in a specified place or shape can be facilitated through adhesion. Tapes and glues are some examples of adhesion technology in common use throughout society. Adhesion is also prevalently in nature, occurring in spider webs[61, 62], snails[63], gum[64], and insects[65] and lizards such as the Tokay gecko (*gecko gecko*)[66, 67, 68, 69]. In this thesis we plan to expand our understanding of adhesion in elastomer systems by specifically examining how adding adhesion to shapes such as crumples[55], and a Ron Resch[70, 71] origami pattern might yield

new applications such as roughness tolerant or switchable adhesion. Meaningful adhesion measurements require knowledge of the methods used. Here the basic theory of adhesion is discussed along with two common methods of testing adhesion, the post or probe tack test and the peel test.

1.4.1. Basics of Adhesion

Adhesion is often characterized by an attractive force between two dissimilar surfaces. If the contacting surfaces adhere; the system is in a lower energy state than if they were separated. In order to separate the surfaces there has to be an energy input usually through the work done by a force. For reversible isothermal contacts between two elastic bodies the change in energy of the system to separate the surfaces is equal to the change in total energy:

$$dF = dU_T = dU_E + dU_P + dU_S \leq 0 \tag{27}$$

where dF is the change in free energy, dU_T is the change in total energy, dU_E is the elastic energy, dU_P is the potential energy of the load, and dU_S is the energy stored at the interface. The energy stored at the interface between the two bodies can be defined as:

$$dU_S = -(\gamma_1 + \gamma_2 - \gamma_{12})dA \tag{28}$$

where γ is the surface energy of elastic body 1 and 2, respectively, and γ_{12} their interfacial energy, and dA is the change in contact area between the two elastic bodies. This equation can also be represented as:

$$dU_S = -wdA \tag{29}$$

where w is the thermodynamic work of adhesion, known as Dupré's energy of adhesion[72]. The energy change between the interfaces is therefore equal to the work of adhesion over the change in area.

Adhesion is usually measured as G. A critical value of G where failure occurs and a crack becomes unstable is a G_C value, a critical energy release rate which may be equal to the work of adhesion in quasistatic experiments. G_C is defined as

$$G_C = d(U_M + U_P)/dA \tag{30}$$

at the point of interfacial failure, where U_M is the mechanical energy and U_P is the potential energy. There is also a dependence on three variables: surface energies of the two surfaces, compliance[73], and contact area. Compliance is a measure of the stiffness and elasticity of a material.

There is no clear consensus as to the best method to measure adhesion, although some tests are more commonly used than others. Three common tests related to our geometries and experiments are the probe-tack test, the peel test and the JKR adhesion test. Each test has different advantages and disadvantages.

1.4.2. Probe Tack Test

Figure 6 shows a schematic of a probe-tack test, where adhesion is measured between a flat surface and a substrate (typically the adhesive being tested). The upper flat surface is often cylindrical for geometric reasons which simplify the analysis. The cylindrical probe is mathematically simpler as only one variable, the radius, is needed to compute the total contact area, as opposed to two: a length and a width. The circular end of a cylindrical post also ensures a more even pressure distribution than the end of a rectangular prism as stress concentrations form at sharp corners.

The test consists of three steps as shown in Figure 7, the lowering step where the cylindrical post is lowered into the substrate with enough force to ensures complete contact has been made. The second step is holding the post in position where it remains in contact with the

substrate surface for some predetermined time. The third and final step is the removal of the post by an upward debonding force. The angle of application and removal of the post is strictly 90° in order to ensure both surfaces are in complete contact and to ensure forces are evenly distributed during the connection and separation steps. If forces are not evenly distributed during the removal step, a crack between adhesive and post may be initiated at one side and analysis becomes complex.

Post testing is often done on surfaces that have hysteretic energy loss. In other words, greater force needs to be applied for debonding than was needed for bonding[73]. High adhesion low compliance surfaces experience large energy loss in debonding as these adhesives tend to be quite soft and may not separate from the post at all points on the surface simultaneously or concentrically from the edges. High adhesion low compliance adhesives which separate in sections leaving other sections still attached, as in cavitation, have a different surface area at pull-off that is not equal to the radius of the indentor.

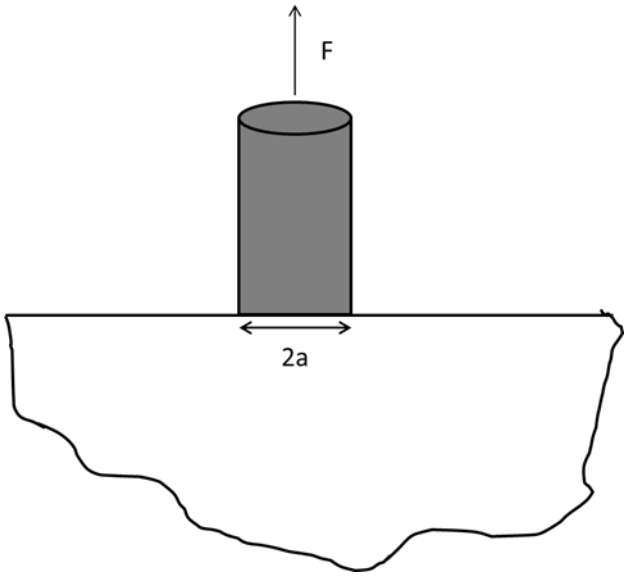

Figure 6. Representation of the Probe Tack test, a rigid cylindrical post with $2a$ diameter is placed into the surface of an elastic adhesive material. Inspired by a figure in Kendall 1971 paper[73].

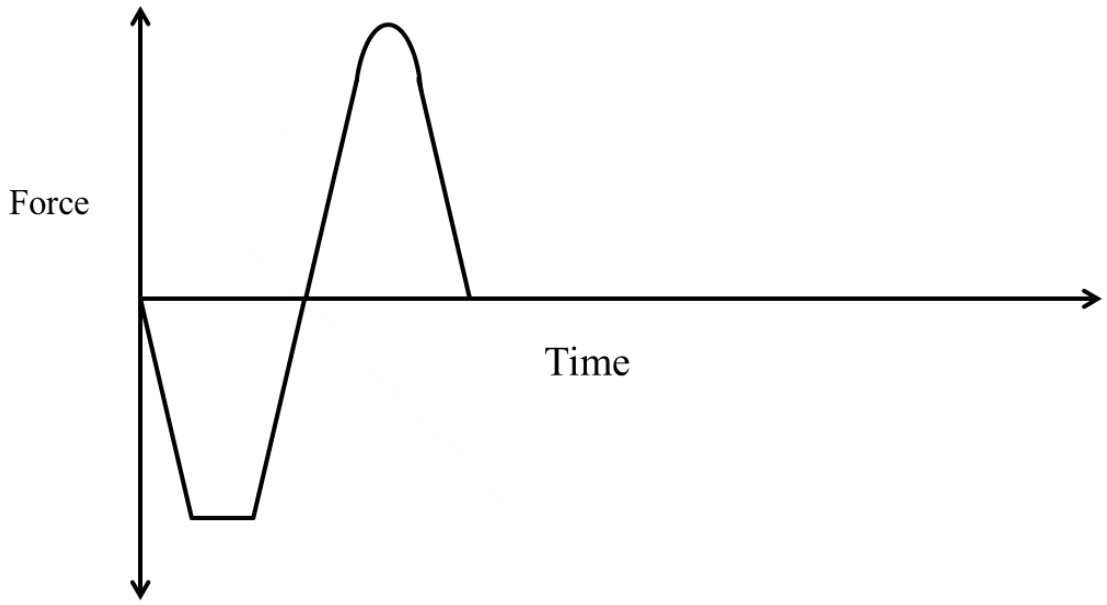

Figure 7. The steps of a Probe Tack test where the post is lowered onto the surface force is applied for a period of time to adhere the post to the substrate. The post is then pulled upward for removal by an upward tensile force. Notice the force increase in the debonding removal step, for an ideal Probe Tack. In instances where the substrate does not come off all at the same time there can be an extended or multiple peaks. Schematic of a probe tack test inspired by a figure in Kendall 1971 paper[73].

The measurements taken from a probe tack are those based on the excess force needed to separate the surfaces of the probe and adhesive which is a measure of the interfacial energy. This measurement is not a direct measure of adhesion it is a measure of the energy release rate, G_C. The energy release rate is determined by the interfacial surface energy and the area. In instances of a force controlled experiment, with no cavitation or fingering instabilities occurring, we can state that the forces are in equilibrium and write the equation as[72:]

$$G_C = F^2(1-\nu^2)/8\pi E a^3, \tag{31}$$

where a is the radius of the cyclindrical post.

1.4.3. Peel Test

The peel test is a method where a thin adhesive layer, is lifted by one end at some angle and speed from a substrate. Unlike the probe tack test, peeling does not break contact over the

entire surface in one step. Peel causes an initial crack in the adhesive layer to propagate as the displacement of the free end of the adhesive layer continues to debond the thin material from the substrate. This debonding is dependent on the rate of displacement, width of the material, and the surface energy between the material and the substrate. The material being peeled is often in a rectangular strip as shown in Figure 8.

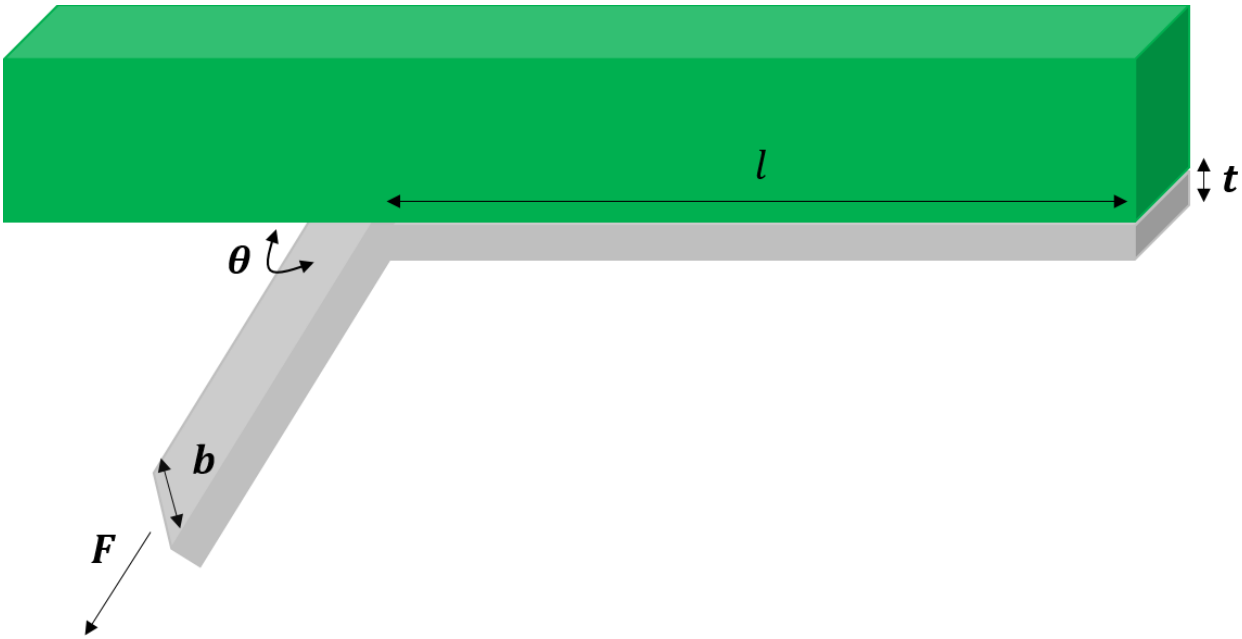

Figure 8. Peel test of a rectangular sheet from a substrate. Inspired by figures from Kendall 1971 and 1975 papers[73, 74].

To determine the adhesion of debonding in a peel test, the force is measured. The force needed to debond the strip depends directly on the energy release rate, G_C. The G_C to peel the strip of a certain width off the surface of a substrate is a fixed property of the system dependent on the material of the strip and the speed of pull-off/debonding. The material properties of the strip dictate the interfacial energy through the chemistry of the bonds. The speed of pull off and compliance of the material together affect G_C by determining recovery time. Slower pull off speeds will allow the material more time for force recovery whereas faster pull off speeds might exceed recovery time. Relating the measured force to the energy release rate mathematically:

$$\frac{F}{b} = G_C(1 - cos\theta). \tag{32}$$

In cases where the angle of peel, θ, is 90° the equation simplifies to:

$$\frac{F}{b} = G_C. \tag{33}$$

Changes in area due to stretching are not typically observed in our experiments. Thus strips in peel are generally considered inextensible sheets[74]. Thickness and width likewise have no effect on the change in surface contact as there is no altered dimensions due to stretching.

1.4.4. JKR Test

The JKR test (Johnson-Kendall-Roberts) is a point of contact test between two elastic solids in the form of two full or half spheres, a full or half sphere and a flat surface (Figure 9), or between two crossed cylinders[75]. The total radius of contact expands from a single point during compression as both solids are moved in closer contact.

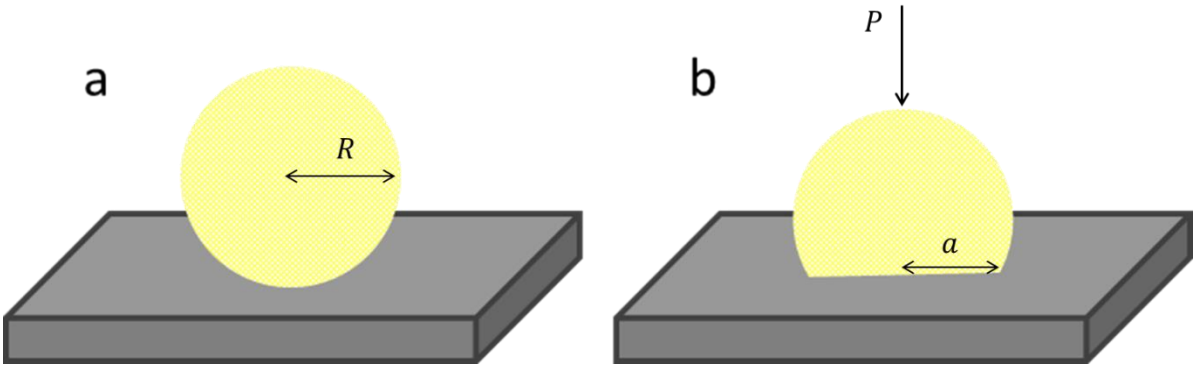

Figure 9. JKR test. Side a is a is a sphere and a flat surface which when pressed down looks like b, where the sphere is now in contact with the flat surface.

The surface energy between the surfaces:

$$U_s = -\gamma\pi a_1^2 = -\gamma\pi(RP_1/K)^{\frac{2}{3}} \tag{34}$$

where a_1^2 is the area of contact between the two solids, R is the radius of the sphere, P is the force, and $K = (4/3)\,(k_1 + k_2)$ the elastic constants of each sphere combined over the volume $k_1 = (1 - \nu_1^2)/E_1$ with k_2 being the same with equation with material properties of the second

solid. The work done through separation is then calculated as the work of adhesion with the force needed to separate the spheres:

$$P = -\frac{3}{2}\gamma\pi R \tag{35}$$

which is independent of the material properties of the solids[75].

The ratio of displacement to load is the compliance which for JKR is:

$$C_0 = \frac{1}{2E^* a} \tag{36}$$

where E^* is the effective modulus, a modulus adjusted for Poisson Ratio:

$$E^* = \frac{E}{1-\nu^2} \tag{37}$$

the effective modulus is additive in the case of two curved elastic half-spaces in contact. The energy release rate is given as:

$$G = \frac{(4E^* a^3/3R - P)^2}{8\pi E^* a^3} \tag{38}$$

valid for cases where the contact radius is small and the ratio of the contact radius to the hertzian contact a/h approaches zero. Hertzian contact is a measure of the contact area divided by the diameter of the sphere, $h = a^2/2R$. In cases where the ratio of $a/h \neq 0$ and the material is incompressible with $\nu = 0.5$ the expression can be modified to:

$$G = \frac{(P' - P)^2}{8\pi E^* a^3} f_{Gp}\left(\frac{a}{h}\right) \tag{39}$$

in terms of load difference where P is the initial load, P' is the end load, and $f_{Gp}\left(\frac{a}{h}\right)$ is:

$$f_{Gp}\left(\frac{a}{h}\right) = \left(\frac{0.56 + 1.5(a/h) + 3(a/h)^3}{(0.75 + (a/h) + (a/h)^3)^2}\right) \tag{40}$$

a relationship of the ratio between contact radius and height of the semicircle. In terms of displacement the equation becomes:

$$G = \frac{E(\delta' - \delta)^2}{2\pi a} f_{G\delta}\left(\frac{a}{h}\right) \tag{41}$$

where δ is the initial displacement, δ' is the final displacement, and $f_{G\delta}\left(\frac{a}{h}\right)$ is equal to:

$$f_{G\delta}\left(\frac{a}{h}\right) = \left(1 + 2.67\left(\frac{a}{h}\right) + 5.33\left(\frac{a}{h}\right)^3\right) \tag{42}$$

which is valid under conditions where full friction exists between the two solids, ie there is no intermediary obstacles, air, or liquid[76].

1.5. Previous Work

The work in this thesis builds on data and measurements from similar experiments to that have been conducted previously in my M.S. work[77, 78]. Notably, the bending experiment apparatus is utilized to explore the mechanics of a tape loop. In this section I will briefly summarize the M.S. research, results, and relevance.

Thin systems have engineering challenges that differ from their 3-D counterparts. Thin systems in configured shapes will have different stress and strain behaviors than the same material molded directly into a similar shape, so it is important to find test geometries which are relevant to origami structures. Our earlier (M.S.) work explored measuring these basic differences in an origami-relevant geometry[77, 78]. Specifically, we linked bending to material properties such as the bending modulus and film dimensions. Notably, the bending test works with materials which are too thin for many other tensile tests. The bending test also allows us to measure dynamic aspects of various material properties through force recovery measurements.

Knowing function and longevity of a structure requires knowing physical properties at all scales; this is particularly true of origami inspired structures made of large bends, sharp folds and singular D-cones. Adequately measuring the mechanical properties of 2-D materials, generally materials of thickness an order of magnitude less in one dimension than in other dimensions,

poses a challenge. Most traditional mechanical tests are designed for bulk samples, samples where the thickness is of the same order of magnitude as the other spatial dimensions. Our experiments measured the properties of 2-D materials, specifically the modulus and force recovery in a nondestructive method.

1.5.1. Bends

Bending is important in thin films because bending is much easier than stretching due to the higher energy cost involved in stretching. Previously, we designed a simple experiment to directly determine the bending modulus of a material by measuring forces as a film is increasingly confined between two parallel walls, shown in Figure 10. Bends were where the film approximated a half cylinder in the middle connecting two equal lengths of film touching two parallel glass plates. The bend was chosen as it is a common shape both independently and in many more complex origami shapes.

In a typical bending experiment, a thin rectangular strip of film was placed between two plates in our apparatus. The film ends were aligned along each respective plate to be parallel and of equal lengths. Initial plate distance was adjusted until there was a slight circular bend in the area of the film connecting the pieces along the plates. Glassy films such as PC often required tape to secure the ends and prevent any lateral movement of the film. Prior to placing a film in the apparatus, the physical dimensions of thickness, width, and length were taken by calipers. If films were too thin, measurement of thickness was conducted by confocal microscopy or image analysis.

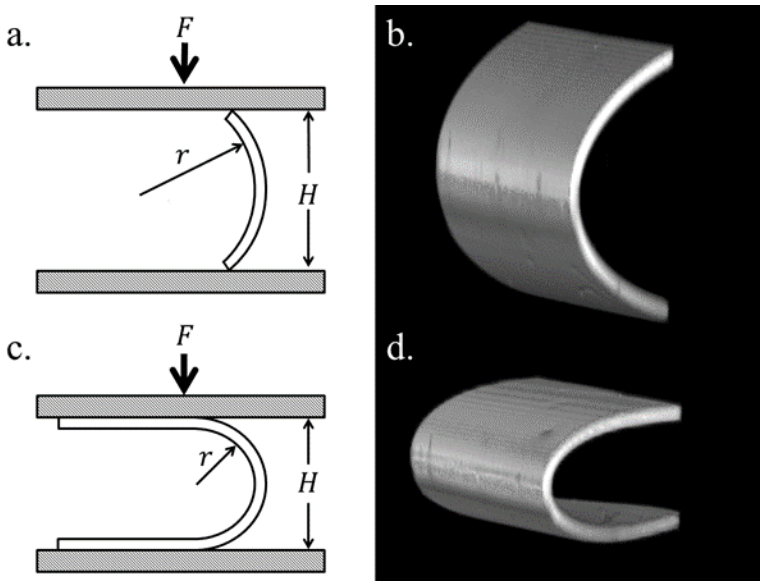

Figure 10. Bend at initial low curvature (a. b.) and bend at high curvature under compressive stress as the two plates are moved closer together (c. d.)[78].

The half cylindrical geometry of our bent films allowed us to use basic mechanical equations to relate applied moments to the degree of bending in the film[78]. Ultimately this allowed us to derive an equation that both described the force with regards to dimensions and material properties and fit our data. We show typical results in Figure 11 where we fit the relation

$$F = \frac{\pi B b}{r^2} \tag{43}$$

to the data. In Eqn. 43, b is the film width, r the radius of curvature, and B is the bending modulus given by:

$$B = \frac{E t^3}{(1 - \nu^2)} \tag{44}$$

where t is thickness, E is Young's modulus and ν is Poisson's ratio.

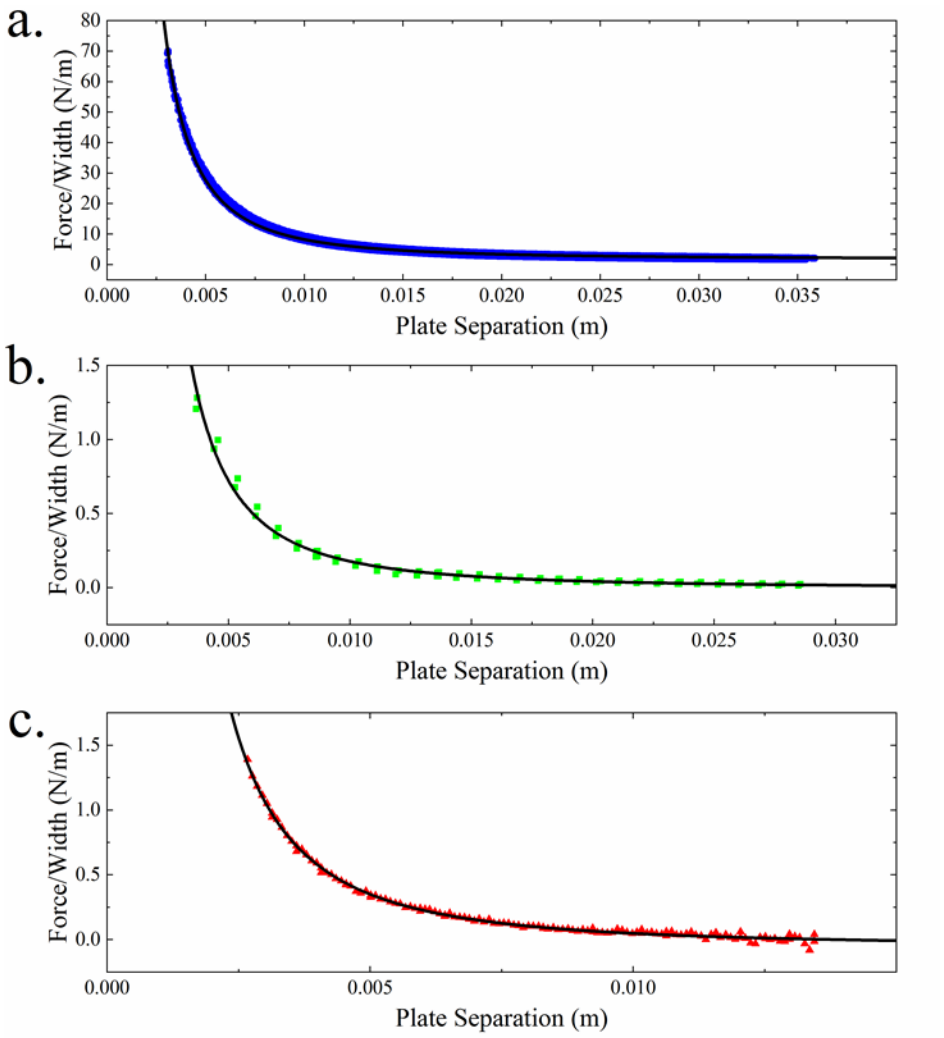

Figure 11. Graphs of force vs. distance for all three materials used: a. PDMS, b. PS, and c. PC[78].

Data from the many different experiments carried out were compiled to measure the bending modulus, where B is plotted against t. A cubic thickness dependence was expected based on Equation 44, the slope of which is equal to E. We obtained modulus values of PDMS, $E_{PDMS} = 1.69 \pm 0.05$MPa, PS, $E_{PS} = 3.5 \pm 0.05$GPa , and PC, $E_{PC} = 1.6 \pm 0.01$GPa[78].

The bending of thin films is a good method of determining modulus for films where other physical properties are known. Modulus values obtained are in keeping with literature values of modulus for all three materials examined: PDMS, PC, and PS. The advantages to this method

are that it is nondestructive, it does not require large samples, and it is accurate for modulus determination of a variety of materials both crosslinked and glassy.

1.5.2. D-cones

D-cones were formed through bending a film in half in one direction, followed by folding the film in half again in a direction orthogonal to the first bend axis, Figure 12. This doubly bent film was then placed between the two parallel plates in a similar manner to the single bend (the ends of the film resting against the parallel plates, the area where the D-cone is formed was facing the camera). Other aspects of the experiment such as: the apparatus, procedure, collection of data, and data processing were kept similar to what was done in testing the single bend.

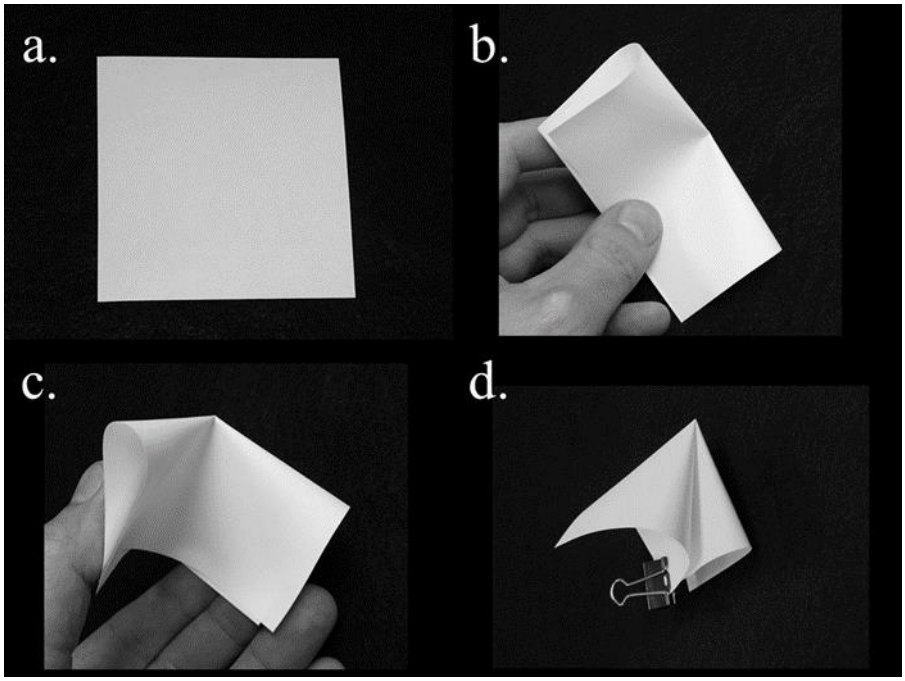

Figure 12. Folding of a paper in half longwise then folded a second time longwise orthogonal to the first fold to form a single D-cone[78].

Our measurements of the double bend supported a null hypothesis that the D-cone did not contribute significantly to the stress-strain behavior of the film. This means the D-cone was not load bearing and thus did not affect the measured forces we investigated. This is mainly because

the D-cone does not exhibit any significant changes from its initial geometry during compression. To model the force-displacement data, we made the assumption that different regions of our doubly bent film all act independent of each other. The dominant system energy was still stored in bending, but now several bends are present in the film. Following the same mechanical approach used previously we found that the double bend only differs by a factor of 4 when compared to the single bend. In detail:

$$\frac{F}{b} = \frac{4\pi B}{R^2}. \tag{45}$$

The modulus values determined from fitting Equation 43, were compared to both values obtained by us using ASTM D412 dogbone T-tests and literature values. The modulus value we obtained for PDMS is within the expected literature range of 1.32-2.97 MPa, with it being towards the lower end consistent with the somewhat lower curing temperature of 85 °C. Our measured PS modulus aligned exactly with literature values of 3.0-3.5 GPa. Our obtained PC modulus was slightly lower than the accepted literature value of 2.0-2.6 GPa[23].

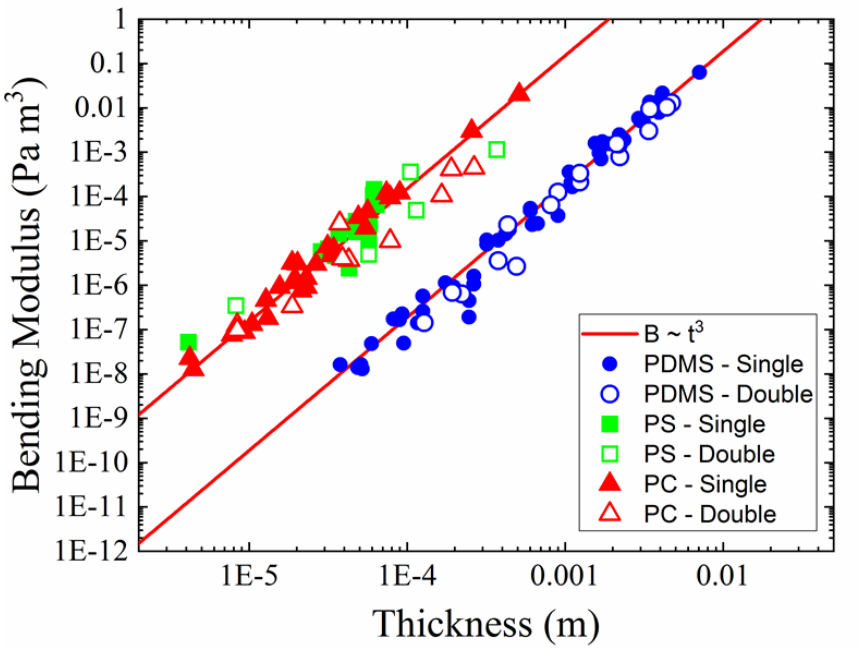

Figure 13. Log-log plot of B from Equation 44 against cubic thickness of all experiments[78].

1.5.3. Strain Dependence

Thin film materials often exhibit moduli that are strain dependent. Softening trends are seen in all three materials, Figure 14, in keeping with expectations for glassy polymers, but unusual for strain hardening PDMS. The strain softening of PDMS from our data at times exceeded the Hookean regime. We attribute the strain softening of PDMS to the nonlinearity of PDMS at strains <40%, which some films were tested above[78].

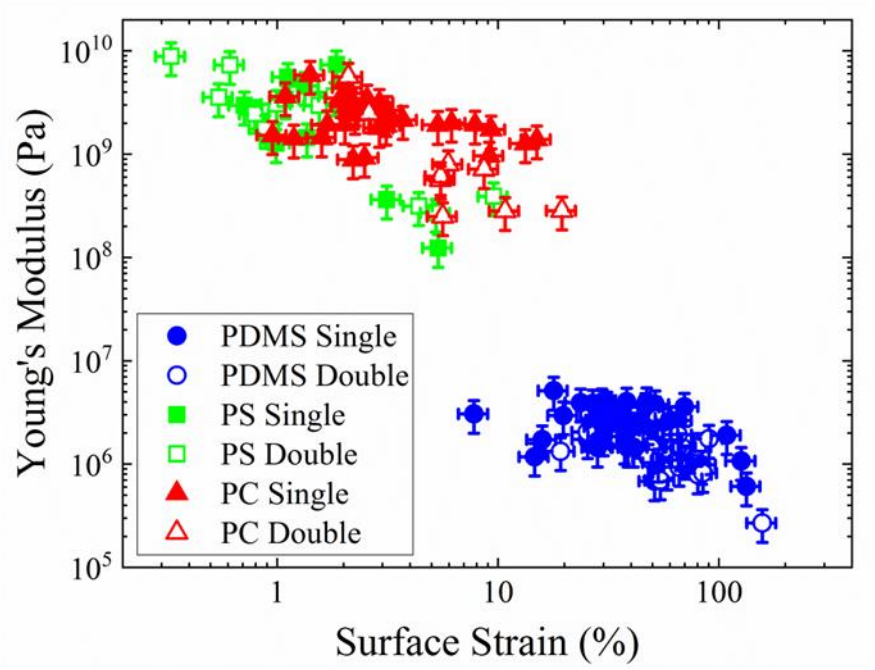

Figure 14. Softening trends of all experiments that show general softening trends over the span of thicknesses examined[78].

Double bend geometry in our two-plate bend method is as effective as the single bend geometry for the determination of the material modulus. The D-cone in the double bend was not load bearing and did not have noticeable effects of the force distance curves. The double bend geometry is comparable to a single bend film of double the thickness. The advantages of our bending method for single bends are also advantages for double bends.

1.5.4. Force Recovery

Next force recovery experiments were conducted on singly and doubly bent films. Force recovery is the observation of dynamic changes a material undergoes when subjected to a constant stress over time. The internal adaptive processes that a material takes in response to a constant stress can differ. The process that a film undergoes is predictive of potential uses in real world engineering applications.

Some of the most relevant modes of time dependent change for our polymeric materials are elastic recovery, relaxation, creep, and failure. Relaxation and creep are two opposite processes that lead to deformation of a material over logarithmic time scales. In relaxation the strain of a system remains constant while the stress decreases through deformation or molecular rearrangement[79]. In creep the stress of a system remains constant while the strain is decreased through expanding deformation that spreads out the load over a wider area[38, 80]. Failure is when a material experiences stress in excess of its maximum stress resulting in fracture where the material breaks[81], buckling, crazing or permanent deformation.

In our experiment we measured the changes in force over time of our material confined between plates which were held at a constant displacement. The plates were moved toward each other at a constant speed until a desired bend curvature was reached. This curvature was maintained in the bend through holding the fixed displacement in our apparatus over the desired timescale. Holding the apparatus in the same position maintains a constant stress on the film. Under this constant stress we measured the changes in force over a logarithmic time scale.

Results, Figure 15, were normalized to 40 s in order to exclude geometric details imparted by the apparatus and to account for the relaxation that takes place during compression. Due to its fragility, stiffness, and low molecular weight PS did not yield usable data. PS films

bent to curvatures high enough to be measurable by the sensitivity of the scale were prone to cracks and crazing. PDMS samples were limited by the maximum force measurements of the scale as samples of too high a thickness had too high a bending force to be measurable with our scale. PDMS and PC showed a logarithmic decay force recovery which we fit with the equation:

$$\frac{F_t}{F_{40}} = -\beta log\left(\frac{t}{\tau}\right) \tag{46}$$

where F_t is the force at a given time adjusted by F_{40} the force at 40 s after the start of the experiment, τ is the relaxation time, t is the time investigated and β is a proportionality constant. PC, however, was also well fit by a stretched exponential function:

$$\frac{F_t}{F_{40}} = A^{[-t/\tau]^{\delta}} \tag{47}$$

where δ is the exponent value of the shift and A is the proportionality constant, a common way to measure glassy polymers. However, due to our experimentation being a constant temperature our δ is small and τ large which makes it essentially the same as the logarithmic equation[78]. Both are depicted as trend lines in Figure 15.

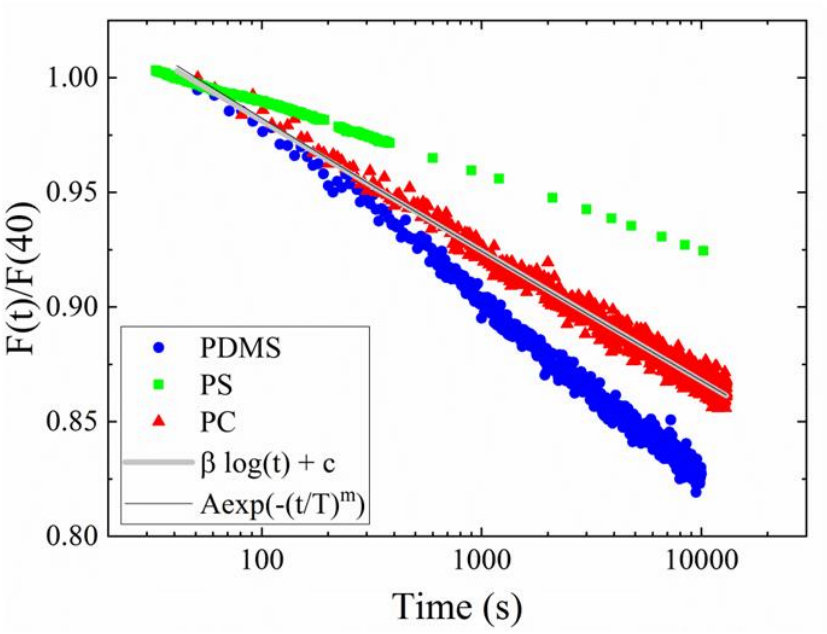

Figure 15. Representatives of PDMS, PS, and PC force recoveries from our data that show that all are well fit by a logarithmic function as well as a shifted exponential[78].

The force recovery of films was not dependent on the material with crosslinked PDMS showing a similar behavior to glassy PC. Both materials had logarithmic decay trends during force recovery. PC was also well fit to a stretched exponential decay function which overlaps the logarithmic decay as there is no temperature variation in our samples over the force recovery time.

1.5.5. Conclusion of Previous Work

Our single bend experiments yielded equations 43 and 44 which gave the realistic material modulus of our thin samples as a result of simple mechanical testing that does not require large amount of sample or necessitate sample destruction. Our bending test also confirmed that D-cones do not affect the load bearing of the sample and that the modulus can still be determined for films in flat geometries containing D-cones. We also determined the relaxation behavior of all of our films, single and double bends, followed logarithmic trends consistently for all three materials. We showed that this method is effective for different

materials of a variety of thicknesses in obtaining materials properties that may not be attainable by conventional means due to specifics of a sample, such as thinness.

1.6. Materials

Polymeric materials were chosen for our experiments due to the unique physical and chemical properties of polymers. Polymers were also chosen as a realistic material system as they are finding expanded usefulness across different areas and disciplines of engineering, biomedical applications, and commercial products. Knowledge of mechanical properties is necessary for polymer systems to be properly utilized in engineering applications. The mechanical properties of polymeric films rely on both the material properties and the dimensions of the film. In our experiments we use three different polymers: polydimethylsiloxane, polycarbonate, and polystyrene films because each has a different mode of failure, compliance, and surface energy.

Polydimethysiloxane (PDMS) is a hybrid polymer that is a flexible elastomer filled with nanoparticulates[23, 82], it is commonly used for insulation of electronic components[83], sealants, or applications that require a hydrophobic surface[14]. Sylgard 184 PDMS has a modulus that increases at higher crosslinking; higher crosslinking is achieved through higher ratios of polymer base to curing agent up to 9:1 and higher curing temperatures, ranging from 25-200 °C. Higher curing temperatures result in higher ultimate tensile strength, compressive strength, and modulus values in the range 1.32-2.97 MPa[23]. This increase in strength is from higher curing temperatures increasing the speed of the crosslinking process resulting in a higher crosslink density.

One of the first polymers to be discovered (1839)[84] and synthesized was Polystyrene (PS)[85]. Isotactic PS is a glassy polymer. The bulky component monomers of styrene are too

randomly bonded in space along the polymer backbone to align regularly preventing full crystallization. Polystyrene solidifies below a T_g near 100 °C into a rigid amorphous material that is brittle and fails in the form of crazing and widening cracks. Polystyrene is also transparent making it a good choice for applications such as lenses and electronics, it is also used in food containers and toys[14]. Bulk PS has Young's modulus of 3-3.5 GPa[86], and a yield strength of 28.7-41.4 MPa which decreases as film thickness decreases[87, 88].

Polycarbonate (PC) is a glassy copolymer comprised of two monomers, Bishphenol A and Phosgene. PC is glassy and transparent with a high refractive index. PC is more ductile than PS and fails not in the form of propagating cracks but in the form of plastic deformation where it stretches and retains the shape introduced by the force[14]. The Young's modulus of PC is 2.0-2.6 GPa[87].

The three materials chosen, PDMS, PC, and PS as stated above are common industrial polymeric materials that have different known modes of failure. We carry out our experiments on these materials in order to show versatility of the methods and determine the mechanical properties for various materials all at once. This provides a wider understanding of the mechanics of the geometries we impose on each film and gives a more useful understanding for engineering purposes.

1.6.1. Sample Film Preparation

Methods of preparation for the three films were chosen based on synthesis and desired end thickness considerations. PC and PS polymers came in pellet form. Pellets were dissolved in appropriate volatile solvents. Solutions of PC and PS were low in centration and viscosity compared to PDMS which prior to crosslinking is a highly viscous liquid. These factors were considered along with desired film dimensions of thickness and area when choosing an

appropriate fabrication method. The desired speed of solvent evaporation for PC and PS was also a consideration. Slowing down evaporation in order to avoid internal pockets of solvent inspired the creation of chambers to retain a small amount of solvent vapor pressure.

1.6.1.1. Methods

Three main methods were used in the making of all of our thin polymeric films: dropcasting, flowcoating, and spin coating, Figure 16. We found these three methods provided us with uniform thin films over a range of sizes for experimentation. The method used depended on the material and desired thickness of the film. Thicker films were dropcast while thinner films were flowcoated or spincoated.

(a) Dropcasting

Solution is added dropwise to the center of substrate until solution spreads flush to the edges of the substrate without spilling over or to the edges of a sample container. If the amount of solution used is small and it is poured directly into a sample container it may not flow fast enough to reach the container edges. If not, the container is turned at a slight angle until the solution covers the entire bottom of the container. The container is then placed on a level surface to complete the coating process.

(b) Flowcoating

Sample solution is placed just behind a blade that is then moved forward along the substrate. The solution is spread out in a thin layer. The blade height is dictated by desired film thickness, as the blade moves forward it pushes the remaining solution forward until all solution has been distributed on the substrate or pushed off the end. To achieve desired thin film properties and avoid unevaporated solvent the blade was kept in close proximity to the substrate.

(c) Spincoating

To spincoat, the substrate is placed on the small rotational stage of a spincoater. The substrate is vacuum adhered to the stage which is then spun at a desired speed, for a specified time in order to spread a sample out to the edges of the substrate. Sample solution is poured onto substrate prior to spinning in order to spread out thick solutions and ensure coverage of the entire substrate. For more dilute solutions with evaporable solvents or for thinner films solutions are poured on during spinning. Speeds varied from 500 rpm to above 2000 rpm and times from 30s to 60s.

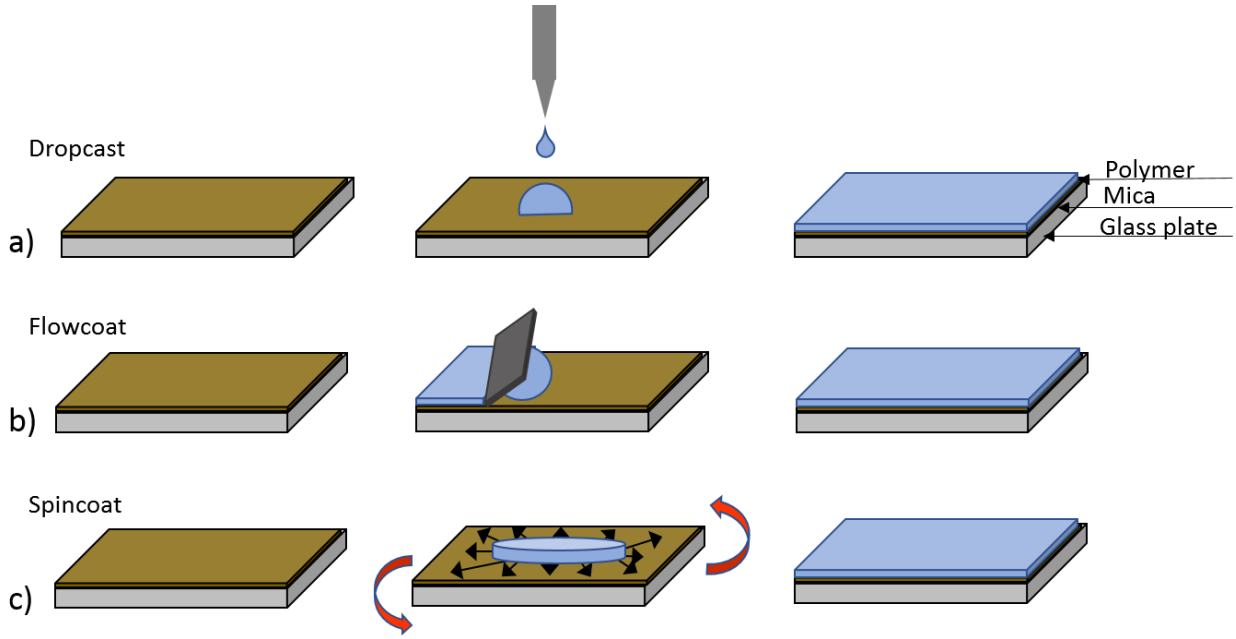

Figure 16. Three methods of spreading polymer solutions over a substrate before annealing. a.) Dropcasting (top) which is the dripping of a solution into a central area that pools and expands outward.b.) Flowcoating (center) the pushing of a solution in a thin layer over a substrate with a long thin tool or blade. c.) Spincoating (bottom) where a solution is spread to the edges of a substrate by quick rotation of the substrate.

1.6.2. PDMS Preparation

Sylgard silicone elastomer base 184 and Sylgard 184 elastomer curing agent are measured out in a desired weight ratio between 10:1 and 50:1, with a 2-5g excess of desired film

weight to account for any loss from polymer coating the walls or stirring tool during mixing. The solution was then thoroughly mixed for 5-10 minutes using a glass pipette as stirring tool. The solution was then applied to desired substrate through methods described in Section 1.6.1.1, in order to create samples of uniform thickness. In dropcasting the film was poured directly into a PS sample container until desired weight was reached. The sample container was then examined to ensure that solution completely covered the bottom including edges and corners.

Spincoating was done on glass slides that had been rinsed with water and coated with a 1:1 Polyacrylic acid (PAA)/deionized (DI) water mixture at 1000 rpm for at least 30 s. PDMS was then spread over the PAA/DI water release layer and put on spincoater at speed between 500 and 2000 rpm for approximately 60 s. Sample solution was poured on prior to spinning in order to spread out the thick solutions and ensure coverage of the entire substrate and during spinning for thinner solvents and films.

Sample containers prepared by all methods were then placed in a vacuum oven for 5 mins at a pressure of 20-25 in Hg. This vacuum cycle was repeated for four cycles to fully release gas bubbles from sample prior to crosslink annealing. Annealing was done by heating in a vacuum oven set to 15 in Hg set at ~85 °C for 90 mins or convection oven under atmospheric pressure at 85 °C; convection oven was used only for thinner or spincoated samples. Once 90 minutes had elapsed samples were promptly removed from oven and placed on counter to quench for a minimum of 30 minutes. Samples were not used until the following day to allow for any additional crosslinking of ends to take place.

1.6.3. PS and PC Preparation

Solutions of PS and toluene were mixed by weight percentage 5-25 % wt. PS, while solutions of PC and chloroform were mixed in ratios of 1-10% wt. PC. Solutions were allowed

to sit for 48 to 96 hours prior to use in order to allow polymer to fully mix with solvent. Solutions were then applied through one of the three methods shown in Figure 16 onto a freshly cleaved mica or glass substrate. Mica was held by capillary force from a drop of water to a glass slide for support and stability. Samples were then immersed in the vapors of their respective solvent, chloroform for PC or in air for PS, by being placed in chambers to slow down the evaporation rates. Samples were left in these chambers for at least 12 hours prior to annealing

1.7. Direction

Additional challenges still remain in the formation, maintenance, and effects of stresses and aging of 3-D shapes made from 2-D materials. For example, a current challenge exists in understanding the effects of surface energies (adhesion) of the thin material with itself and its surroundings. In this thesis we seek to understand how adhesion relates to the geometry of a thin material system such as a bend. Accurately predicting the behavior of thin, shaped adhesive materials could lead to novel applications such as crumples that can adhere to rough substrates or origami that can switch adhesion on and off.

In this thesis we extend our thin polymer film work from the foundation laid out in our previous work[77, 78], into adhesion and new origami inspired designs. Specifically, we intend to explore how adhesion can also be measured in a set up similar to the single bend tests described in[77]. We then extend this testing to "sticky crumples" in order to determine how adhesion changes when a thin strip of 2-D material is formed into a (random) 3-D shaped 2-D material. We will then add roughness to surfaces to determine if crumples can adaptively conform around obstacles and irregular surfaces to create "better than flat" adhesives. Finally, we will explore origami shapes that are switchable adhesives, depending on their configuration. This new

ongoing work should enhance the knowledge and possibilities related to the adhesion of 3-D configured 2-D materials.

2. ADHESION: MECHANICS OF A TAPE LOOP

2.1. Introduction

A tape loop, Figure 17, is a simple, common way to attach two flat objects together such as hanging up a poster. A tape loop is made by taking a strip of adhesive bending it over a 180° angle until the ends overlap and stick together forming a circular loop. The outer adhesive side is then used to attach the items together. However, the mechanics of the attachment and detachment process of this common method are a bit more complex than might be assumed.

The loop remains circular and is undeformed if no external force is introduced. This cross-section retention is material, substrate, and time independent. If the loop is used and pressed between two surfaces the force and compression cause a shape change in the loop from circular to a more elongated shape that is flatter along the top and bottom with high curvature at the ends. While compressed between the two objects it remains in the configuration, retaining the highest possible surface contact area with each. After separation of the two attached objects from the tape loop there is a slight opening with the oval shape being retained rather than a return to the original cylindrical shape. This means that the system can exist in multiple configurations under the same loading conditions (see Figure 17). Geometry is for some reason, dependent on the history of the system.

Figure 17. A tape loops in two stable configurations. The left is a newly formed tape loop with a rounded shape. The right is a tape loop is after compression and has a more flattened oval shape.

The change in configuration shows a hysteretic loss of energy during the sticking on and peeling off cycle. The elasticity of the loop is insufficient to restore the loop to its original shape; therefore, equilibrium is not dictating the tape loop shape. Multi-configuration stability and hysteresis might be expected from pressure sensitive adhesives, that is, adhesives designed to lose energy to viscosity, however, we also observe the effect with dry (low-loss) adhesives. This is of particular interest due to the rise of adhesive designs that are reusable and have minimal energy loss, such as gecko inspired adhesives.

Common though the tape loop is, it is interesting that it is not easy to find a complete, simple, mechanical description of the system. Particularly, as details like the aforementioned bistability are difficult to understand from a terse energy balance. The goal of this chapter is to give a more complete description of the adhesion of a loop, and by doing so we turn the tape loop into an adhesion measurement system.

Our experiments focused on using dry adhesives of thin polymeric films that have varying energy loss at the interface. Our goal was to isolate the effects of the compression and retraction cycle. Pressure sensitive adhesives were not used for simplicity of measurement, as they are designed to dissipate energy so, insight into the system bistability would require extra steps to try to separate energy differences attributable to the cycle and those attributable to the viscous loss in the adhesive. Other non-dry adhesives such as glues, epoxies, and elastomers in the process of crosslinking would be difficult to work with cleanly as strips of tape will undergo hardening during experimentation. The compliance change and surface energy changes would affect the stability of the system, measurements, and potentially damage experimental equipment set ups, so we exclude these systems as well.

Experimentally we observed that the shape hysteresis is not simply a product of energy dissipation during debonding it is a general geometric feature of adhesive loops. We also determined that the "Sticky Elastica" model can be modified to the tape loop geometry. This model provides us theoretical insight and enables the system to be used as an adhesion measurement system. The usefulness of the tape loop as a system to measure adhesive energy was experimentally verified using different preparations of PDMS, this work has been published[89]. Our results led to the discovery of an incredibly simple method of measuring a tape loop system's adhesive properties using only a ruler for measurement.

2.2. Methods

To characterize the force behavior of a tape loop over the compression and extension parts of a cycle we created loops of "dry" adhesive polymer films. To create loops analogous to tape loops rectangular strips were cut from each polymer film. The strips were then measured for dimension of length, width, and thickness. Measurements were done prior to experiment to

prevent inaccuracy due to possible stretching (especially with lower modulus samples). Thickness was measured by image analysis and confocal microscopy due to the soft nature of the films yielding unreliable results when compressed with calipers. Film weight was measured after the experiment in order to ensure the cleanest film surface is measured during the test. The strip was then put into a half loop shape with both free ends in contact with parallel walls. The bend of the half loop connecting the two ends was free standing in the air. A half loop was used to mimic the tape loop for reasons of geometric symmetry and to avoid considerations of doubly thick overlap regions. The walls serve as the two surfaces that the loop adheres to and as a means of facilitating compression and retraction.

After a film was carefully inserted between the plates such that it had equal contact with each plate and a semi-circular bend in the gap between the plates, Figure 18, the compression cycle was started. During the compression cycle one plate was moved by a controlled step size and constant speed closer to the other plate which remained stationary. Compressing the film increased the curvature of the bent region of film. Force changes were measured with corresponding distance changes for a representation of the work done as bend curvature was increased. Video was recorded during the process that was used to measure loop height and bend radius using a particle tracking program[77].

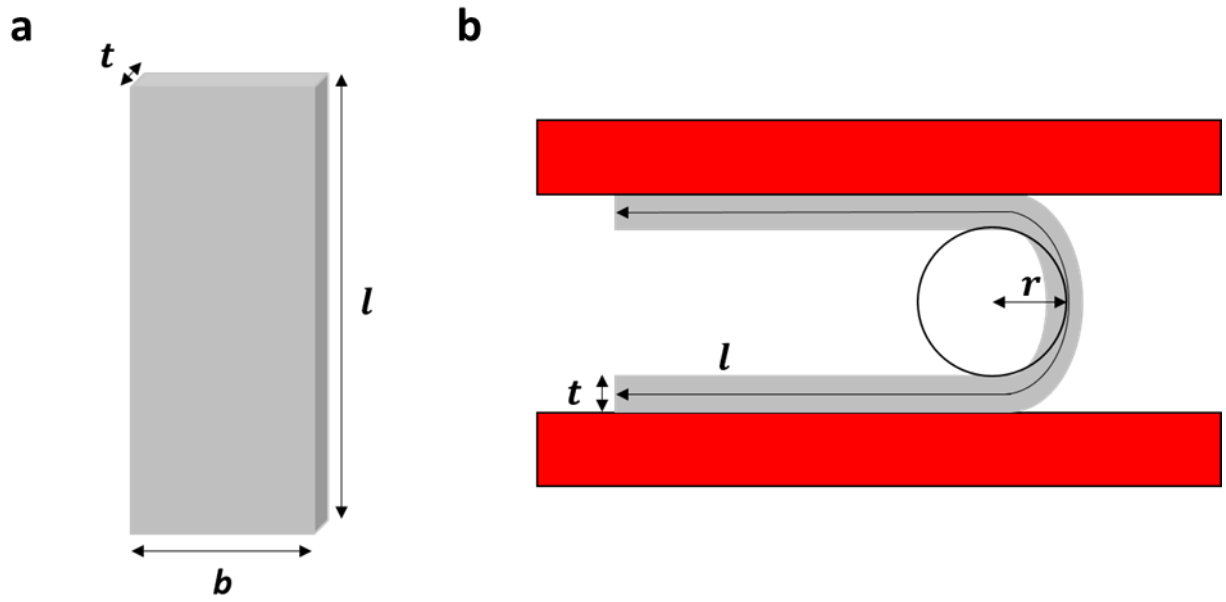

Figure 18. a. Measurements of polymer strip dimensions prior to insertion into apparatus (b.). b. a strip in the apparatus. Note the rounded semicircular bend of radius, r.

The experimental apparatus constructed on the large scale is shown in Figure 19. The two plates used were glass slides; the stationary plate was attached to a Denver instruments scale while the mobile plate was attached to an actuating Newport Motion Controller Model ESP 301 motor. Mirrors were set up to reflect a view of the scale measurement within the focal area of the Pixelink 954000025 camera capturing the experiment. A Tamron CCTV telescoping lens was attached to the camera to improve the clarity and brightness of the picture captured by PixeLINK software. A ruler was also in frame to serve as a scale reference for data processing. This experiment was also carried out on a smaller scale on a confocal microscope using a nanoindenter motor.

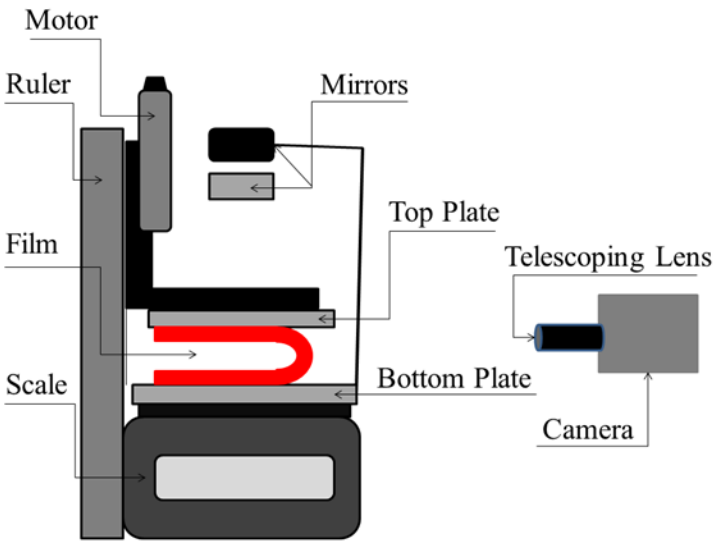

Figure 19. The in air large scale experimental apparatus set up for bending a thin film between two plates: scale, actuating motor, mirrors, and camera position.

Polymeric sample strips were prepared from PC, PS, and PDMS[90] of different cross-linker ratios. Different crosslink ratios of elastomer to curing agent of 10:1, 20:1, 30:1, 40:1, 45:1, and 50:1. These different ratios produced different crosslink density films that had different modulus and adhesive properties. Films were made in a variety of thicknesses from microns to millimeters using the previously mentioned methods of spincoating, flowcoating, and dropcasting.

Once film was loaded into apparatus as shown in Figure 20 with slight bent curve an actuating motor was moved at a constant slow speed down until film was compressed a certain distance, Figure 21. The motor was then moved up to either the start distance or a point above the desired start point in order to facilitate debonding Figure 22. The motor was set to the same speed for both up and down movements. A speed of 0.00851 mm/s was used for most experiments chosen as it was suitably slow to avoid unwanted mechanical instability and due to video capture equipment considerations. Video was taken of both compression and retraction. Plates were cleaned with acetone between experiments.

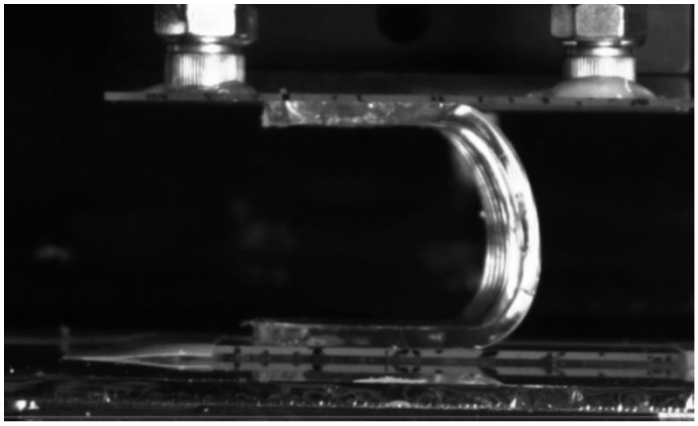

Figure 20. A picture of a strip of thin film placed between the two plates in apparatus. Thicker film was chosen for enhanced visibility. Sample shown is 2.64 mm thick 40:1 PDMS.

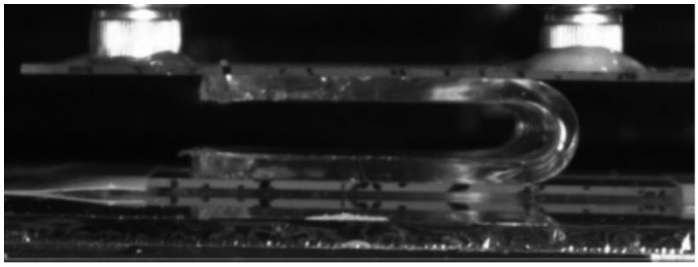

Figure 21. A picture of a strip of thin film placed between the two plates in apparatus at a point of high compression, low plate separation. Thicker film was chosen for enhanced visibility. Sample shown is 2.64 mm thick 40:1 PDMS.

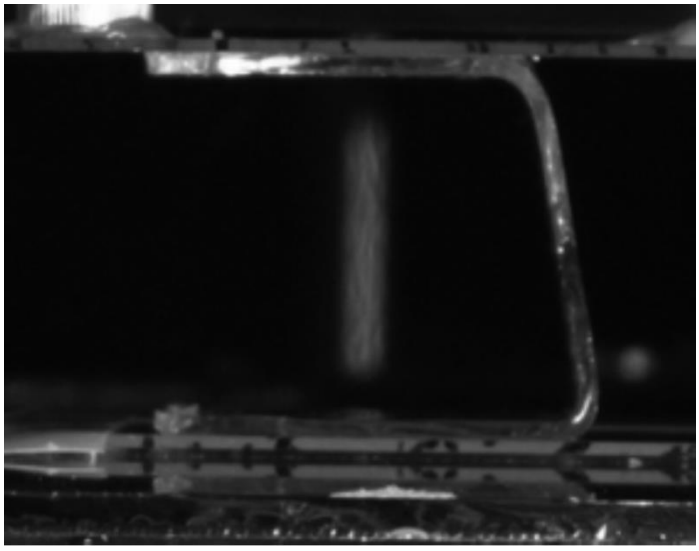

Figure 22. A picture of a strip of thin film placed between the two plates in apparatus at a point of retraction where the film is in peel. Notice the square like appearance of the film where the free part of the film is at approximately ~90° to the two glass plates. A thicker film was chosen for enhanced visibility (in this case, the film is 1.40 mm thick 40:1 PDMS).

Plate distance and force measurements were graphed as force-distance curves. Force-distance curves were examined for commonality of trends. These trends were then used in conjunction with models to create a mathematical representation of the changes in the tape loop shape at each step of indention and retraction.

2.3. Model

In order to properly describe the system in mathematical terms we used several different models. Initially we used a scaling model involving a critical length in the system around which the behavior changes. While it describes well the forces attributable to the work being done it does not give insight into the shape of the system at all points in a cycle. As one of our main interests was the stability of the tape loop system in multiple configurations we then turned to a model that accounts fully for the shape, the sticky elastica model. Below we outline our models and discuss the conditions of each.

2.3.1. Scaling

Initial modeling was constructed using an elastocapillary length as the lengthscale of relevance to the tape loop system. Above and below this length, the system changes into one of two regimes. We identified the relevant elastocapillary length as:

$$\ell_{ec} = \sqrt{B/\Delta\gamma} \tag{48}$$

where B is the bending modulus from Eqn. 44, and $\Delta\gamma$ is the work of adhesion[91]. Two behavior regimes are expected as H goes below ℓ_{ec} in compression and above ℓ_{ec} during retraction, where H is the distance between the two confining plates in the experiment.

The first regime, $H > \ell_{ec}$, has the system unconfined, bending is not dominant in the total energy of the system and can be ignored. In order for the inextensible tape loop to accommodate increase in H an amount of area $b\delta H$ has to open along the interface, b is width

and δH is the change in length equal to the change in plate distance. The opening of a new contact area requires a work done of $F\delta H$. The energy balance of the area opening to the work being done is the tensile value $F \sim \Delta\gamma b$, the same as a 90° peel-test.

The second regime, where $H < \ell_{ec}$, the system is highly confined and strongly bent. Bending dominates adhesion in this state, and so adhesion can be ignored. The energy balance between the bending and work in this regime is $F = \pi B b / H^2$ a compressive force that follows 'adhesion free' bending results for this regime[78].

The two limits suggest that rescaling distances by ℓ_{ec} and forces by $\Delta\gamma B$ will describe a universal behavior of the tape loop system. This scaling predicts a single force-displacement curve which for $H < \ell_{ec}$ scales as $F \sim H^{-2}$ and for $H > \ell_{ec}$ force approaches a constant value of -1 asymptotically.

2.3.2. Sticky Elastica

Scaling gave a universal force-displacement curve for the tape loop system, however, it does not give the detailed shape of the tape loop. An additional model was needed for the calculation of both loop shape and full force-displacement curve directly. We adapted the 'Sticky Elastica' model to the geometry of the tape loop for consideration of the full system energy. This method of analysis has the advantage of boundary conditions with incorporated material specific details of the loop with the surfaces. Importantly, we note that the curvature of the film at the point of contact with the plate is influenced by adhesion, which may not be obvious from simple scaling arguments.

The Sticky Elastica model begins with the free energy of the system. The system is initially a straight piece of film with width b of length L with ends touching two plates separated by distance H, Figure 23 a). Initially $L = H$. As the plates move closer together by an amount

δL the gap between the plates becomes $L - \delta L$ and the film will start to cover some of each plate with a length equal to $L - \ell/2$. Equal contact between the two parallel plates up to a point $\ell/2$ leaves a central curved area between the plates free of contact, denoted by the curvilinear coordinates s and θ, Figure 23 b). The coordinate θ is the angle of the curve at a point and is measured in a positive direction from a line perpendicular to the plates at that point. The coordinate s follows the contour of the film. The free region has a length of ℓ.

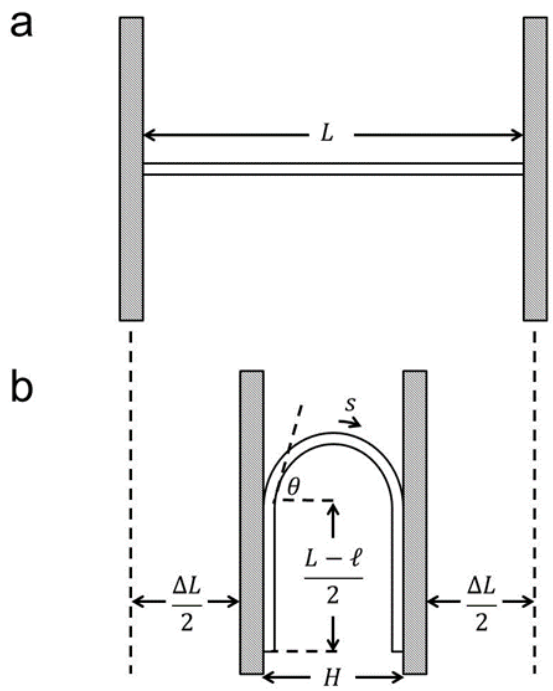

Figure 23. The film for our energy modeling starts straight with both ends touching a plate of a distance L apart a). As the plates compress b) more film is in contact with the plates and a curvature appears in the film section between the two plates.

$\theta(s)$ is thus the function which describes the position of the sheet. Of course, the film also cannot pass through the plates and is thus bound in the region between them. Symmetry suggests that we can place the origin in the center of the free part of the film, and using this coordinate system the boundary conditions can be established as $\theta(\ell/2) = -\pi/2$ and $\theta(-\ell/2) = \pi/2$. Further, due to the symmetry of the system it can be inferred that $\theta(0) = 0$.

The free energy of the entire sheet can then be given as:

$$U = \int_{-\ell/2}^{\ell/2} \left[\frac{B}{2}(\theta')^2 + \Delta\gamma\right] ds - L\Delta\gamma - \alpha\left(L - \Delta L - \int_{-\ell/2}^{\ell/2} cos(\theta) ds\right) \quad (49)$$

where $\Delta\gamma$ is the work of adhesion, $\theta' = d\theta/ds$ which describes the angle made between a segment of film and the plate through a line normal to the plate as a function of position s along the plate, α is a Lagrangian multiplier maintaining the inextensibility constant as the film is not stretching[92, 93]. The Lagrange multiplier physically has units of force per unit of width of the film. The term $-L\Delta\gamma$ is the energy scaling based on the total dimension of the film, the length multiplied by the work of adhesion, the force required to propagate a crack between the film and substrate opening contact area. We assumed no shear or stretching in the film and have thus omitted the additional terms. The symmetry of the system allows us to change the limits resulting in

$$U = 2\int_0^{\ell/2} \left[\frac{B}{2}(\theta')^2 + \Delta\gamma\right] ds - L\Delta\gamma - \alpha\left(L - \Delta L - \int_{-\ell/2}^{\ell/2} cos(\theta) ds\right). \quad (50)$$

In order to minimize the equation to identify a minimal curve, $\theta(s)$ we need to conduct variations of the curve shape, $\theta(s)$, the free length ℓ, and the multiplier α as they change simultaneously as noted by Wagner and Vella. The minimization yields a differential equation:

$$\theta'' = -(\alpha/B) sin(\theta). \quad (51)$$

This equation can be integrated once to give:

$$\theta' = \sqrt{2(P/B)cos(\theta) + c_1}, \quad (52)$$

where c_1 is a constant of integration. We have also made the substitution $\alpha = P$.

The minimization of Eqn 52 above yields a boundary condition:

$$\theta'(\ell/2) = \sqrt{(2\Delta\gamma)/B} = \left(\sqrt{2}/\ell_{ec}\right). \quad (53)$$

This means that the adhesion of the film changes the curvature at the point of contact between the film and the surface it is adhered to. This boundary condition means that c_1 must equal $(2\Delta\gamma)/B$ which can then be substituted into Eqn 52. The differential equation can then be solved with the help of the Jacobi Elliptical Integral functions. We find:

$$\theta(s) = 2am\left(\sqrt{\frac{P+\Delta\gamma}{2B}}, \sqrt{\frac{2}{1+\Delta\gamma/P}}\right), \tag{54}$$

where am is the Jacobi Amplitude Function. From this solution we can determine the length of the free region of film,

$$\frac{\ell}{2} = F\left(-\frac{\pi}{4}, \sqrt{\frac{2}{1+\Delta\gamma/P}}\right)\sqrt{\frac{2B}{P+\Delta\gamma}}, \tag{55}$$

where F represents the elliptic integral of the first kind. This result is the same one reached by Majidi in a previous work[93].

2.4. Results and Discussion

Films of PDMS weight ratios 10:1, 20:1, 30:1, 40:1, 45:1, and 50:1 elastomer base: curing agent were measured in our apparatus. Different ratios produced different crosslink densities leading to different bending moduli. Larger ratios formed elastomers with lower crosslink density. Less crosslinked samples were softer (lower modulus) and interacted more strongly with surfaces. We expected higher adhesion from these softer less crosslinked films.

Tape loops of 10:1 PDMS samples were identical to those done in previous bending research[78]. Low hysteresis and adhesion was observed for samples in the thickness range previously studied, Figure 24. This was anticipated and served as a control for comparison to softer more adhesive samples. Hysteresis for 10:1 PDMS samples was more evident at thicknesses of ~1.5 mm and below (Figure 24 and 25), and appeared to increase as samples became thinner. The hysteresis of thinner samples of 10:1 PDMS is thought to be due to a

combination of decreased bending modulus for thinner films and fixed adhesive interaction magnitude. A range of 10:1 thicknesses below 1.20 mm have smaller forces upon compression than those of their thicker counterparts.

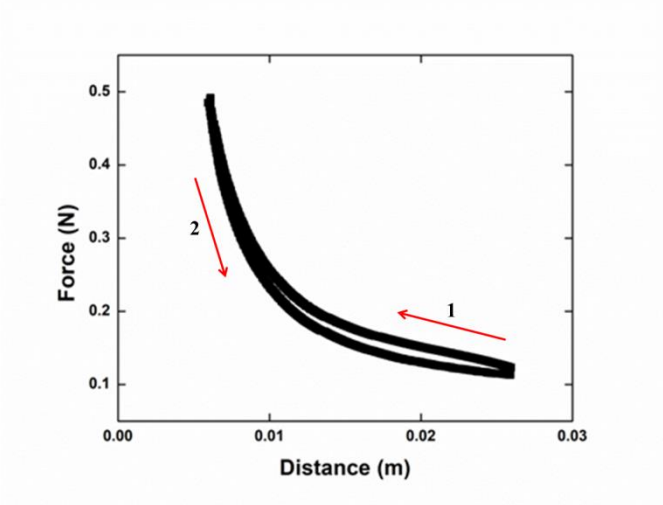

Figure 24. A force-distance graph of a 1.00 mm thick sample of 10:1 PDMS with length of the strip was 81.78 mm and width of 69.19 mm. Notice the small hysteresis between compression and retraction curves.

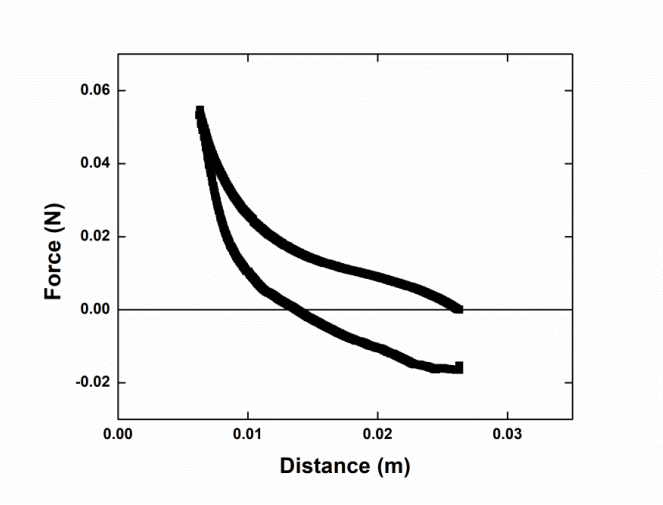

Figure 25. A force-distance graph of a 0.72 mm thick sample of 10:1 PDMS with length of 80.50 mm and width of 67.27 mm. Notice the hysteresis between compression and retraction as the curve goes below zero force.

Lower crosslink density samples had increasingly larger hysteresis, even for thicker samples, as seen in Figure 26 which shows hysteresis force-distance graph of 20:1 PDMS film

and Figure 27 which shows a 40:1 PDMS force-distance curve. The shape of the retraction curve for the 20:1 PDMS sample appears almost parallel to the indentation curve. At lower crosslinking the retraction curve dips down progressively lower.

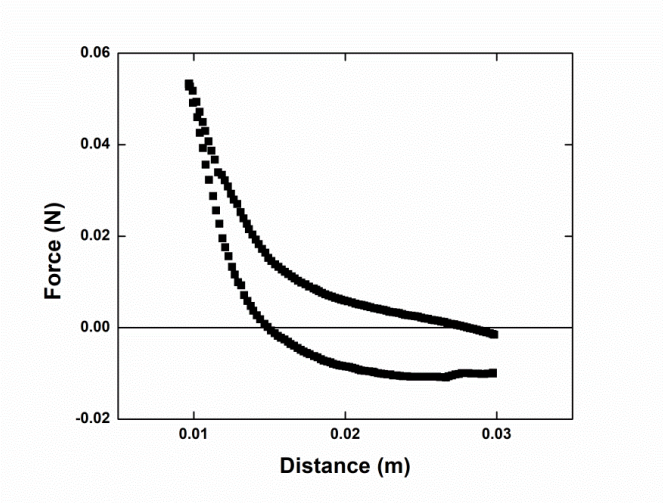

Figure 26. A representative 20:1 PDMS film. Film dimensions are length 80.36 mm, width 26.08 mm, and thickness 1.15 mm.

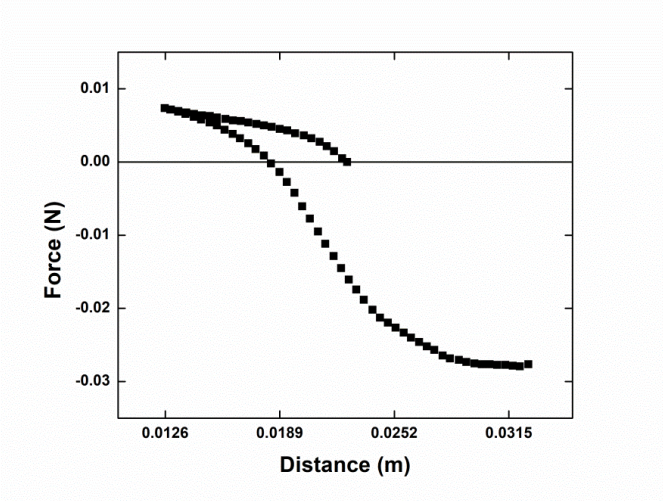

Figure 27. A representative 40:1 PDMS film. Film dimensions are length 81.35 mm, width 27.09 mm, and thickness 1.38 mm.

In order to properly model the entire cycle of the compression and contraction curve we need to examine the entire cycle. As mentioned, samples for thicker 10:1 PDMS and other non-adhesive samples formed complete cycles that remained above zero forces and aligned with each

other without hysteretic separation along the bending curve. The complete cycle for an adhesive sample does not follow the same curve Figure 28 represents a more complete cycle. The graph was adjusted slightly from raw data in in order to ensure forces are close to zero aiding in comparing different samples to each other. At the beginning of the cycle, force grows positively during compression, becomes negative and plateaus during retraction for a significant distance before the cycle is repeated. This cycle is repeatable, the same sample can be put through the experiment multiple times and produce the same cycle behavior through the different points of compression and retraction.

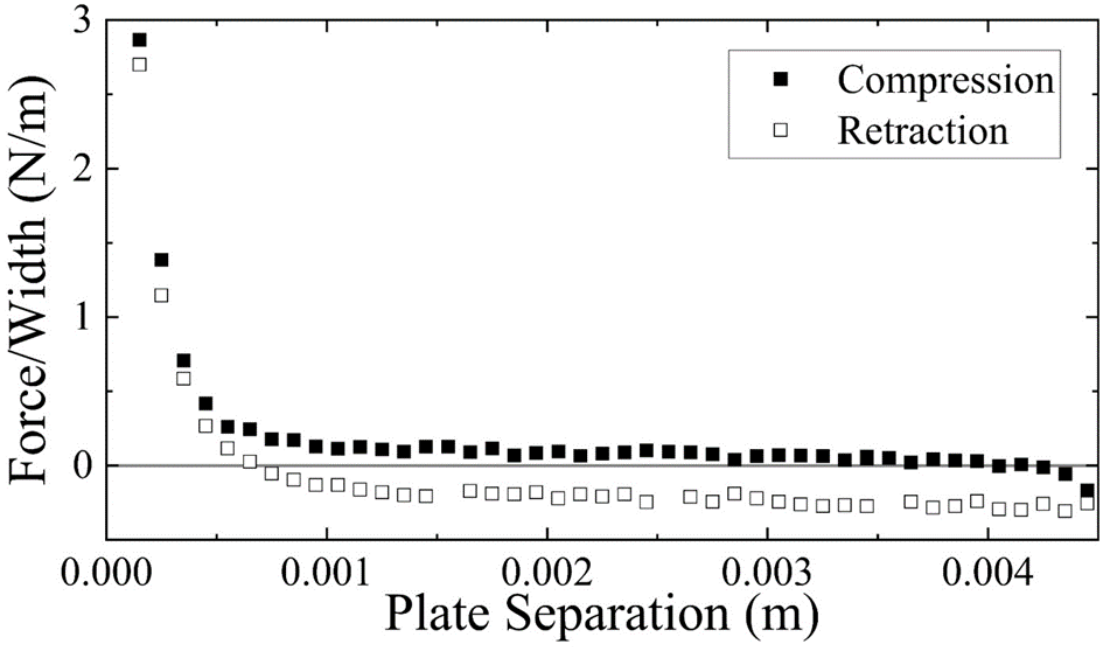

Figure 28. A standard curve for tape loop compression and retraction experiment on a 10:1 PDMS strip of thickness 56.4 mm. Force has been divided by width to get initial forces close to zero and allow for simpler comparison with other samples. Note the increasing force of the compression curve and the fast drop below zero of the retraction curve. Below a certain force the retraction curve plateaus.

As the plate separation increased from the point of maximum indentation, the adhesive force pulling on both sides of the film caused increased curvature near the contact point between the film and the plate on each plate. As separation increased further the section of film between

the plates became highly curved at the contact point and nearly flat between the two contact points (see Figure 29). As plates separated further and peel continued beyond this point the curvature at the contact points did not change significantly, a roughly constant 90° angle between the free and adhered parts of the film justifying use of Eqn 33. We assume equal sections of film were peeled on both sides due to symmetric geometry.

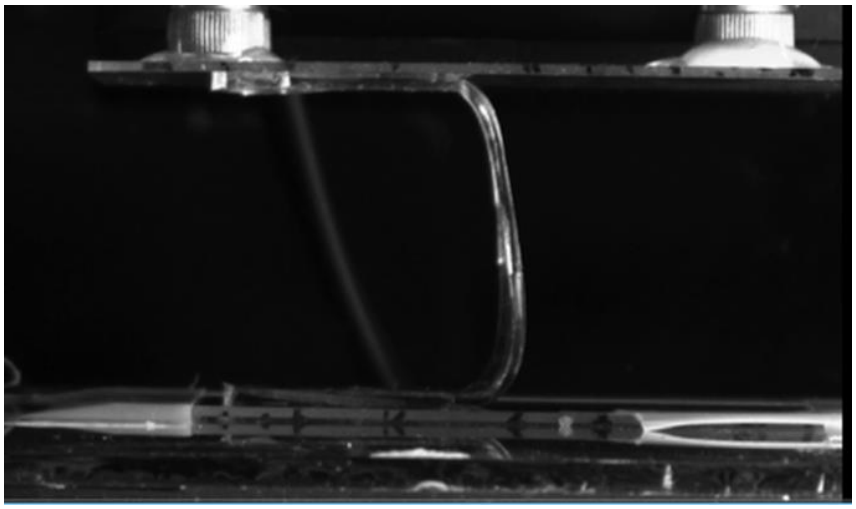

Figure 29. 1.13 mm thick PDMS film of 30:1 at increased plate separation distance; note curvature increase near the plates and film is nearly straight between them.

2.4.1. Limiting Behavior

The analytic solutions allow for discussion of limiting behavior. Limiting behavior is the force behavior of the system at different points of interest in the cycle, notably, where force is at or below zero. The limiting condition of the asymptotic increase in force, $P \to \infty$, during compression will not be discussed here as it has been discussed in a previous work as the product of bending. The limits of force below zero and at zero are discussed below as they are factors of the adhesion and elastocapillary length of the tape loop.

As H increases past the elastocapillary length and grows larger the force goes to zero then negative. After the initial curve into negative force from positive the negative curve then flattens out and the system reduces to peel, as shown in Figure 28. The crossing point at $P = 0$ is of

interest as it depends on film properties. Since the elastocapillary length depends on the properties of the film we pursued if the reverse was also true, the measurement at this limit can give insight into the film properties.

When compression was stopped at any point in the experiment where $H < \ell_{ec}$ in the pull off portion of the experiment at some point force passes through $P = 0$ as it goes from negative to positive. This point has a unique solution which can be found by integrating Eqn. 51 twice to yield a shape function of $\theta(s) = a_1 s + a_2$. Setting the boundary conditions of θ at $s = 0$ and $s = \ell/2$ we can determine the values of the variables a_1 and a_2 to be 0 and $-\pi/\ell$ respectively.

The solution to the amplitude Jacoby elliptical integral function becomes:

$$\theta(s) = 2am\left(\sqrt{\frac{\alpha - P}{\frac{\Delta\gamma}{2}}}\frac{s}{\ell_{ec}}, \sqrt{\frac{2}{1 + \frac{\Delta\gamma}{\alpha - P}}}\right) \tag{56}$$

which can be used to find the limits. At $P = 0$ the plate distance results in the film being in equilibrium.

During retraction as the force approaches 0, $P > 0$ the limit of Eqn. 54 goes to $\theta = \sqrt{2/\ell_{ec}}$. From geometry $\theta' = 2/H$ which gives:

$$H = \sqrt{\frac{2B}{\Delta\gamma}} = \frac{\sqrt{2}}{\ell_{ec}} \tag{57}$$

which is an interesting result as it is a simple equation where the only additional input is plate separation. Meaning the adhesive qualities of a film can be measured by use of a ruler.

2.4.2. Zero Friction, Zero Force Apparatus

An additional apparatus was created to isolate and quantify our experimental tape loops at the point of zero load. Designed, built and run by Tim Twohig, the apparatus, Figure 30,

colloquially referred to as “Tim’s boat” is a horizontal apparatus with two glass plates; like the vertical apparatus one plate is stationary while the other plate is mobile. The stationary plate is fixed to a pole while the mobile plate is fixed to a “boat”. The boat, a 3-D printed container, rests on the top surface of water. The boat on the water enables the mobile plate to move freely as friction is negligible between the boat and substrate below the water surface (depth is typically several centimeters). A counterbalance weight is added to the boat to compensate for the weight holding the stationary plate.

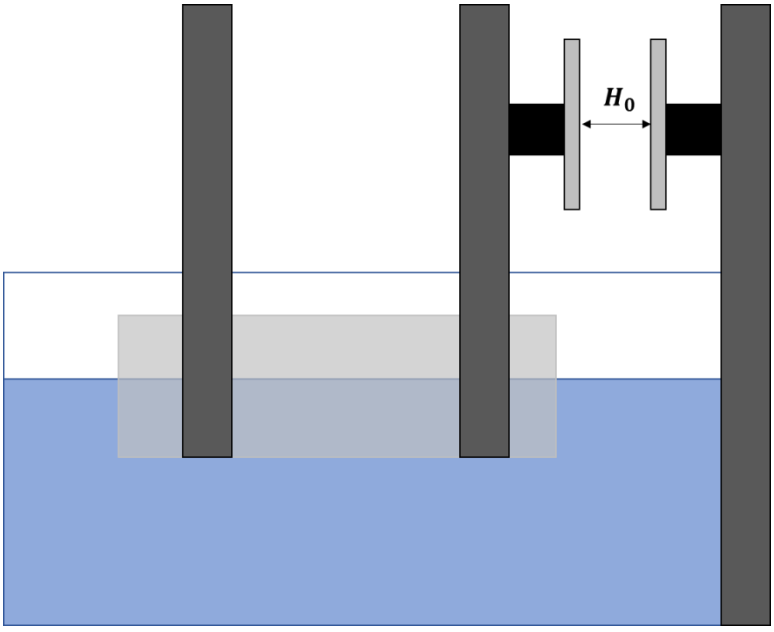

Figure 30. Zero friction zero force apparatus, “Tim Boat”. A plate is attached to a pole standing in flat floating “boat”, this plate is mobile and can move over the water surface to reach film equilibrium. The “boat” contains a counter balance weight. The second plate is stationary and fixed to a pole that is also fixed in place.

Here films were cut into two approximately equal strips. The strips were measured prior to insertion into apparatus for dimensions of length, width, and thickness. Both strips were inserted into the apparatus as mentioned previously with the end along the plate facing toward the center of the plates a small distance from each other and the bends facing outward to create a

symmetrical disconnected loop, Figure 31. The loop is not a continuous connected loop for the same reasons as previously mentioned, in order to avoid a doubly overlapped region.

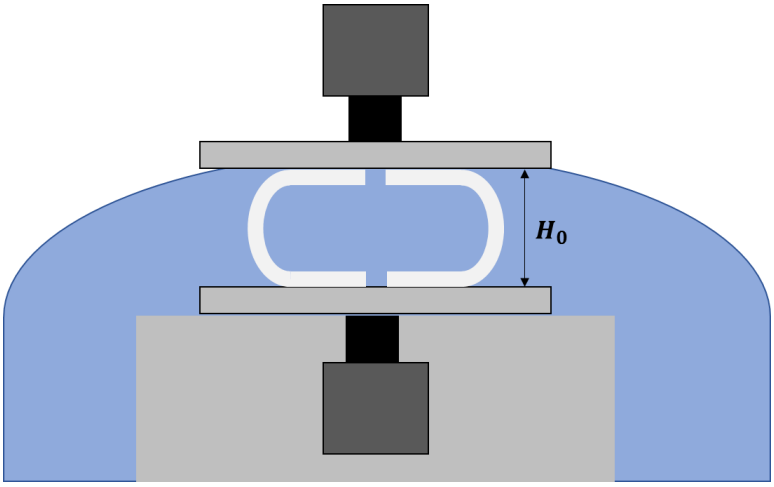

Figure 31. Schematic showing the tape loops in the "boat" apparatus.

Once both strips were placed along the plates the experiment was started. The mobile plate was moved by hand to a separation that was less than the elastocapillary length of the film loops. The elastocapillary length is the length where the surface energy of a bend is the same as the elastic energy, above and below this length are dominated by different energies. The loops were compressed for a short span of time prior to release of the mobile plate. The system was then allowed to relax to equilibrium. After sufficient relaxation time pictures were taken and H_0, the equilibrium plate separation was measured with image processing software.

2.4.3. Compression Discussion

During compression a curve that follows the "pure bending" limit prediction is seen in our experimental results. While compression data in adhesion experiments often shows smaller adhesion values than pull-off data, we note that we observe zero influence of adhesion upon compression. To examine why the compression curve differs from the retraction curve we examine the interfacial crack stability.

First we need to know how the 'crack' propagates along the interface. We start by looking at the energy of a crack propagating along the interface, simplifying Eqn 49 by placing the mechanical energy into a new term, the energy release rate G:

$$dU = (G - \Delta\gamma)dA. \tag{58}$$

The change in energy dU is a product of the change in area dA dictated by the energy release rate G and the change in the interfacial energy $\Delta\gamma$. From this equation a virtual crack closing by dA can be imagined. If $G = \Delta\gamma$ the system is at equilibrium the system energy is zero and the crack has no incentive to open or close along the surface. If $G < \Delta\gamma$ there is an energetic cost to opening the crack (decreasing the contact area); closing the crack will reduce the free energy. If $G > \Delta\gamma$ the free energy is reduced by opening the crack; increasing the surface to air and adhesive to air interfaces. In short, crack will only open and propagate if $G > \Delta\gamma$ otherwise the crack closes or remains stationary.

In our experiment, the tape loop is confined between the two moving plates, which are held fixed. This restriction is known as a fixed grip condition and means that the total mechanical energy, U_m, can be written as:

$$U_m = 2\int_0^{\ell/2}\left[\frac{B}{2}\left(\theta'(s)\right)^2\right]ds. \tag{59}$$

as no work is done by fixed plates, and all that remains is bending. The energy release rate is defined as:

$$G = \frac{dU_m}{dA}. \tag{60}$$

Which in our case is:

$$G = 2\int_0^{\ell/2}\left[(\propto -P)cos\left(\theta(s)\right) + \Delta\gamma\right]ds = -\Delta\gamma. \tag{61}$$

In other words, the film should increase contact with the wall. However, if we examine the second areal derivative of free energy, we find:

$$\frac{dG}{dA} = -\frac{1}{b}\frac{dU_m}{d\ell} = 0 \tag{62}$$

where $d\ell$ is the change in length of the film along the wall and b is film width. This means that the film is marginally stable. If dG/dA were less than zero than the crack would be able to propagate.

The crack is said to be marginally stable as it cannot close or open along the surface unless the plates are moved (as in peel). This stability of the crack has consequences for the system such as the observed hysteresis. If the system starts far from the free energy minimum, it cannot move the crack to find equilibrium.

The internal forces on the film can be seen in Figure 32. During plate separation where P is the negative normal force of the plate on the film, α is the internal forces in a segment of film, and $\Delta\gamma$ is the work of adhesion. In this state the work of adhesion opposes the work done by the plates as it propagates the crack to peel the film away from the surface. Without adhesion, (Figure 32 c), the internal film forces balance with the work of the plates must be simply, $P = \alpha$ and the differential equation (Eqn 54) becomes:

$$\theta^{"}(s) = 0. \tag{63}$$

The solution is a circle. The system starts far from the minimal state, but cannot propagate the interfacial crack to reach it. Essentially ℓ is no longer a minimizable quantity, the adhesion boundary condition does not occur, and adhesion only enters the free energy as a constant.

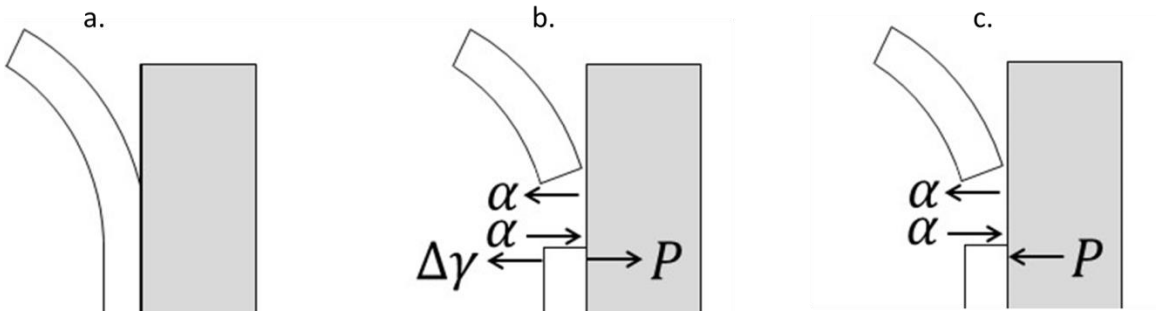

Figure 32. Force balances on the film as shown in a), in b) the force of adhesion is present as the plates separate, in c) adhesion appears absent as the plates compress.

2.4.4. Application of Models

As mentioned previously the indentation curves from compression were well fit to the model used in our previous experiments on bending[78] shown as Model I in Figure 33. As the desired goal is a complete representation of the cycle using elastica models we modeled this part using zero adhesion or circular elastic, Model II, which overlays Model I in Figure 33. For the retraction curve which did not fit Model I or Model II we used a Sticky Elastica model shown as Model III in Figure 33, where it is also well fit to our data.

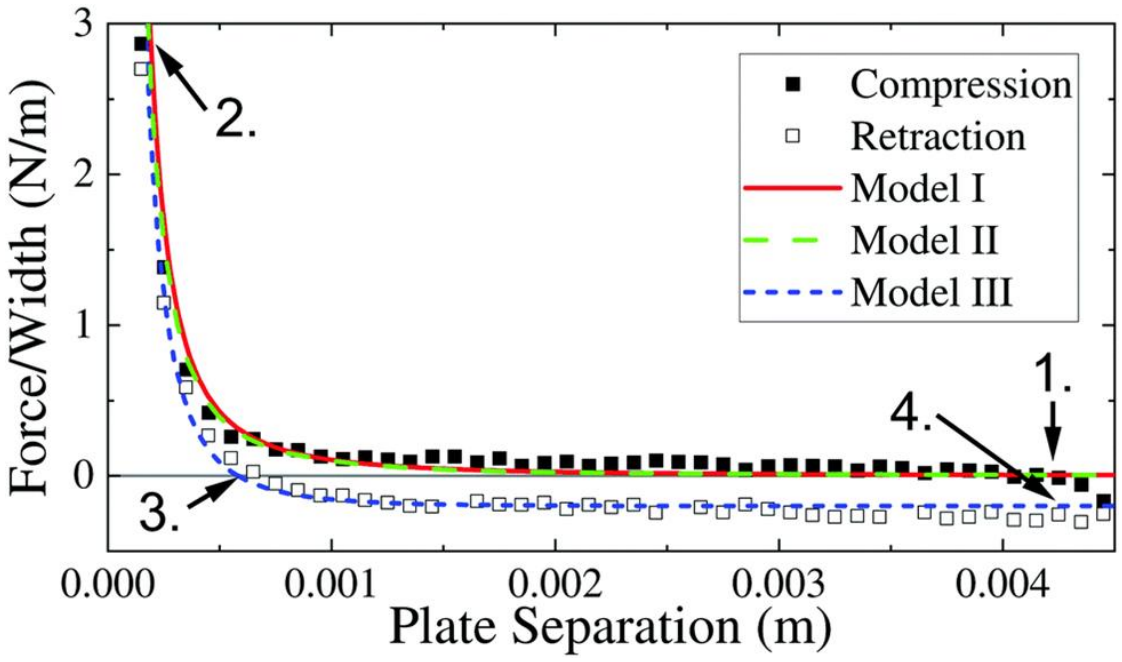

Figure 33. Models used to fit experimental data. Model I is the bending model from previous work. Model II is the zero adhesion Elastica model. Model III is the sticky Elastica model. Notice how well fit Model I and Model II are to compression data while Model III is well fit to retraction data.

Model III encompasses the initial drop in force to zero as well as the further drop in force accompanying adhesion and the subsequent plateau region. The sticky elastica is able to model this change in force as it takes into account the forces of adhesion along the length of the film and the curvature difference between the compression cycle and the retraction cycle when adhesion is present. The adhesion affects the forces by introducing a tensile stress that pulls at the plates equal to the amount of force needed to open and propagate the crack between the two surfaces, Eqn. 50. As it accounts for the changes simultaneously, as stated previously, it accounts for the changes that do not conform to a simple bending equation. Model III is well fit to our data.

2.4.5. Limit of $P = 0$

The point where $P = 0$ was examined with the low friction "Tim's Boat" apparatus using 10:1 PDMS of a variety of thicknesses. In the experiment each film arrives at its natural

equilibrium point, approximately that of the elastocapillary length. Figure 34 shows the equilibrium plate separation, H_0, as a function of the independently measured bending modulus. In addition, the plate separation at zero load could be extracted from all cycle experiments in both the microscale and macroscale experiments. All data correlated well to the trend line predicted by Eqn 57, showing it is valid across multiple length scales. For clarity, we fit the data with the general square root power law $H_0 = cB^{0.5}$, where c is a constant, which yielded a value for the work of adhesion of $\Delta\gamma = 0.15 \pm 0.1\,{}^{N}/_{m}$, in good agreement with the average value of work of adhesion measured in directly fitting force-displacement curves.

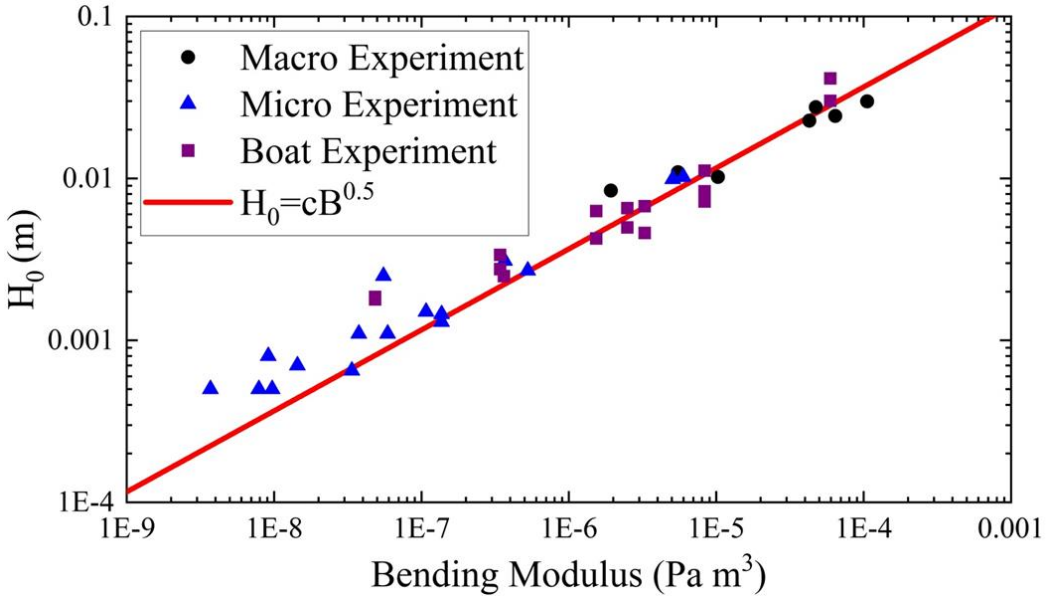

Figure 34. Zero friction boat experiment displaying the plate distance, H_0, of each film tested compared to the zero force point of previous experiments.

2.4.6. Shape

After confirming that models of Euler Elastica fit well to all points, we turned our attention back to shape. In order to determine the success of our model to show the entire cycle of forces and shape occurring in the tape loop cycle we need to compare them. To do this comparison we carried out cataloging the curves of the free film in experiments done using

confocal microscopy. The confocal curves were then overlaid with elastic fits as shown in Figure 35 in red.

We see that the elastomer shows a significant change in conformation between compression and retraction curves. After loading the film has a gentle circular curve. As the plates move closer together the curvature becomes larger. The bend in the film goes from the circular bending shape to the almost rectangular shape it assumes during peel. This shape difference can be mathematically represented by the change in curvature along the contact points of the film to the top plate. When the curvature in the free area of film is high and rounded the areas of film along the plates are of low curvature. As the plates pull apart the free area of film becomes lower in curvature until it is essentially flat, as this occurs the sections connected to the plates increase in curvature.

At the end of the compression cycle there is a small length, high curvature bend in the film Fig 35 a). As the plates separate the free film grows and curvature falls slightly. Further plate separation results in shapes with high curvature near the plates and long flattened regions between Fig 35 b).

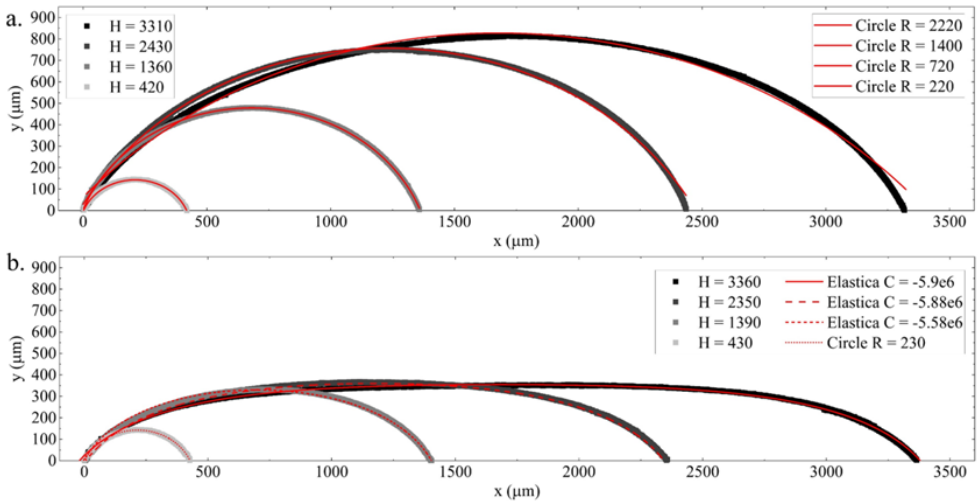

Figure 35. Compression and retraction shapes of film measured on confocal. Actual data points fall off some from the red fit lines due to gravity, a parameter not incorporated into the model.

The compression data curves are fit with the Model II which corresponds to Euler's Elastic with zero adhesion (rectangular elastica). The retraction curves are fit by varying $\Delta\gamma$ in Eqn. 54. The Elastica fits well to all stages of the curve. Deviations in the fit are attributable to gravity which slightly distorts the film in less constrained plate separations.

2.4.7. Measurement of PDMS

The data gathered provided information that allowed us to characterize the bending modulus and adhesion for the different ratios of PDMS films. Much as in the low adhesion single bend experiments (Section 1.5.1) indent curves allowed the measurement of modulus values as compression was insensitive to the adhesion of the system. Here, the G_c values were obtained through applying peel equations to each experiment, or through fitting Model III. The modulus and G_C of different ratios of PDMS are shown in Figure 36. Interestingly they show an inversely proportional trend with modulus decreasing at larger ratios while adhesion increases at large ratios. This is consistent with expectations that samples of PDMS with lower crosslink density are more compliant and tackier.

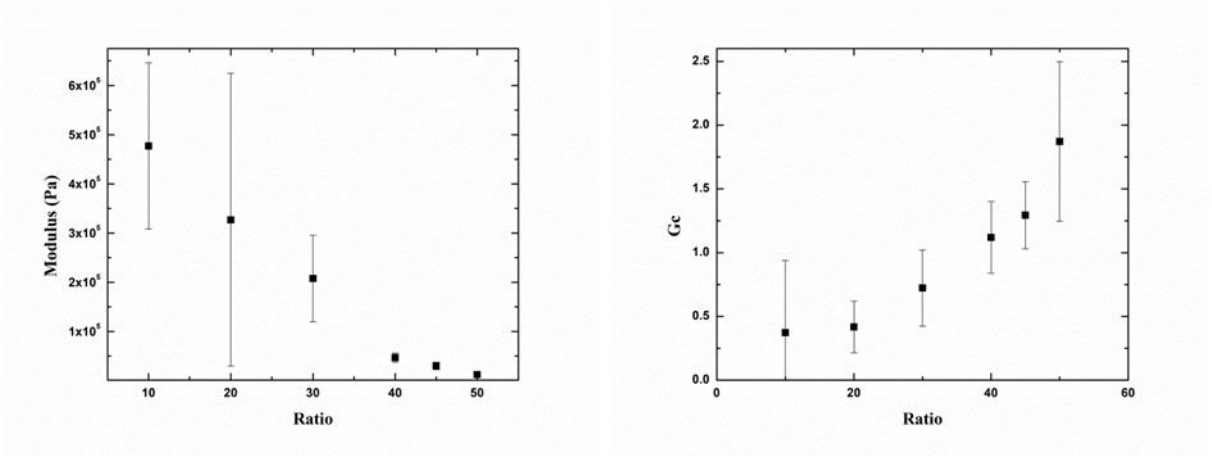

Figure 36. Graphs of the crosslink ratio compared to the modulus and G_C respectfully. Notice the inversely proportional trends. Error bars are included due to slight variations across multiple samples.

2.5. Conclusion

The tape loop investigation yielded models for the compression, retraction cycle, the shape, and conditions at the different boundaries. These models allowed us to measure trends between the crosslink density of Sylgard 184 and both modulus and work of adhesion. Specifically we find an inverse trend between modulus and crosslink density.

We could verify the work of adhesion directly by considering a scaling argument for the long distance force displacement plateau as a 90° peel experiment. This was found to agree with our more sophisticated model.

The compression part of the cycle is insensitive to adhesion and well fit by the scaling model derived in previous research with non-adhesive films. The retraction cycle is sensitive to adhesion. The hysteresis of the cycle between retraction and contraction is explained by the interfacial crack's stability.

Through examination of limits in the elastic model we determined that $P = 0$ is a particularly useful limit. Here, the plate separation is found to directly relate to the work of adhesion. Using an experimental method involving a friction free floating apparatus we were able to establish that the mathematical equation simplified from the Elastica is valid.

3. CRUMPLE ADHESION

3.1. Introduction

Adhesion on rough surfaces requires a balance of compliance and contact surface area. Even small amounts of surface roughness have been shown to lead to decohesion. Adhesion is even harder on surfaces with roughness at different hierarchies of length scale as even if the adhesive bonds well to lower hierarchy levels, it must deform around higher levels and store elastic energy. One can think of this elastic energy as a force resisting adhesion[94]. Lower compliance materials experience increased stress as they elastically deform around such obstacles[95]. Once the load pushing the high compliance adhesive into the rough surface is removed the built up elastic energy can contribute to debonding/peeling[95].

Size and spacing affect adhesion as well; with larger more numerous obstacles being harder for adhesives to effectively overcome the compressive forces caused by their deformation[94]. Higher elastic modulus films take less force to remove from rough surfaces as the roughness structures move closer together. The force to pull off a low elastic modulus film is decreased on those with higher roughness. Low modulus adhesives that require hardening on or drying after being placed on a surface also have a disadvantage as shrinkage during this step can result in debonding[96].

We sought to answer the question: can an adhesive made up of a low compliance inextensible sheet in a crumple geometry have advantages over corresponding flat thin film sheet adhesives, solid adhesives, or liquid (curable) adhesives on rough surfaces. The basis of our idea was rooted in the attempt to engineer an adhesive capable of making a high degree of surface area contact with a surface that has a hierarchy of length scales. The crumple was chosen due to its complexity – it is made up of structures on a variety of random lengthscales. In this chapter

we will outline experiments carried out to determine peak forces needed to separate crumples from surfaces of varied, but idealized, roughness.

3.2. Materials and Methods

3.2.1. Materials

PDMS films were made as described in previous chapters, Sections 1.6.1, 1.6.2, and 2.2. To directly explore the adhesive component, we make stickier PDMS crumples by altering the crosslink ratios as was done with the adhesive strips described in Figure 36 and in Section 2.2. PDMS ratios used were 10:1, 15:1, 30:1, 40:1, 45:1, and 50:1, as the lower ratios 10:1 and 20:1 had no pull off force they were not considered useful in the crumple experiments. This was in keeping with lower ratio PDMS yielding lower adhesion in the tape loop measurement experiments, and the current experiment could not detect any overall adhesion with these samples.

3.2.2. Methods

Two plate mechanical compression and retraction tests were carried out on crumples of the representative material PDMS in different crosslink ratios: 10:1, 15:1, 30:1, 40:1, 45:1, and 50:1. A film was cut into a square or rectangular sheet. Dimensions of each sheet were measured except thickness in the case of low modulus films, prior to crumpling. Low modulus film thickness was measured with confocal microscopy after experiments in order to preserve the integrity of the sample (e.g. cleanliness of the surfaces) for experiments. Each sheet was compressed from the outside in by a gloved hand until a roughly spherical crumple was formed (Figure 37). Due to the method of crumple formation, exact internal structures were random; to our knowledge no two crumples were identical.

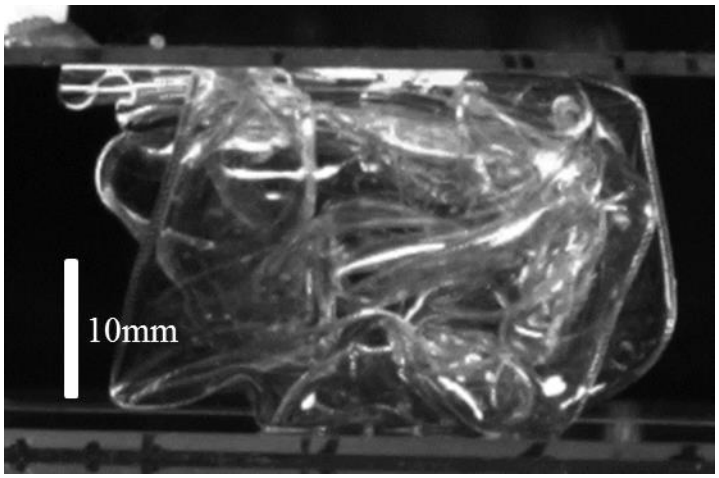

Figure 37. Example of a crumple of 10:1 PDMS used in experiments. The PDMS sheet had a thickness of 0.34 mm, length of 81.39 mm, and width 37.12 mm.

Formed crumples were placed onto clean glass slides in the large or small scale apparatus mentioned previously. The crumple was pressed into one of the plates while the other plate was moved until the crumple touched sufficiently to established contact area for adhesion with minimal compression, Figure 38. The plates were then moved to compress the crumple to a predetermined distance at a set speed. Once the plates achieved compression the plates were moved in retraction at the same set speed in a distance excess of the start position in order to have one plate completely separate from the crumple. This complete separation gives a full force-separation curve with a minimum force that can be used to determine the peak force needed to separate the crumple from the plate.

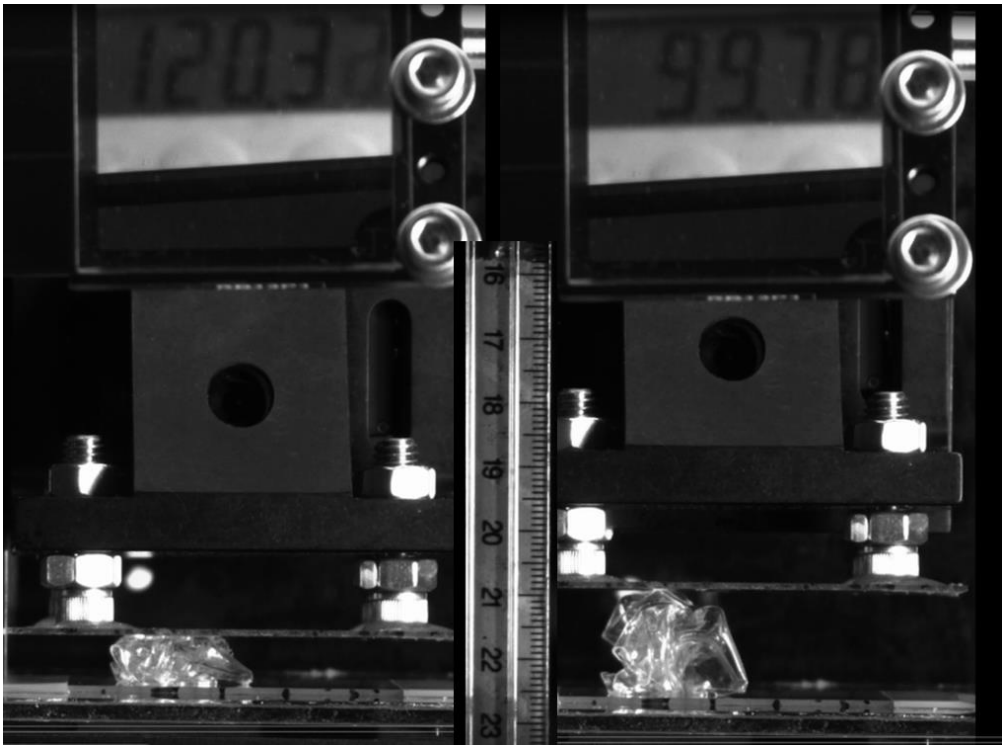

Figure 38. Crumple in an experiment. Left picture shows crumple after being placed into apparatus and compressed to add load and surface contact while the right picture shows plate separation.

Initially crumple samples were tested with repetition using smooth glass plates on the top and bottom sides of the experiment. Following initial crumple experiments on smooth glass plates, idealized roughness was added to bottom plates to test our hypothesis that crumples have improved adhesion on rough surfaces. The idealized roughness was one capillary or two capillary tubes laid flat and secured centrally to the plate aligned parallel to the shortest sides. The two capillary tube plate had a spacing of one capillary tube distance separating them from each other. Capillary tubes used were Kimble Chase Geresheimer borosilicate glass with an outer diameter between 1.5-1.8 mm.

In order to test if gravity influenced which side of the crumple separated completely a top plate with roughness was added to the experiment. Two rough top plates were made in the same

way as the bottom plates with one and two capillary tubes, respectively. Rough top plate experiments were carried out with the opposite bottom plate being smooth.

Crumple samples were each tested three times in succession with variation of either the top or bottom slide roughness while the other slide was a smooth non-rough slide. The order of slide roughness was varied from experiment to experiment in order to not have order be a factor. The three experiments (smooth, 1 tube, 2 tubes) were done in succession on the same sample.

Videos were taken of compression and retraction cycles. The videos were analyzed for forces and distances using particle tracking software. This data was compiled into force-distance curves for each experiment. Samples tested with all three roughness slides were compared to each other.

3.3. Results and Discussion

3.3.1. Model

The crumple is a different geometry than the tape loop so is not directly comparable to a peel test. Therefore, the force curves cannot be interpreted in the same manner. However, as stated above, the geometry takes on a roughly cylindrical shape when compressed and might be treated similarly to a probe tack test. Equations 31 for the probe tack test might be a suitable starting point for a model. To use this equation, however, an effective modulus will need to be used in place of the material modulus as a crumple being a complex structure containing air does not have the same modulus as a solid column of material would.

The crumple being structurally different is not directly measuring adhesion, however, the peak force should be related to G_C, but measurements might be influenced by other factors. The adhesion of crumples, therefore, might be better described by the area of the hysteresis curve below the experimental zero than by the minimum force. This approach should take into account

other factors contributing to the measurement besides G_C which is an oversimplification for such a complex system on a rough surface.

JKR is common test to perform for adhesive systems. As the crumple is initially a spherical shape JKR analysis could provide values that relate to G_C. The main difference would be that the value would be a combination of multiple forces. Peak force might be important as an indicator for comparison of the performance of the crumples, however. Analyzing a crumple in instances where both plates are smooth and comparing those results to the results of idealized rough surfaces could provide an indicator if there is a significant difference between the adhesion of the crumple based on substrate roughness.

A hint to the behaviour might be found in the relationship between the contact radius and the overall crumple radius. The slopes of the contact radius vs the displacement (δ) value for crumples are so far irregular. In a general JKR experiment initially the radius of the contact circle increases rapidly from a small point of contact into a larger circle as the distance is decreased and it and the substrate are pushed together. As compression continues between the sphere and substrate from increased displacement the material begins to resist further spreading, smaller increases in radius, before achieving a maximum radius of contact. No consistent trend was observed. Results varied, most had different slopes as seen in Figure 39 including: linear slopes, step-like slopes, or slopes that appear opposite to the anticipated. More analysis remains to be done as the change in radius differs on the dynamic crumple.

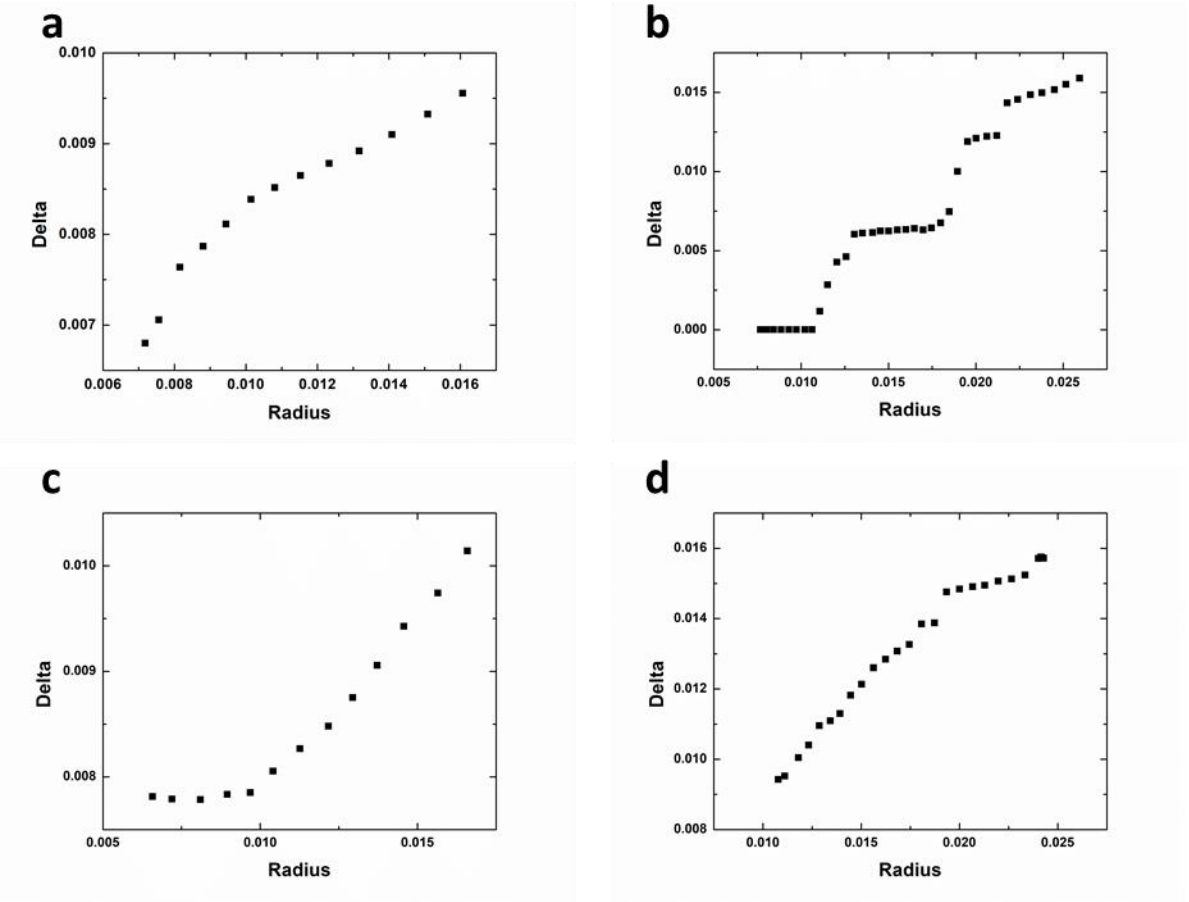

Figure 39. JKR analysis of $a = \sqrt{R\delta}$ where a is the contact radius along the y axis, δ is the indentation step along the x-axis and R is the radius of the sphere. As can be seen in these four examples the slope for a crumple, a dynamic structure, varies.

For current purposes we are primarily comparing the performance of the crumple on smooth or idealized rough surfaces. Detailed analysis of crumple adhesion would be insightful, but is not necessary for this goal. Due to the complex geometry two different metrics – the peak force and the total work done in a cycle – will be used to determine performance.

3.3.2. Force-Displacement Cycles

Figure 40 shows a typical compression and retraction cycle for a crumpled PDMS sheet. The crumple starts at some nonzero force as it experiences load from its initial confinement between the two glass plates and additionally due to the weight of the film (the force sensor is

below the sample, typically we remove the weight before considering measurements). As the plates are compressed the force rises with a slope that follows a power-law, $F = F_0 H^{-\alpha}$, Eqn. 26 as can be seen from the trend line added in Figure 41. The force increases monotonically to some maximum force obtained at small plate separation. Keep in mind that plate distance was a bit smaller for rough samples in places due to the volume of the obstacles resulting in higher local compressive forces. As the plates separated the forces dropped quickly to zero and then below zero until hitting some peak tensile force (a minimum force), after which the tensile force decreases in magnitude. The compression cycles shown in Fig 40 and 41 shows a hysteretic energy loss from the work of adhesion needed to separate the crumple from the plate.

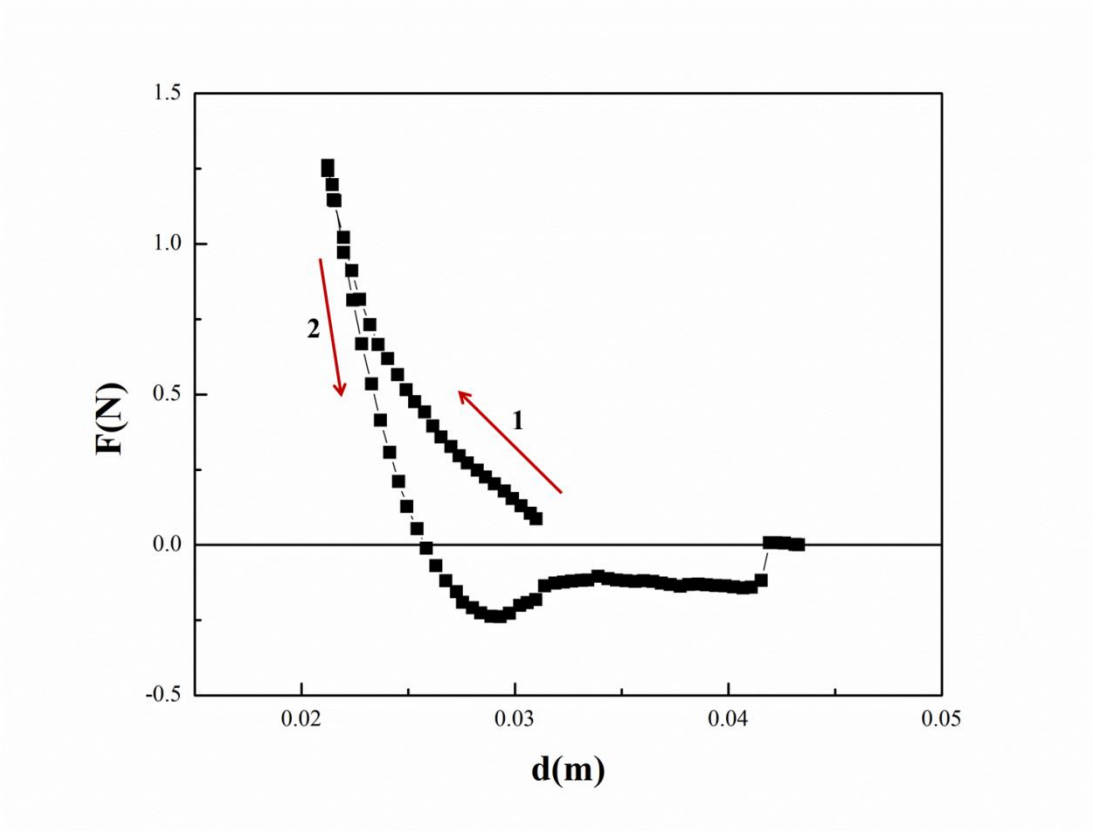

Figure 40. A force vs. separation graph of a 40:1 PDMS crumple between two plates, forward and receding curves. Notice the hysteretic loss due to adhesion and the clear drop of forces to zero as the sample completely separates from the substrate. Dimensions of the sheet of PDMS are thickness of 3.25 mm, length of 82.11 mm, and width of 81.89 mm. The radius of the crumple was 2.48 mm on average during compression.

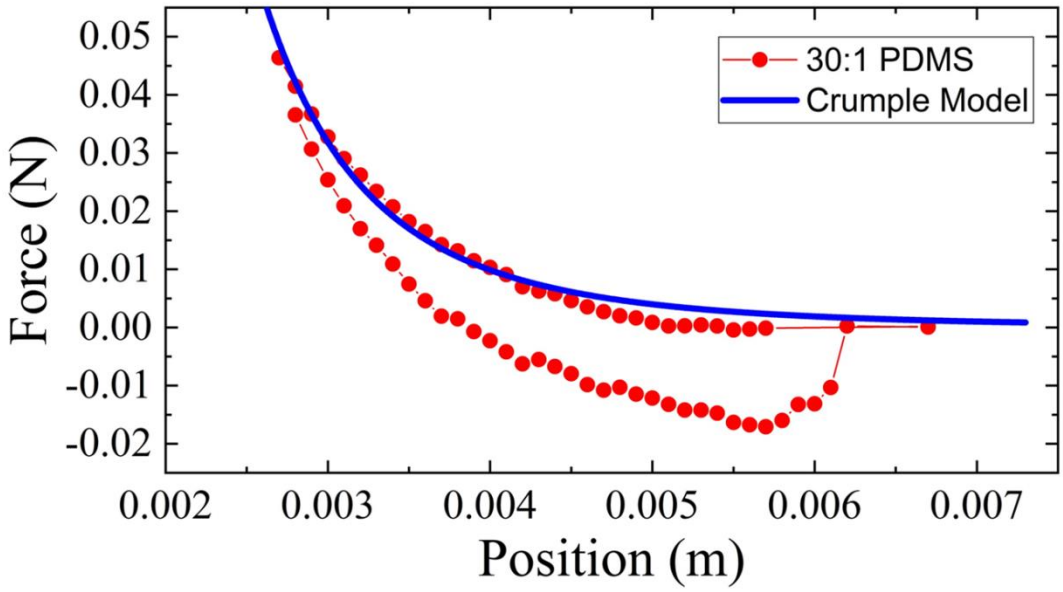

Figure 41. A 30:1 PDMS sample. Note the fit of the crumple model trend line in blue. Values of trend line were F_0 of 1.91E-12 N and α of 4.06. The crumple dimensions were thickness of 2.32E-5 m, length of 44.3 mm, width of 43.9 mm, and an average radius of 0.0122 mm.

When no load or confinement was applied to crumples they tended to undergo dynamic rearrangements and opening, especially in cases of higher modulus, lower adhesion, and thicker films. The rise in forces back to zero does not necessarily follow the same curve every time. Curves can have a smooth sharp tensile peak, an elongated plateau, or decreases in tension that appear as steps. In this way, the hysteresis of the crumple differs notably from that of the tape loop. The tape looped reached a negative value and plateaued as long as there remained film attached to the plates that could be peeled off. Crumples are dynamic, complex shapes which tend to shift during retraction as the confining force is decreased, especially prevalent in less tacky or thicker samples. The evenness of crumple pull off from each plate varied by sample with some being about equal while others pulled more quickly off of one plate versus another, this can be attributed to randomness. In short, statistical or average behavior must be considered.

Hysteresis varied depending on PDMS ratio, Figure 42, with our experiments showing that 50:1 PDMS had the highest adhesion similar to the tape loop experiment. Samples of 10:1

PDMS still showed hysteresis even though they have smaller energy release rates in general. Not all films crumpled films showed hysteresis. Figure 43 shows a 15:1 and a 40:1 PDMS sample that all did not show much hysteresis. This might be attributed to other factors besides crosslink density such as thickness, asymmetry of thickness, or potential contamination. The 15:1 PDMS has the highest forces comparative to other samples which might be attributable to sample thickness. Samples below 20:1 ratio did not often show negative (tensile) forces and so are not considered further in our adhesive crumple discussion.

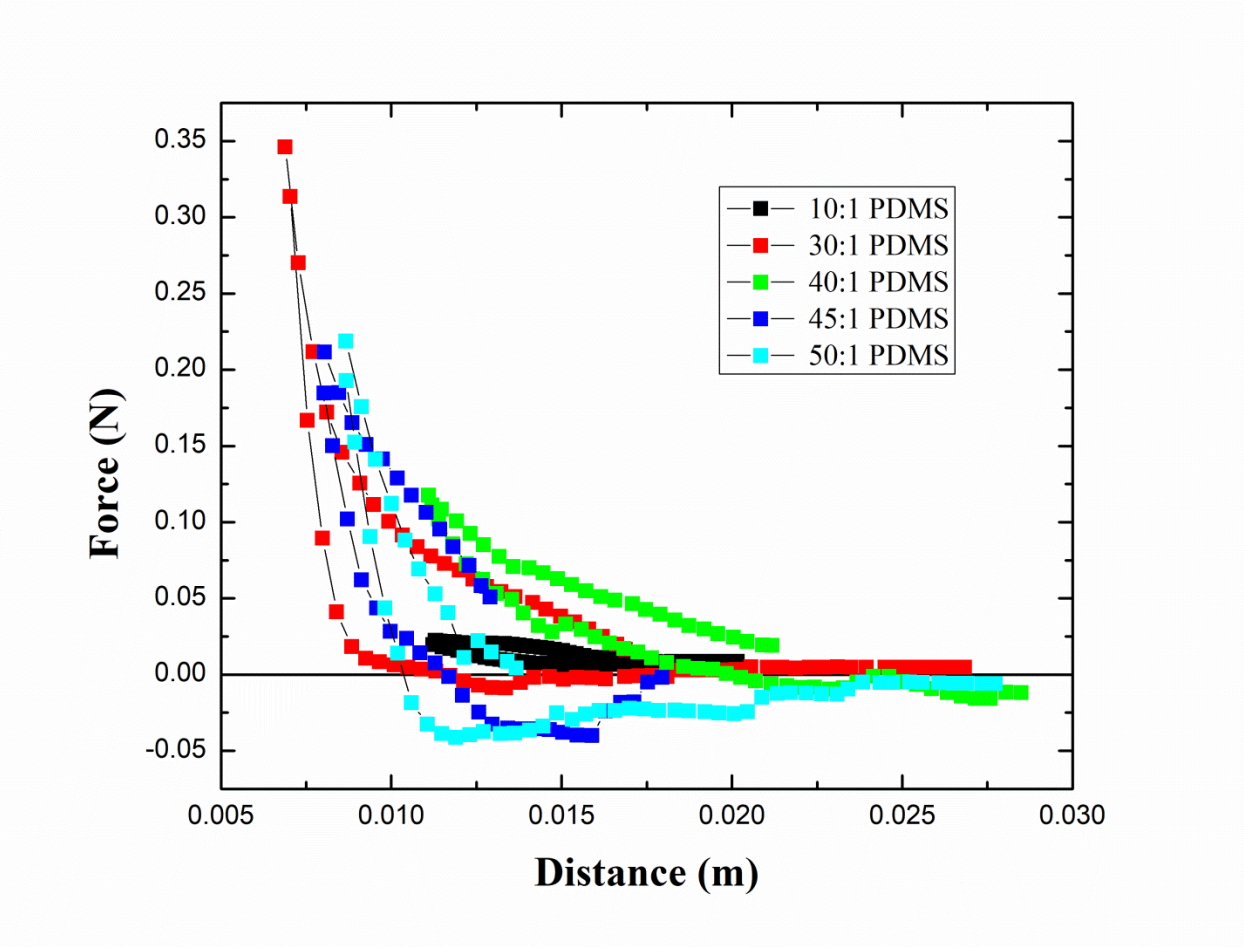

Figure 42. Crumple ratios of tested samples of different crosslink ratios. Note the increase in hysteresis as the crosslink density decreases at higher ratios.

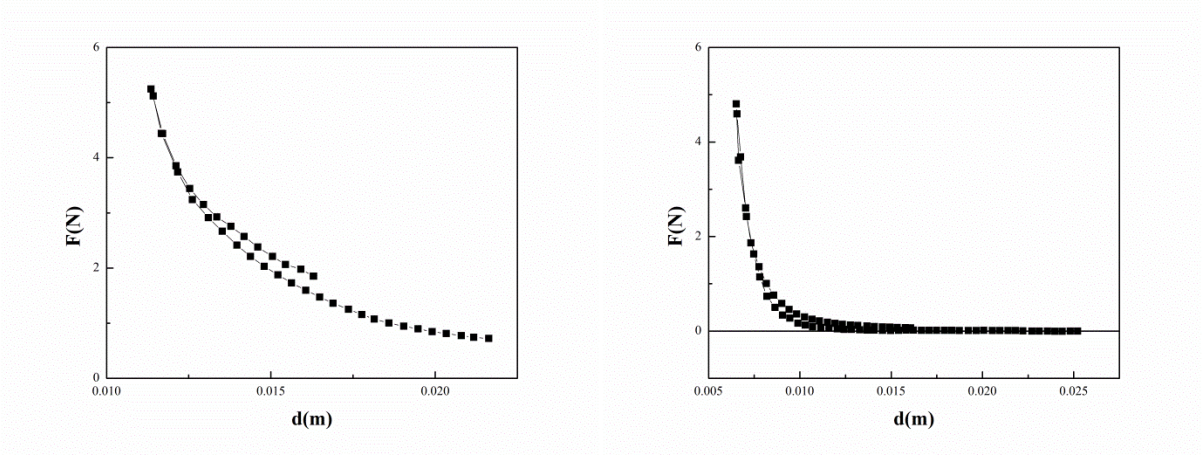

Figure 43. Low hysteresis in crumpled adhesive films samples on the left a 15:1 PDMS sample and on the right a 40:1 PDMS sample. The 15:1 PDMS film had dimensions of thickness 1.19 mm (averaged), length of 80.98 mm, and width of 75.47 mm with the average crumple radius in compression being 23.65 mm. The 40:1 PDMS sample had film dimensions of 0.569 mm thickness, 54.49 mm length, and 53.32 mm width with an average radius of 14.52 mm.

After experiments with crumpled PDMS films and flat plates we then added the roughness component. Plates were change for a variety of roughness on the top plate or the bottom plate respectively. Both the top and bottom plate were made rough to account for gravity effects. No experiments were carried out on samples with roughness on the top and the bottom concurrently. All three roughnesses in an experiment can be seen in Figure 44.

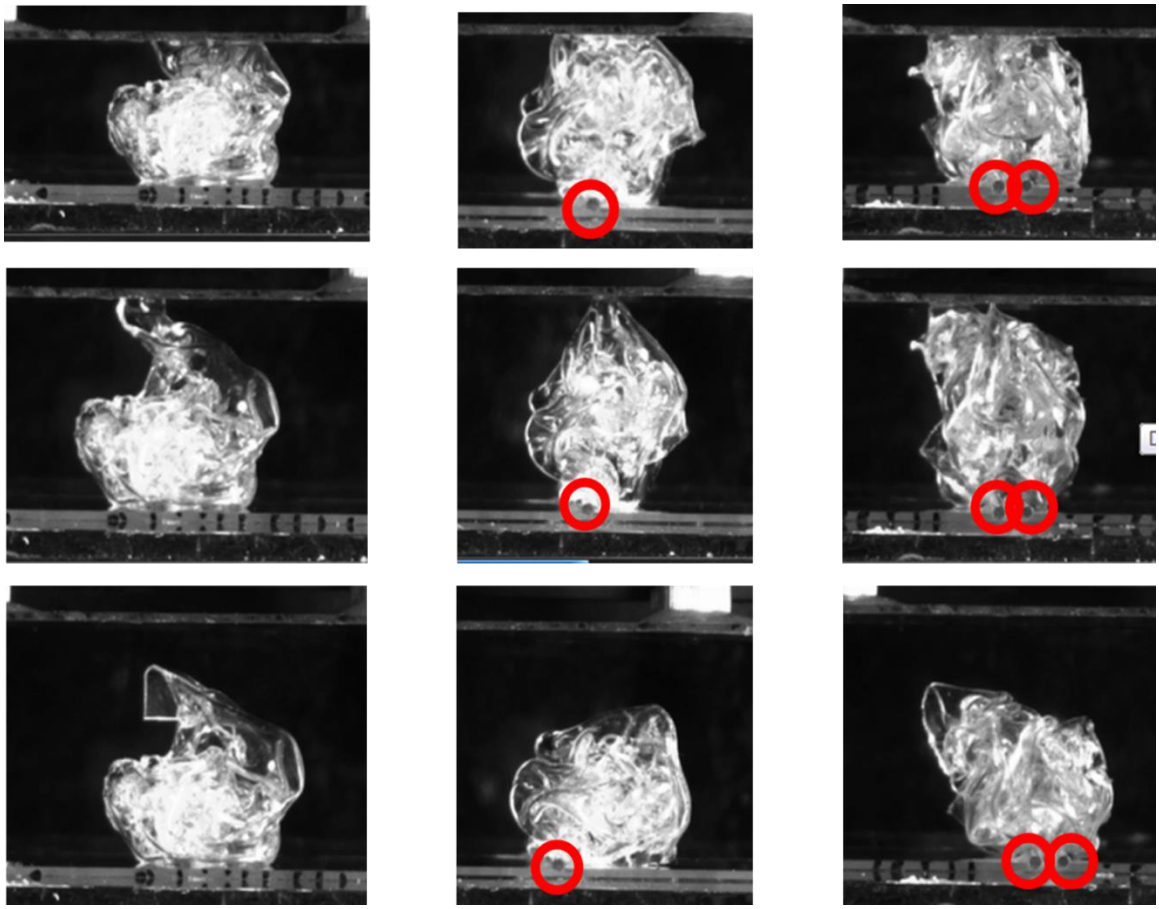

Figure 44. PDMS experiments at different points of the retraction cycle on all three bottom plate roughnesses. Note how there is not much difference in the separation and all remained on the bottom plate even for samples with roughness. All three experiments were done using the same 50:1 PDMS film with dimensions of 0.483 mm thickness, 54.04 mm length, and 54.01 mm width, the average radius of the crumples was 12.01 mm, 10.96 mm, and 12.76 mm, respectively.

Visually, there was no discernable difference between samples on smooth or rough surfaces. Roughness did not dictate which side would start to debond first or which side would debond fully. Figure 44 shows how all three roughness samples remained attached to the rough bottom plate and debonded from the smooth glass plate on the top. This was also true in some samples where roughness was on the top, adherence to the top or bottom plate occurred for all variations of the experiment with no recognizable pattern. The plate the crumple was pressed

into before compression also did not dictate which plate the film would remain attached to. This supports the idea that the crumple is adhering well to the rough surface.

Investigation into the surface contact of the crumple further supports the crumple's indifference to these rough surfaces. Pictures taken using laser scanning confocal microscopy to determine the contact area are shown in Figure 45. Here the dark grey sections are the contact region, the dark black line at the bottom of the right picture is the obstacle, and the lines running across are the laser interfering with itself. Both show patchy irregular contact areas much like the contact splitting seen in organisms such as spiders[97, 98]. Contact splitting is a set of beneficial effects found in fibrillary and other small contact adhesives in large numbers as it has reduced strain from peel and on rough surfaces and uniform stress and adhesion on each contact point[99]. This patchy contact area is not surprising due to the different scales of structures of a crumple. The surface area does not appear to decrease even in the presence of the obstacle. Due to the complexity of the crumple the contact area of a crumple is also complex and warrants more detailed, quantitative study.

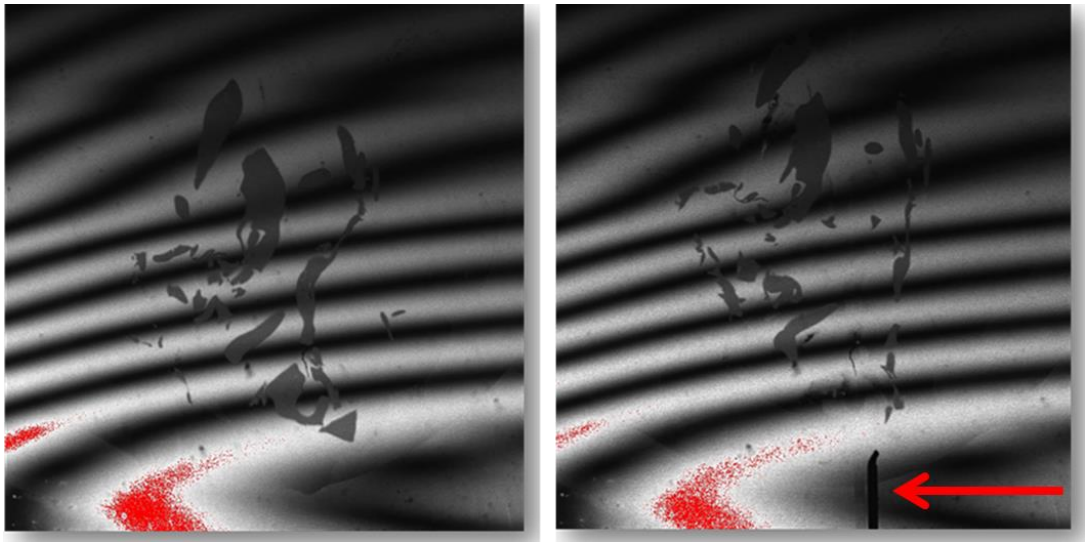

Figure 45. Contact area as shown on a confocal microscope image. The contact points are the dark grey. Lines of black, white, and red are laser interference. The red arrow points to the surface roughness below the sample on the right.

Comparison of force curves, peak forces, and work done also showed the trend visually observed in experiments and contact areas. Data shown in Figure 46 through 50 highlights the indistinguishable curves for films of various crosslinker ratio. There was no significant difference between the crumples on the smooth plates and those on the rough plates.

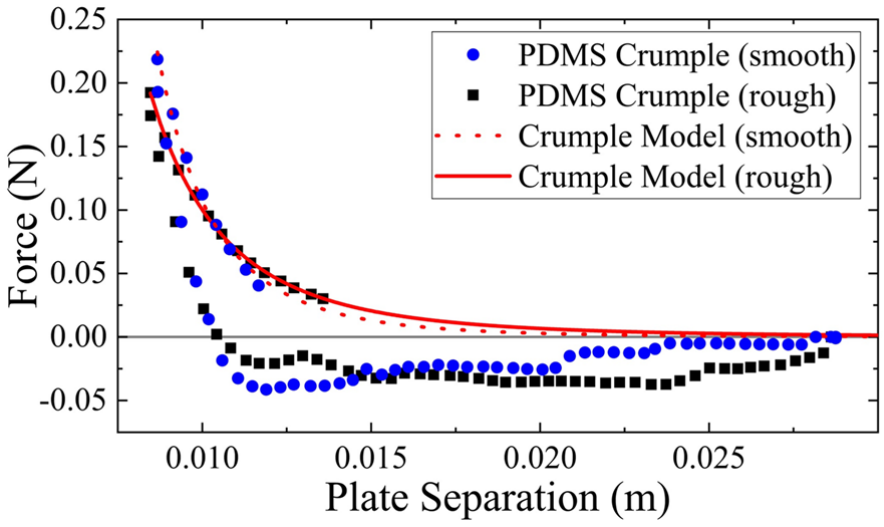

Figure 46. Crumples on a rough surface and a smooth surface. Note how closely they overlap. Also shown are the fits of the crumples model to each.

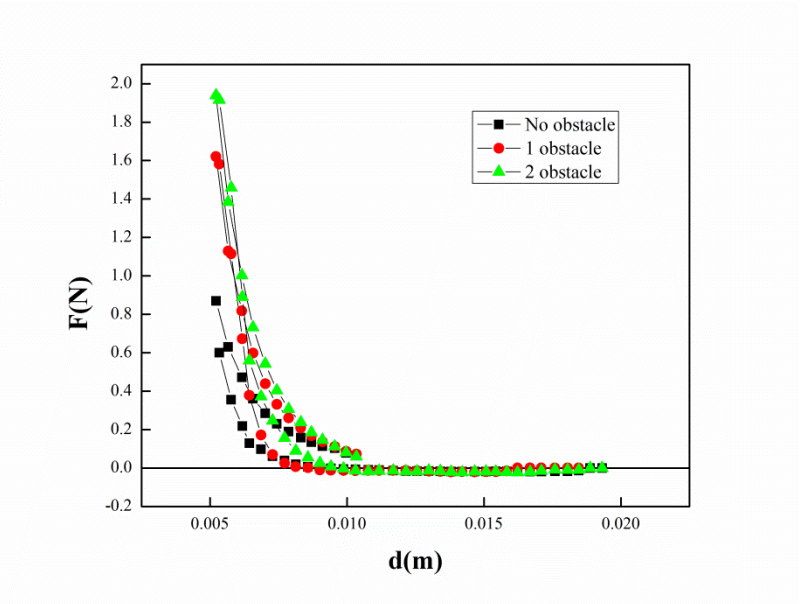

Figure 47. A single 30:1 Sample of PDMS run through all three roughnesses consecutively Film dimensions were 0.576 mm thick, 53.67 mm length, and 53.12 mm width with average crumple radii of 10.17 mm, 14.79 mm, and 12.96 mm, respectively.

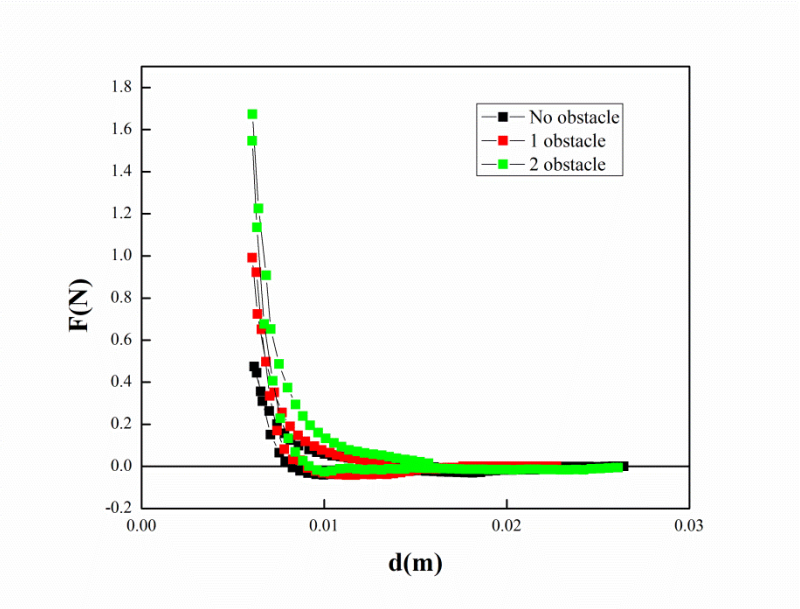

Figure 48. A single 40:1 Sample of PDMS run through all three roughnesses consecutively. The dimensions of the film were 0.41 mm thick, 53.71 mm length, and 53.61 mm width, with crumple radii of 11.80 mm, 10.05 mm, and 12.63 mm, respectively.

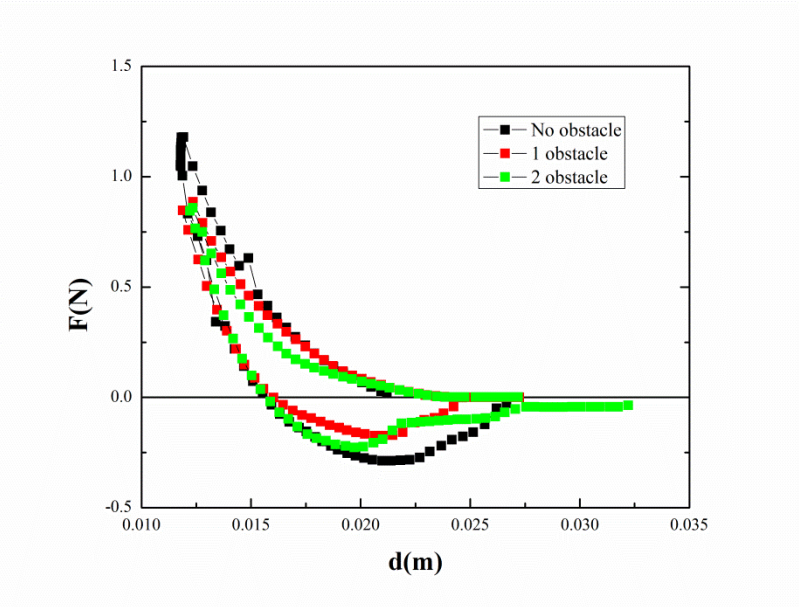

Figure 49. A single 45:1 Sample of PDMS run through all three roughnesses consecutively. Film dimensions were 0.9 mm, 82.20 mm length, and 81.86 mm width, with crumple radii of 17.25 mm, 19.91 mm, and 17.92 mm, respectively.

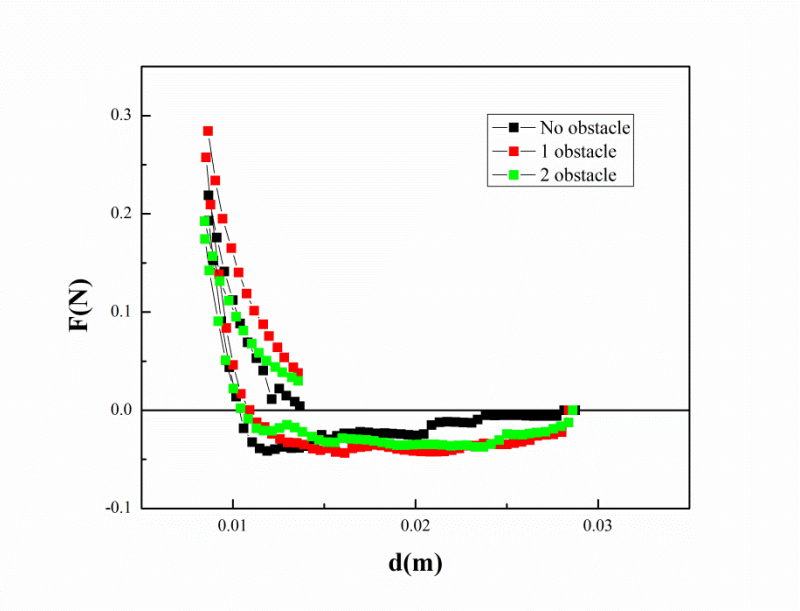

Figure 50. A single 50:1 Sample of PDMS run through all three roughnesses consecutively. Film dimensions were 0.48 mm thickness, 54.04 mm length, and 54.01 mm width, with crumple radii of 12.01 mm, 10.96 mm, and 12.76 mm, respectively.

Pull-off forces also showed no difference for rough or non-rough samples. On average there were larger pull off forces at lower crosslink densities/ lower modulus (the higher ratios). We plot the average pull off force in Figure 51. Compared to the work of adhesion from the tape loop experiment it differs in exact value, as expected, however, it displays the same trend of higher forces seen at the lower crosslink densities. Despite complex geometry, pull off forces seem related to crosslink density. The complexity shows that as predicted the value of G_C is not calculable from only the pull off force due to the complexity of the corresponding geometry. More work remains to be done in order to determine the appropriate methods to connect the adhesion of the crumple to the contact area and geometric considerations.

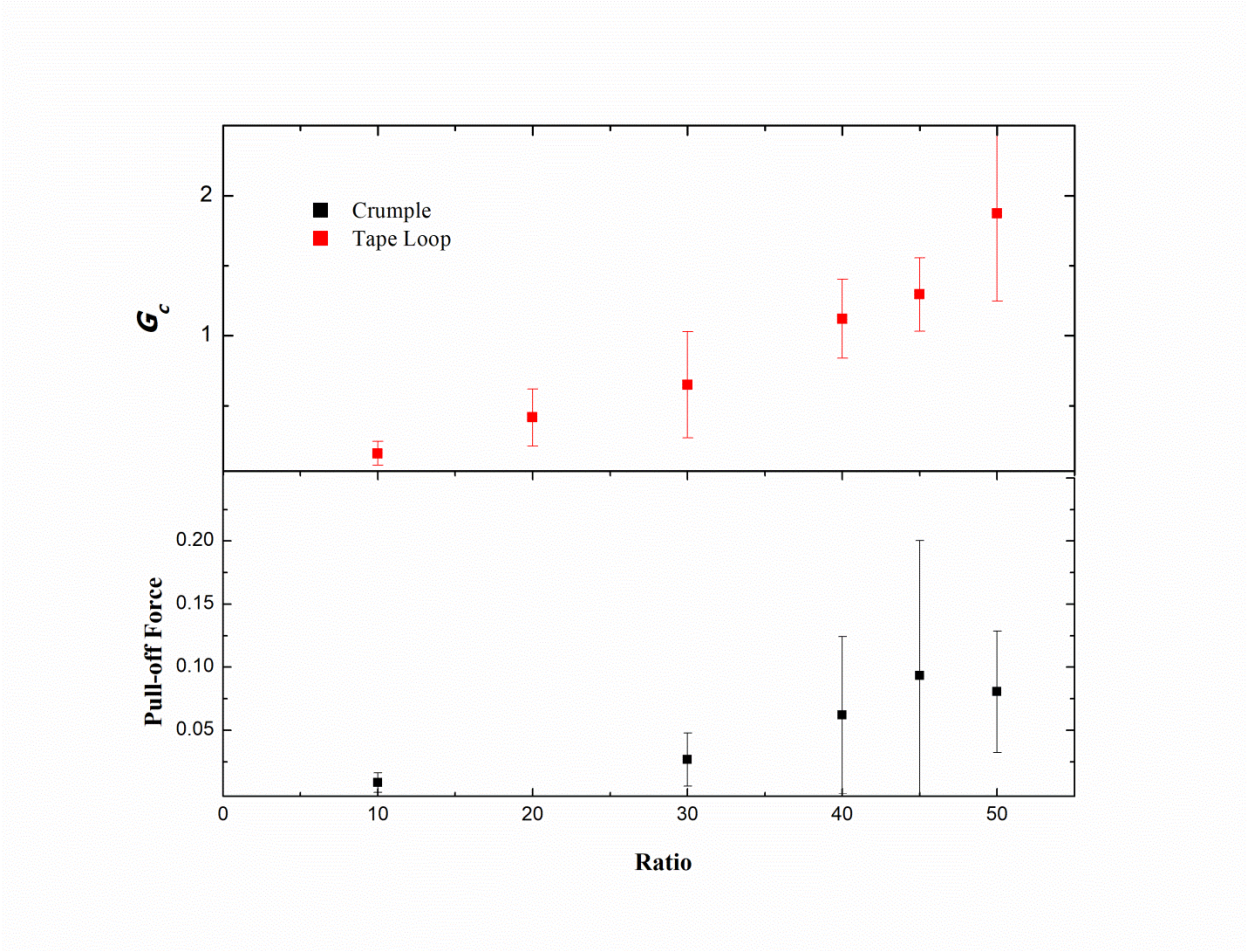

Figure 51. The average pull off force of crumple experiments with y-values shown on the left axis on the same graph as the tape loop G_C values with y-values shown on the right axis.

3.4. Conclusion

Similar to measurements in other geometries, crumpled films of higher crosslink ratio PDMS have stronger adhesion than less crosslinked PDMS. We can see this from the greater hysteresis of high ratio films compared to low ratio films among other measurements. Unlike adhesive strips which formed a force plateau as they peeled, crumples showed a quick decrease, sometimes showing numerous steps, before achieving pull off. The force displacement curves were therefore in some ways similar to those of probe tack tests where force jumps as different regions of adhesive fail separately.

We added roughness to determine if the crumple adapts well around obstacles, the driving thesis of this project. Our experiments show there is no significant difference in the pull off force comparatively between a crumple on the smooth surface or either of the rough surfaces. Results support our hypothesis that crumples are roughness tolerant adhesives.

In our preliminary investigations into the contact area of the crumple on a surface, we observed a patchy pattern reminiscent of contact splitting. The contact appeared similar comparatively for the smooth and rough surfaces examined. This further supports the idea that the hierarchy of structures of a crumple are able to deform around objects on the surface

Further work is still needed to fully explore the possible advantages of adhesive crumples on rough surfaces. Contact area of a crumple with the surface is complex and requires further investigation. The roughness used in our experiments was intentionally simple. 3-D printing of other variations of roughness would add to a deeper understanding. All of the experiments were performed at the same speed for consistency. However, as adhesion also has a speed dependence in soft systems other speeds could be tested. The contact area as stated is complex, as such more quantitative contact information should be taken for a better understanding of how these random systems conform around obstacles.

4. SWITCHING ADHESION WITH ORIGAMI

4.1. Introduction

An adhesive is often most useful when it requires high force to separate it from a surface. However, high force can be detrimental if eventually removing the adhesive is desired. For example, when hanging a painting on a wall temporarily - removal of a high force capacity adhesive might damage the wall. One way to prevent damage and yet maintain high forces is to have a mechanism in place that switches the adhesive from high force to low force, i.e. making a switchable adhesive.

Switchable adhesives are those with high adhesion that can nonetheless be easily released from a surface when an external stimulus is introduced. This stimulus changes the fracture mechanics that dictate whether a crack can form by altering the interfacial chemistry strength of the adhesive, releaseablity through mechanical means, or contact area in order to decrease the force needed. This gives the advantages of both permanent adhesives and temporary adhesives to a single adhesive system[100].

One of the key features needed to make a switchable adhesive is to have one of the three properties that determine the force to be changeable. The failure force determined through fracture mechanics can often be written:

$$F = \sqrt{\frac{G_C A}{C}} \tag{64}$$

where C is the compliance or stiffness, A is contact area and G_C is critical energy release rate. This equation is oversimplified and doesn't apply in all situations, for example in systems which have progressive failure, like peel[72]. Weaker physical bonds adhere less strongly than covalent bonds so are easier to remove in general, with better potential for reusability (low G_C).

Decreasing the contact area results in easier removal of an adhesive as well. Low modulus systems detach with less force than high modulus systems[100]. Lowering any of the three parameters (G_C, area, or compliance) via external stimuli reduces the amount of force needed to remove an adhesive.

Mechanical switching is a type of switching which affects compliance without directly changing modulus. A structure might be preloaded to hold a specific shape. When the preload is removed the structure might then recover to its original configuration. If the original configuration reduces one of the switchable parameters, the change in structure can make it easier for a crack to form and propagate along the interface. This creates an "on" configuration that requires an amount of force, F_{on}, for separation and an "off" configuration that requires an amount of force for separation, F_{off} that is different from that of the "on" configuration. Comparison of the F_{on} and F_{off} force is convenient in the form of a ratio, the switching ratio. Higher switching ratios which result from higher force in the "on" position and lower force to remove in the "off" position are generally the goal. Changes to geometry independent of other changes are enough to create high ideal switching ratios which approach infinity[100].

In our work, we look at structures that have the potential for mechanical switching. In particular, structures we considered are origami patterns that alternate between a rigid configuration and a soft configuration based on loading conditions. The soft configuration (high compliance) should require less force to initiate fracture between the adhesive and the surface and initiate peel.

The origami architectures we have chosen to explore as switchable adhesives are known as the Ron Resch patterns[70] shown in Figure 52 and 53. Ron Resch was an artist in the 1960s who made tessellation patterns in 3-D from 2-D materials. The applications of these patterns are

increasing as we find new ways to utilize them. We looked primarily at a triangle pattern and a square pattern that have closed and open configurations. These patterns were also chosen as they have smaller unit cells that can be used independent of a long-range tessellation.

The triangle pattern has folded equilateral triangles that form periodic radial patterns of six triangles (Figure 52). For our purposes, we are only using a segment of the tessellation. When the shape is folded, and six of the triangles which are oriented radially around a center folded area, are compressed together to form a hexagon with a flat surface. This flat surface can be laid flush against another surface. If the load holding the triangles compressed together is removed the triangles separate as the structure returns to a more relaxed position. As the shape opens, the triangles tilt out of plane developing a "curve" such that the structure can no longer lay flat against a surface. Therefore this shape offers the potential to be used as a switchable adhesive as it has the two separate configurations that can be used as on (strongly adhered) and off (weakly adhered) modes.

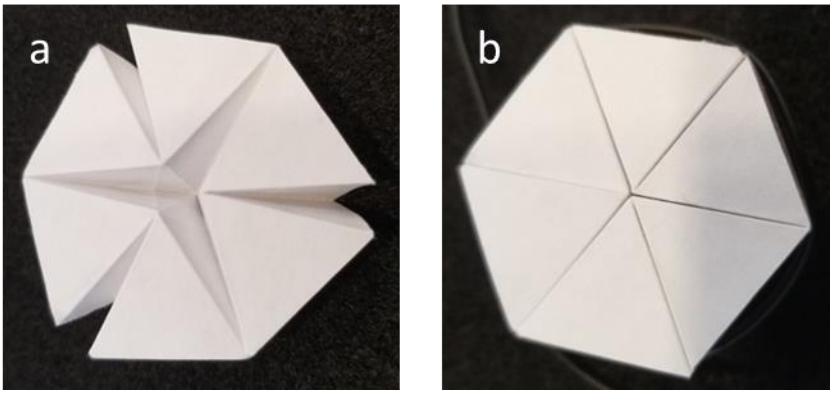

Figure 52. Unit cell of a Ron Resch triangle origami pattern. In the initial state the triangles are somewhat separated from each other due to the elasticity of the folds and the shape is open with a slight curvature. Once the triangles are brought together a flat hexagonal configuration is produced.

The square pattern shown in Figure 53 (the water bomb as it is colloquially called) has some similarities to the triangle pattern and some differences of note. Similar to the triangle

pattern the square pattern has a curved open configuration and a closed flat configuration. The degree of curvature of the square pattern is much higher than that of the triangular pattern with possibilities of rotational adhesion considerations analogous to insects and biologic organisms which will be discussed later in this Thesis. The squares also offer a tunable surface area as increasing area can be done through the inclusion of more squares to make larger overall square or rectangular patterns.

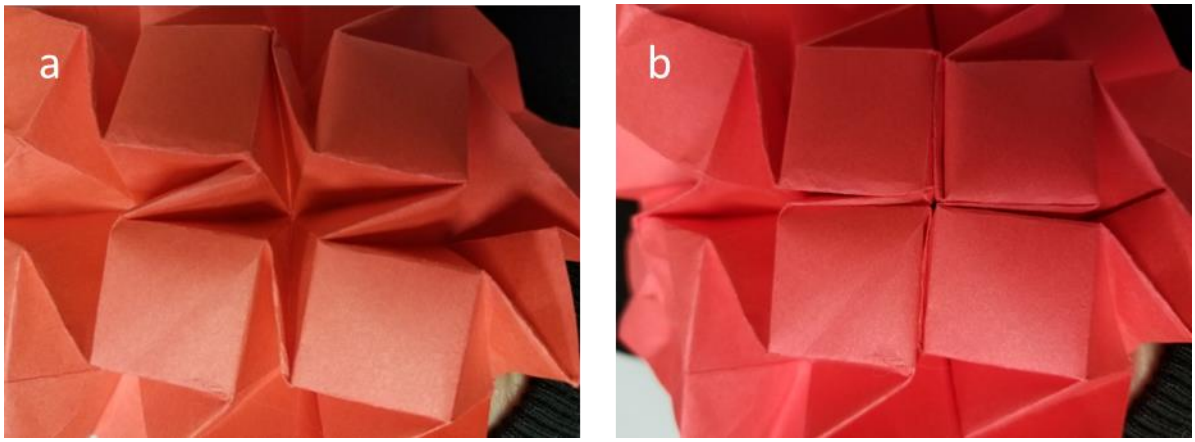

Figure 53. The square pattern of water bomb. Note how the relaxed unloaded configuration is curved in the plane of the image and open, while the closed configuration is flat in the plane of the image.

4.2. Experiment

The sections of tessellations of interest were initially drawn in PowerPoint. These patterns were printed and used to guide folding of PC for testing. Initial experiments were carried out by folding a section of PC sheeting by hand in accordance with the pattern. The PC was cut by scalpel into the exact dimensions needed for the pattern. In hand folding PC experienced some breakage or extra thickness along fold lines that were detrimental to the experiment. Later experiments carried out cut the PC with a Cricut machine which allows the introduction of small puncture points along the fold lines which facilitates easier, cleaner folding.

This modified pattern was then used to print PC sheets for easier folding. With both methods, the sheets were then folded along the pattern lines to achieve the desired Ron Resch segment.

Adhesive substrates were used as a means to test the switchable adhesion of the origami shapes. The adhesive substrates chosen were low crosslink density PDMS of ratios 40:1 and higher. PDMS was chosen as it is a dry adhesive, providing a way to test the pull off force more directly than use of a PSA. Adhesion was not applied directly to the PC initially as one side being adhesive was sufficient to test the concept. PDMS with its low modulus and high curvature bends that do not form the folds needed for neat origami shapes, was not considered for use directly as an origami shape. Further experiments should be carried out on origami that has adhesive on the segments of the unit section is desirable. This adhesion should be only on the triangle or square faces as adhesive on the other areas might result in self-adhesion in the folding areas which would limit or prevent the switching mechanism.

In order to secure the origami shape in the apparatus and to measure the pull off forces strings were used. The strings secured the origami shape to the motor. The string also provided the force to lift the shape off of the substrate via tension. Strings, in our case fishing line were cut and threaded through a centrally positioned hole in the upper folded area away behind the contacting surface. That is the topmost D-cone areas of the folds that are on the other side of the flat surface side achieved in closed configuration. The threads were then fed through a 3-D printed holder or directly tied or clamped to a linear actuating motor or a tensile tester. For experiments testing in the "on" position the 3-D printed holder remains resting on the sample to maintain load and hold the shape. The strings go through the holder. For samples in the "off" position the sample holder is removed after placement or not used at all.

The sample holder shown in Figure 54 consisted of 3-D printed triangles, Figure 52, that fit on top of the origami structure and were then enclosed in an outer sheath that held them snugly. This outer 3-D printed structure has a small hole through the top to allow the string to pass through.

Figure 54. 3-D printed apparatus for the triangle origami pattern. Where the 3-D printed structures are placed triangle side down onto each triangle and then pushed together to create a load holding the pattern in the "on" configuration.

The Ron Resch segment in the "on" configuration was pushed flat into the surface of a tacky PDMS substrate until the two surfaces adhered fully. The motor then moved up pulling the Ron Resch segment from the surface in either the "on" positon or the "off" position (Figure 55 and 56, respectively). The off position 3-D printed triangles were removed prior to allow the switch in configuration. Experiments with square pattern were similar but sometimes used binder clips to hold the 3-D printed apparatus snugly together for the more rigid on position as at the time of this writing there exists no 3-D printed holder. Figure 57 shows the square pattern in on position held together with clips and an unrestrained off position.

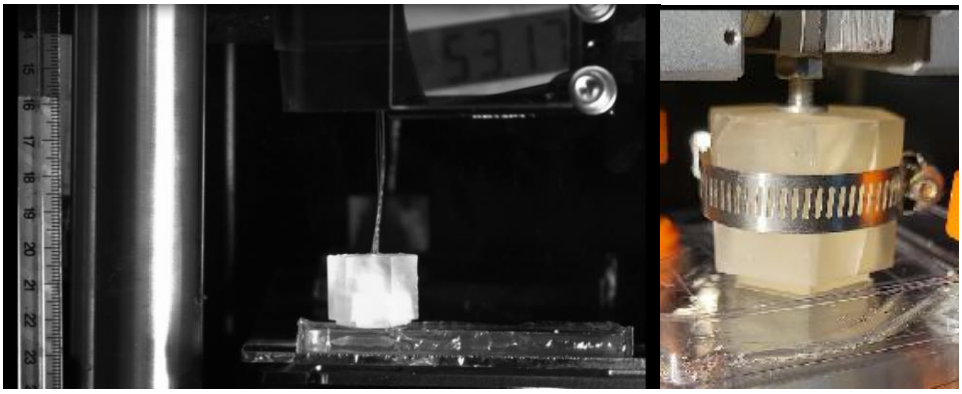

Figure 55. An experiment in the "on" position. The PC pattern is flush against a 40:1 PDMS substrate. The holder keeps the pattern in a constant load condition through the experiment. The string emerges from a single area and is attached to the linear actuation motor which moves upwards.

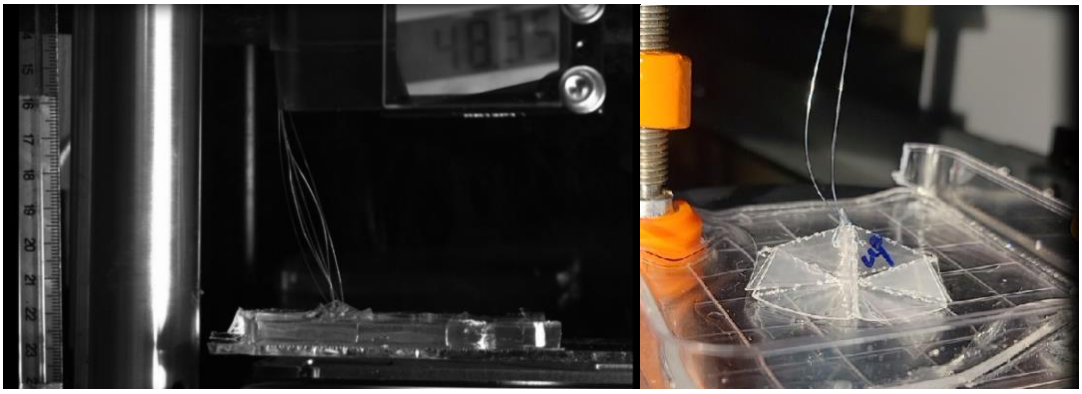

Figure 56. An experiment in the "off" position. The PC pattern is flush against a 40:1 PDMS substrate. The holder has been removed so there are no load conditions present during the experiment. The string emerges from a single area and is attached to the linear actuation motor which moves upwards.

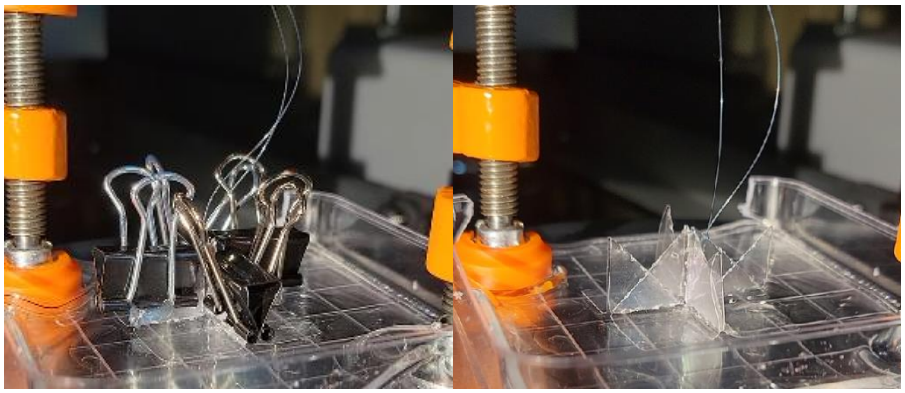

Figure 57. The square pattern of origami in both experimental setups, on the left secured in closed "on" position and on the right open "off" position.

The motor moved at a set speed. Videos were taken and were analyzed by means similar to that of other experiments using particle tracking programs. Data obtained yielded force distance curves. Careful attention was paid to the method of removal i.e. peel or coming off as a single unit.

4.3. Results and Discussion

We predicted that the Ron Resch pattern in its closed rigid "on" state will be similar to a post test. We also predicted that when we switch the configuration to the softer "off" state we would see more of a peel during failure. This thought process was from the slight curvature of the on position for the triangles origami allowing a crack to form more easily between the substrate and the sample at the edges. Moving the motor upward increased the tension on the string which provided the force needed to propagate the crack until there was complete separation for "off" configurations or complete removal for "on" configurations.

Data comparing the changes in force over time of a sample on 40:1 PDMS and one on 50:1 PDMS are shown in Figure 58 and 59, respectively. For the 40:1 PDMS substrate as time progressed for samples tested the "on" position configuration saw a sharp force increase (red in the figure) which reached a peak tensile force before rapidly changing to zero. The "off" position has a steady decrease in force that slopes down to a small peak force before dropping to zero. The 50:1 PDMS substrate was slightly different as both on and off showed sharp peaks before drops in force to separation. This could be a result of the increased adhesion from 50:1 PDMS. The force might be large enough to prevent the triangle from opening creating gaining curvature. There is also a possible speed element as the 50:1 PDMS is softer and more viscoelastic than the 40:1 PDMS. Meaning that the crack might propagate slower at a slower pull off speed for the 50:1 PDMS due to flow. The test speed was 0.00851 mm/s for both

samples shown in Figure 58 and 59 which may have been insufficient to open the crack quickly enough for peeling on the 50:1 PDMS substrate.

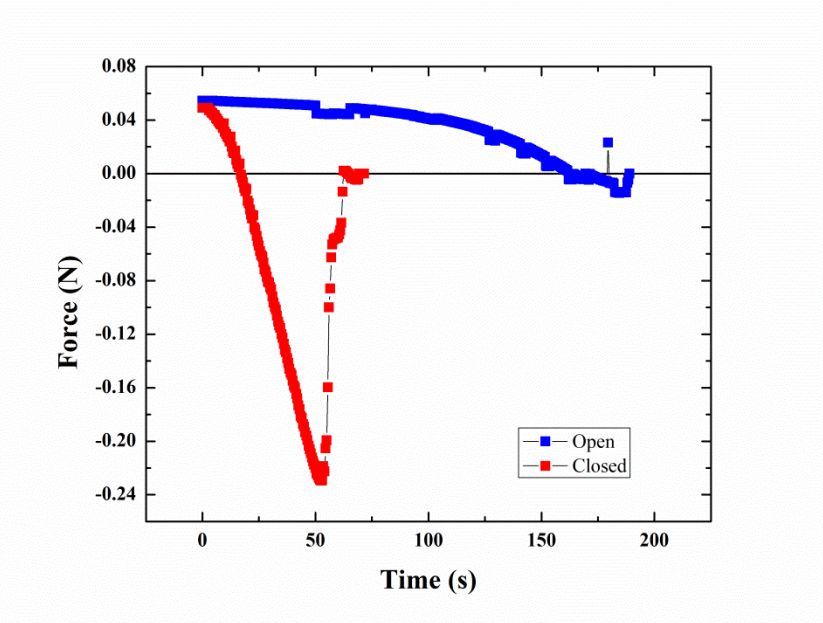

Figure 58. Hexagonal origami pattern on a 40:1 PDMS substrate. Substrate thickness was ~4 mm.

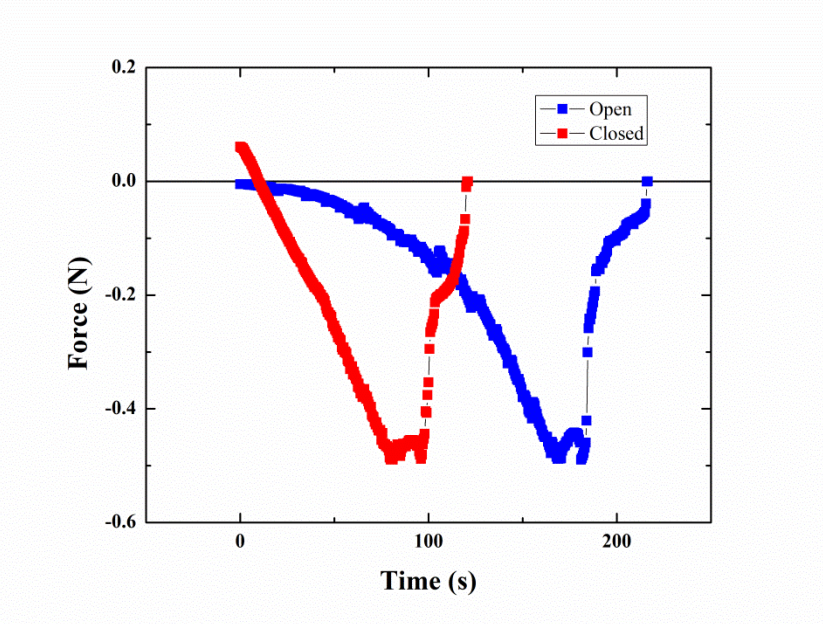

Figure 59. Hexagonal origami pattern on a 50:1 PDMS substrate. Substrate thickness was around ~4 mm.

Plotting force vs the surface contact diameter graphs further support these observations. The 40:1 PDMS substrate sample seen in Figure 60 shows a slope that is sharp at the point of high force for the "on" configuration (red squares). For the "off" or open configuration, force appears to slope more gently until complete separation. Figure 61 shows the amount of the shape remains on the substrate over time which gives information on the type of separation that is occurring. In the "on" position the change in distance increases slightly initially, possibly from pulling up and stretching some of the low modulus substrate, before a vertically sloped line showing that there is a complete separation of the entire structure all at once. This complete separation of all points almost simultaneously is what is commonly seen in a post-test separation. The distance in the "off" position is gradual as more and more of the structure is removed from the surface from one end to another, as in peel.

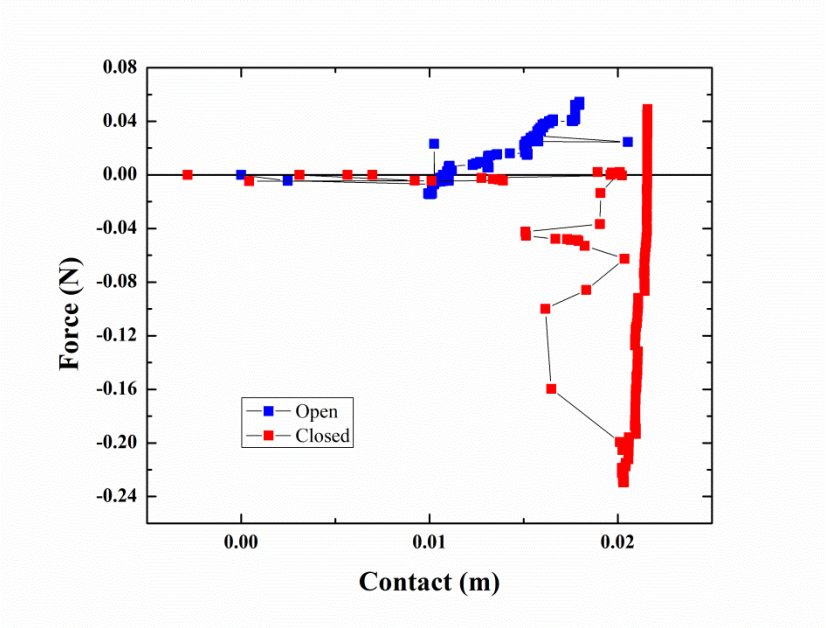

Figure 60. Force-vs the diameter of contact area with the substrate for the hexagonal origami pattern on a 40:1 PDMS substrate of thickness ~4 mm.

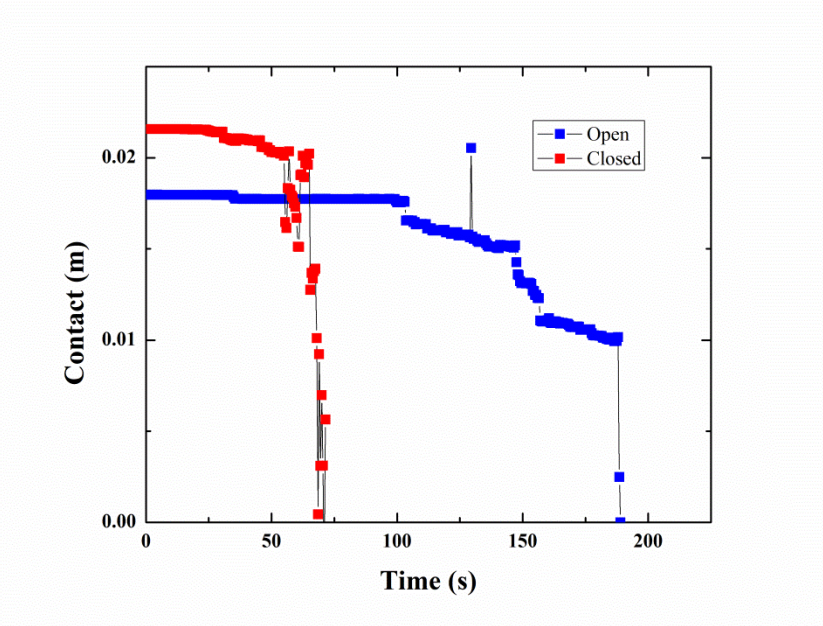

Figure 61. Graph of the change in the diameter of the sample in contact with the substrate over time for the hexagonal origami pattern on 40:1 PDMS substrate of thickness ~4 mm graph.

The 50:1 PDMS substrate force-distance graph is shown in Figure 62 and the time vs distance graph is shown in Figure 63. Both differ from those of the 40:1 PDMS. The force-contact area graphs shows that both the on and off state show similar trajectories. The comparison when observing just the change in contact area is also fairly similar. The main difference being that the "off" configuration stayed on the substrate longer. This can be attributed to the slow speed of the motor and the increased viscoelasticity of the 50:1 PDMS compared to the 40:1 PDMS.

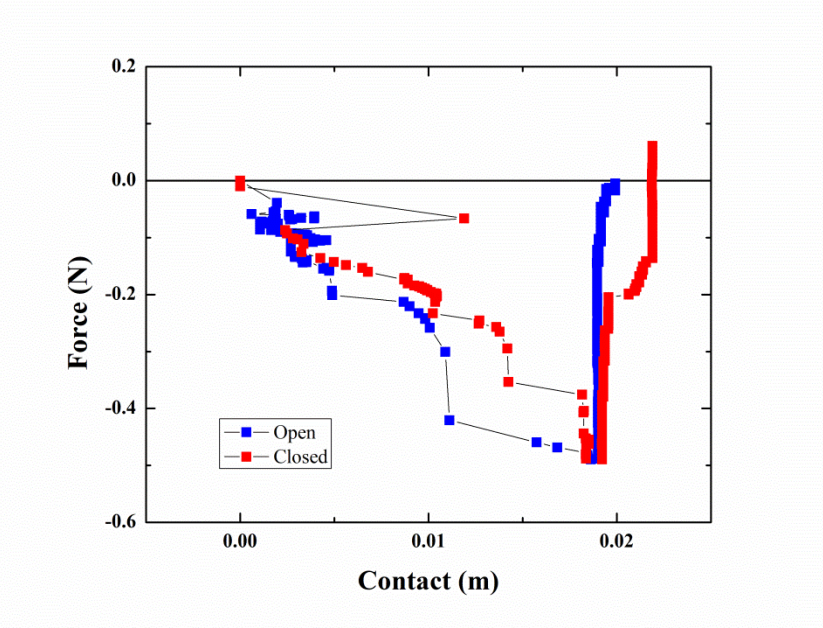

Figure 62. Force over time of triangular pattern on 50:1 PDMS substrate.

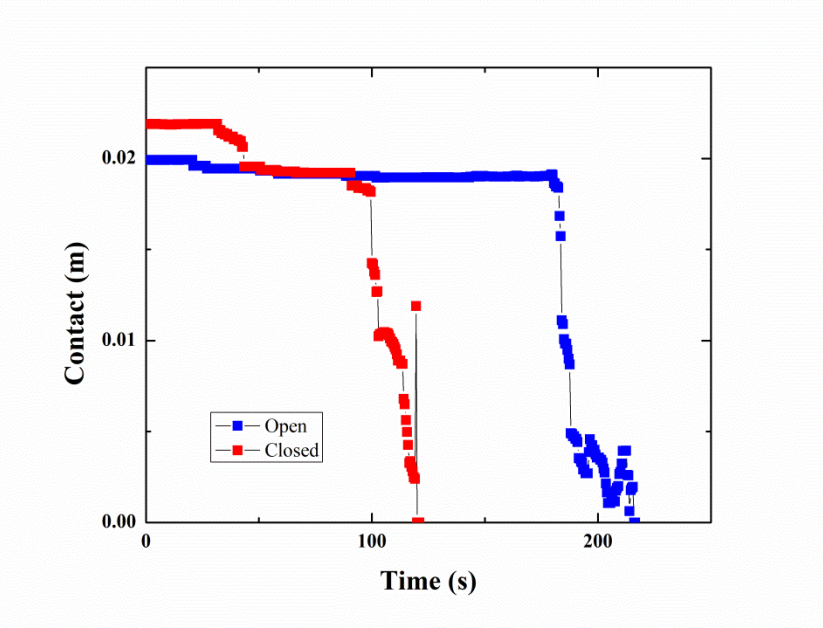

Figure 63. Width of film remaining of triangular pattern on 50:1 PDMS substrate over time.

Square pattern has shown the same trends as the triangular pattern. The closed squares require significantly more force to remove than the open squares. The process of removal from the PDMS substrate is much quicker when the squares are open.

4.3.1. Modeling

The triangles in the on position showed two modes of failure that were observed during separation. The primary mode was pull off all at once or via increased cavitation, similar to a post-tack test. The second was through crack formation along one side or corner that led to complete separation at an angle. This was possibly due to some angle introduced in the set up or as a result of string placement, and is also common in misaligned post-tests. The second mode was somewhat different from traditional peel as it retained the angle through the entire structure for rapid separation, as opposed to an angle of the section being lifted while the remaining is flush to the surface. In both instances the triangles remain stiff and flat in a hexagonal shape.

In order to model our structures we need to modify the post-test equation, Eqn 31, to account for the different geometry. The area of a hexagon is $A = \left(3\sqrt{3}/2\right)a^2$, where a is the length along a side of the hexagon as well as from a corner to the center, Figure 64, as it is composed of equilateral triangles. The post-test generally uses the area of a circle, $A = \pi a^2$, where a is the radius of the circle, Figure 64. Making this change to Eqn. 31 from Section 1.4.2, the post equation gives:

$$G_C = F^2(1-\nu^2)/12\sqrt{3}Ea^3. \tag{65}$$

The same behavior is predicted for the squares with areas of $A = a^2$, where a is a side length, if the length and width of squares are equal, i.e. there are the same number of squares one way as the other the equation is simply:

$$G_C = F^2(1-\nu^2)/8Ea^3. \tag{66}$$

If the length and width are not equal, that is an unequal number of squares in the length and width, one of the a's (side length shown in Figure 64) will be changed to a ratio of a for the

entire section to account for the difference in area. It is appropriate to use ratios as all of the squares composing the section are of equal length.

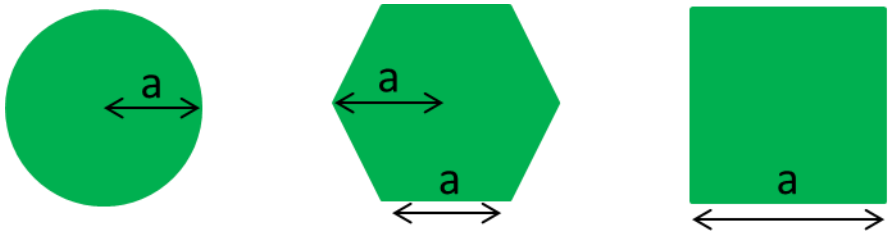

Figure 64. Values of a used in the computation of area for three shapes, the square, hexagon, and square.

The triangles in the off position also have two modes of separation dependent on where the initial crack propagates. The first and most prevalent is from the outer edge as it begins to curve away from the substrate. The lift at the edge of the triangle increases the tension which initiates a crack at either a side or corner. The second mode is where once loose crack formation occurs in the newly opened central area, during pull up the tension on the string then quickly propagates the crack peeling outwards towards the edges.

While we could look at the adhesive sample like a hexagon as previously for the rigid on state, it is not a reasonable assumption for the softer off state. Due to the separation between the unit triangles in the off state we can assume that each acts independently of the others. As we assume that the failure mode is peel, it can be said that there are six triangles peeling together and sequentially. This allows us to modify peel (Eqn. 32), to account for the changing width of a triangle. During peel a triangle unlike a square will not have the same width for all points, Figure 65, the width b changes. As can be seen in Figure 65 the width at the base of a triangle is larger than at the corresponding corner across from it, in this instance if peel begins at the base the amount of force needed will decrease as the width decreases. In the opposite scenario where

crack propagation begins at a point of the triangle more force will be required as width increases, the amount of force should still be lower than that of a square with equal side length.

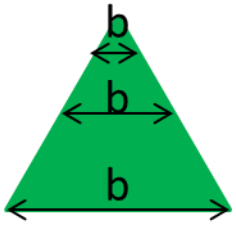

Figure 65. A simple schematic showing how the width of a triangle changes at different points. A consideration when applying it to the peel equation.

The squares might be a bit different in their peel off due to their increased flexibility in the off state. There might also be some rotational forces present. We additionally predict that the system would be similar to contact-splitting mechanisms employed on the legs of insects. Insect legs divide up the contact area[101] through having a large number of small contacts that make up a large contact area[102]. These small contacts are often an array of hairs which end in flattened plates called spatula[103]. Much like what we have already observed through our central detachments of the triangle pattern adhesion that is twice as strong in the center of each contact than along its borders[104].

It was found that insects are able to attach to inverted surfaces effectively through a combination of gait pattern[105, 106] and directional forces of the setae. Experiments on spiders showed that the pads are semicircular requiring the spider to slightly rotate its legs to achieve and hold the structures at an appropriate angle of 30° [107]. Curved adhesive pad structures on a surface achieve adhesion through proper alignment and a pushing force for preferential contact area, as pulling changed the contact area, of triangular shaped setal tips; similar to our triangular pattern, however, in insects they are not always tightly grouped together into a hexagon. Shear forces both improve adhesion to surfaces and can be used to remove the curved parts through

pulling[97]. The role of shear forces remains a topic for further investigation in our origami structures.

Distal pushing is used to remove the contact points of the spider[97]. Insects as a whole utilize four main movement mechanisms for removal of their adhesive structures that all rely on increasing rotational and shear forces: twisting, rotation, pulling, and shifting[108]. In this way the mechanism is similar to that of our origami mechanisms as we pull after inducing a curvature and increasing shear and in the case of the square pattern rotational forces.

4.3.2. Switching Ratio

The measure of change in adhesion of interest was the switching ratio, the difference in force required for removal of the on and off positions. The switching ratio for both the triangles and the squares was significant as can be seen in Figure 66 and 67 In the closed rigid on position force was quite large with pull-off forming a single peak. In the open soft off configuration the pull off differed some in shape between the triangles and the squares, however, the force was significantly less for both. The triangles in off configuration did not have defined peaks at pull off rather the broad plateau peaks expected for peel. The squares in off configuration had a peak similar to that of the on position but slightly broader and showing a peak of lower force. The time that debonding occurred differed between experiments with some debonding faster in the on position and others debonding faster in the off position, as this did not affect the force needed we do not consider it as an important aspect of analysis.

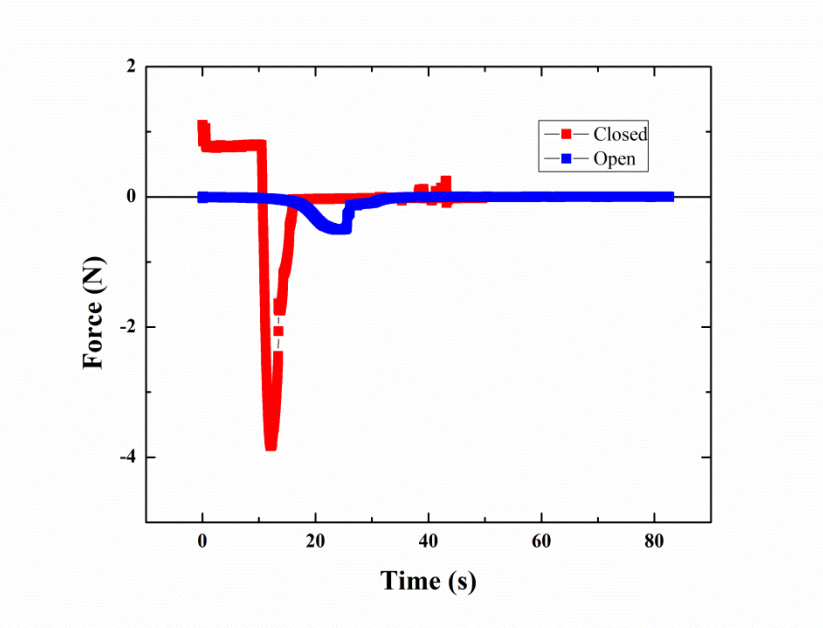

Figure 66. The switching ratio of triangle origami shapes on a 40:1 PDMS substrate at 5 mm/min with the closed shown in red and the open shown in blue. Note the large difference in force. The tension is positive as the experimental setup was changed.

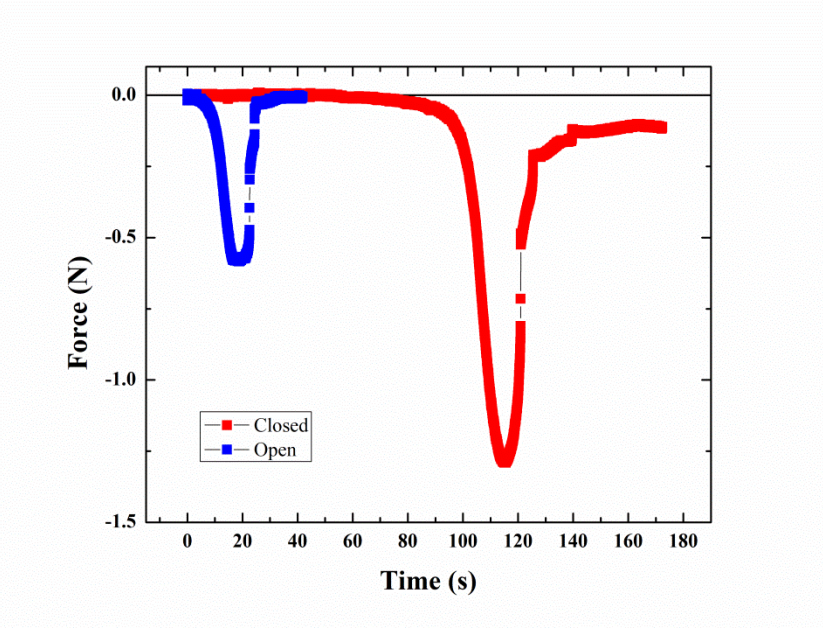

Figure 67. The switching ratio of square origami shapes on a 40:1 PDMS substrate at a speed of 25 mm/min with the closed shown in red and the open shown in blue. Note the large difference in force. The tension is positive due to a change in experimental setup from initial experiments.

The switching ratios for both shapes on different crosslink density substrates is shown in Table 1. All ratios were above 2 with the largest ratio going as high as 52. Meaning that in all experiments the rigid on configuration required 2 to 50 times more force for debonding than the corresponding off position required. There were three main speeds 5 mm/min, 10 mm/min, and 25 mm/min. There is no consistent pattern to the switching ratio based on speed. The crosslink ratio on substrates of 40:1 PDMS and 30:1 PDMS had the highest switching ratios, attributable to higher G_c and other considerations mentioned earlier in this chapter.

Table 1. Switching ratios for both triangles and square patterns. The data collected from multiple experiments of origami patterns hexagon and square at different speeds and on different substrates.

Shape	**Speed**	**Substrate Ratio**	**Rigid "on" position Peak Force**	**Soft "off" position Peak Force**	**Switching Ratio**
Triangle	5 mm/min	40:1	0.31	0.06	4.90
Triangle	10 mm/min	40:1	2.03	0.05	44.47
Triangle	25 mm/min	40:1	4.81	0.10	46.75
Triangle	5 mm/min	50:1	2.11	0.55	3.84
Triangle	10 mm/min	50:1	3.91	0.76	5.17
Triangle	25 mm/min	50:1	5.55	1.66	3.35
Square	5 mm/min	20:1	0.34	0.04	9.49
Square	10 mm/min	20:1	0.74	0.044	17.07
Square	25 mm/min	20:1	1.07	0.17	6.20
Square	5 mm/min	30:1	0.47	0.03	18.77
Square	10 mm/min	30:1	0.67	0.01	52.15
Square	25 mm/min	30:1	1.12	0.12	9.23
Square	5 mm/min	40:1	0.76	0.02	30.90
Square	10 mm/min	40:1	0.69	0.23	2.98
Square	25 mm/min	40:1	1.43	0.32	4.52
Square	5 mm/min	50:1	0.46	0.04	10.38
Square	10 mm/min	50:1	0.48	0.08	6.09
Square	25 mm/min	50:1	1.24	0.34	3.59

Comparison of the triangle shape to the square shape can be rudimentarily done from the values in Table 1. The contact area of the squares is 1069.29 mm² for a unit cell studied which contained 4 squares with sides of length 16.35 mm. The contact area of the triangles was

961.272 mm^2 for the unit cell studied which contained 6 triangles with side lengths of 16.9 mm. However, there was no consistent pattern between force needed per mm^2 being larger for all squares or all triangles in our experiments; just as in other variables the main consistent pattern is between on and off configurations of each shape. More work is needed to determine if one has significant advantage over the other. While no clear advantages have come from experimental data each has an advantage based on shape for function such as triangle pattern being more easily constrained in the on configuration through a central holding mechanism while squares have versatility of easily adding additional squares in the unit for larger contact area.

Our experiments have shown that the force is significantly lower in the off state than in the on state. This has supported our predictions and expectations from modeling and biomimetic considerations that these origami structures have the potential to be viable switchable adhesives. The goal of a switchable adhesive is also repeatability due to environmental and financial considerations our experiments showed repeatable consistent results. As articulation is small we are not concerned about fatigue at the joints of our structures.

4.4. Conclusion

Based on the ability of the Ron Resch segment to change its base curvature as it is actuated, the Ron Resch segment could be used for switchable adhesion. The "on" or flat state approximates a post test and has stronger adhesion than the slightly curved off state which peels from the substrate. It requires more force to lift a post where the area needs to separate from a surface all at the same time than for a peel where less energy is needed once a crack is formed; increasing force propagates the crack until there is complete separation. Further testing of both patterns on additional substrates, at additional speeds and with additional sizes and patterns will illuminate the trends more clearly.

5. CONCLUSION

We extended our thin film work of determining the modulus by bending a film between two plates into a method to determine thin film adhesion based on the force differences between contraction and retraction. Then using a similar two plate compression test used in our previous work with the compression of crumples we compressed "sticky crumples" to measure their adhesion. Roughness was then added to the plates for crumples to see if crumples had the advantage of deforming around obstacles. Finally a segment of a Ron Resch tessellation offers a promising mechanism for switchable adhesion due to its change in conformation from a flat surface to a slightly curved surface.

Bent strips are a good adhesion test for films of different dimensions and crosslink ratios. The bent strips assume geometry upon retraction that is comparable to each side peeling at a close to 90° angle from each respective plate. Degree of crosslinking is related to adhesion and modulus for PDMS films, showing opposite trends. Higher crosslink ratios have higher adhesion and lower modulus which lower crosslink ratios have lower adhesion and higher modulus.

Crumples are sticky when made of sticky sheets. Crumples made of sticky sheets have compression curves along the lines of those shown by our previous compression tests with crumples made of stiff, adhesion-free sheets. Sticky crumples have retraction curves that show strong hysteresis that does not plateau like that of adhesive strips in peel and appears more comparable to probe tack adhesion tests. Crumples are tolerant of roughness and can conform around obstacles. Our initial measurements open the door to a more complete investigation of the complex sticky crumpled system.

A unit cell of a Ron Resch tessellation pattern shows promise as a means for switchable adhesion. The change in conformation might require less energy to separate the surfaces in one

conformation than in the other. The initial switchable origami adhesion experiments show a clear effect, and open the door to explorations of many different kinds of bistable origami structures in the future.

This thesis creates many new foci to expand on the mechanics and uses of sticky sheets. . Our models illustrate the work and shape of the common tape loop cycle and provide a simple way to measure the adhesion of the tape loop. We believe that our initial work with sticky crumples offer the potential to be used in adhesive applications connecting rough surfaces that are not well connected by other temporary adhesives such as tape. We also think that the Ron Resch origami pattern is a useful shape for mechanically switchable adhesion system, but will lead to much more optimized origami structures. In short, our work will open many new avenues of research.

REFERENCES

1 Modjarrad, K., & Ebnesajjad, S. (Eds.). (2013). *Handbook of polymer applications in medicine and medical devices*. Elsevier.

2 Omidian, H., Park, K., & Sinko, P. J. (2016). Pharmaceutical polymers.

3 Hu, J., Meng, H., Li, G., & Ibekwe, S. I. (2012). A review of stimuli-responsive polymers for smart textile applications. *Smart Materials and Structures*, *21*(5), 053001.

4 Patil, A., & Ferritto, M. S. (2013). Polymers for personal care and cosmetics: Overview. *Polymers for Personal Care and Cosmetics*, 3-11.

5 Davies, G. (2012). *Materials for automobile bodies*. Butterworth-Heinemann.

6 Umoren, S. A., & Solomon, M. M. (2019). Protective polymeric films for industrial substrates: A critical review on past and recent applications with conducting polymers and polymer composites/nanocomposites. *Progress in Materials Science*, *104*, 380-450.

7 Jones, R. A. L., Jones, R. G., Jones, R. A., & Jones, R. (2002). *Soft condensed matter* (Vol. 6). Oxford University Press.

8 Odian, G. (2004). *Principles of polymerization*. John Wiley & Sons.

9 Strobl, G. R., & Strobl, G. R. (1997). *The physics of polymers* (Vol. 2). Berlin: Springer.

10 von Schmeling, H. H. K. B. (2011). Eighty years of macromolecular science: from birth to nano-, bio-and self-assembling polymers—with slight emphasis on European contributions. *Colloid and Polymer Science*, *289*(13), 1407-1427.

11 Sperling, L. H. (2005). *Introduction to physical polymer science*. John Wiley & Sons.

12 Lefebvre, M. D., Dettmer, C. M., McSwain, R. L., Xu, C., Davila, J. R., Composto, R. J., ... & Shull, K. R. (2005). Effect of sequence distribution on copolymer interfacial activity. *Macromolecules*, *38*(25), 10494-10502.

13 Förster, S., Zisenis, M., Wenz, E., & Antonietti, M. (1996). Micellization of strongly segregated block copolymers. *The Journal of chemical physics*, *104*(24), 9956-9970.

14 Allcock, H. R. (2019). *Introduction to materials chemistry*. John Wiley & Sons.

15 Lodge, T. P., & Muthukumar, M. (1996). Physical chemistry of polymers: entropy, interactions, and dynamics. *The Journal of Physical Chemistry*, *100*(31), 13275-13292.

16 Pascault, J. P., Sautereau, H., Verdu, J., & Williams, R. J. (2002). *Thermosetting polymers* (Vol. 64). CRC press.

17 De Gennes, P. G. (2005). On polymer glasses.

18 De Gennes, P. G. (2000). Glass transitions in thin polymer films. *The European Physical Journal E*, *2*(3), 201-205..

19 Maestrini, C., & Kramer, E. J. (1991). Craze structure and stability in oriented polystyrene. *Polymer*, *32*(4), 609-618.

20 Tuğcu, P., & Neale, K. W. (1987). Necking and neck propagation in polymeric materials under plane-strain tension. *International journal of solids and structures*, *23*(7), 1063-1085..

21 Kramer, E. J. (1983). Microscopic and molecular fundamentals of crazing. *Crazing in polymers*, 1-56..

22 Bauwens-Crowet, C., & Bauwens, J. C. (1986). Annealing of polycarbonate below the glass transition temperature up to equilibrium: a quantitative interpretation of enthalpy relaxation. *Polymer*, *27*(5), 709-713.

23 Johnston, I. D., McCluskey, D. K., Tan, C. K. L., & Tracey, M. C. (2014). Mechanical characterization of bulk Sylgard 184 for microfluidics and microengineering. *Journal of Micromechanics and Microengineering*, *24*(3), 035017.

24 Adam, G. A., Hay, J. N., Parsons, I. W., & Haward, R. N. (1976). Effect of molecular weight on the thermal properties of polycarbonates. *Polymer*, *17*(1), 51-57.

25 Pitman, G. L., & Ward, I. M. (1979). Effect of molecular weight on craze shape and fracture toughness in polycarbonate. *Polymer*, *20*(7), 895-902.

26 Ohara, A., & Kodama, H. (2019). Correlation between enthalpy relaxation and mechanical response on physical aging of polycarbonate in relation to the effect of molecular weight on ductile-brittle transition. *Polymer*, *181*, 121720.

27 Klompen, E. T. J., Engels, T. A. P., Govaert, L. E., & Meijer, H. E. H. (2005). Modeling of the postyield response of glassy polymers: influence of thermomechanical history. *Macromolecules*, *38*(16), 6997-7008.

28 Fox, T. G., & Flory, P. J. (1954). The glass temperature and related properties of polystyrene. Influence of molecular weight. *Journal of Polymer Science*, *14*(75), 315-319.

29 Ward, I. M., & Hadley, D. W. (1993). *An introduction to the mechanical properties of solid polymers*.

30 Lodge, T. P., & Muthukumar, M. (1996). Physical chemistry of polymers: entropy, interactions, and dynamics. *The Journal of Physical Chemistry*, *100*(31), 13275-13292..

31 Brinson, H. F., & Brinson, L. C. (2008). Polymer engineering science and viscoelasticity. *An introduction*.

32 Lakes, R. (1987). Foam structures with a negative Poisson's ratio. *Science*, *235*, 1038-1041..

33 Przemieniecki, J. S. (1968). Theory of Matrix Structural Analysis 11 McGraw-Hill Book Co. *New York*, *21*.

34 Benham, P. P., & Crawford, R. J. (1987). *Mechanics of Engineering Materials: Graph. Darst.* Longman Scientific & Techn.

35 Katsikadelis, J. T. (2016). *The boundary element method for engineers and scientists: theory and applications*. Academic Press.

36 Treloar, L. R. G. (1942). The structure and elasticity of rubber. *Reports on Progress in Physics*, *9*(1), 113..

37 Muskhelishvili, N. I. (1953). *Some basic problems of the mathematical theory of elasticity* (Vol. 15). Groningen: Noordhoff..

38 El-Khalek, A., & AM, E. (2009). Steady state creep and creep recovery behaviours of pre-aging Al-Si alloys. *Materials Science and Engineering. A, Structural Materials: Properties, Microstructure and Processing*, *500*.

39 Pye, J. E., Rohald, K. A., Baker, E. A., & Roth, C. B. (2010). Physical aging in ultrathin polystyrene films: Evidence of a gradient in dynamics at the free surface and its connection to the glass transition temperature reductions. *Macromolecules*, *43*(19), 8296-8303.

40 Designation: D638 – 14 Standard Test Method for Tensile Properties of Plastics, ASTM International.

41 Fraiwan, A., Kwan, L., & Choi, S. (2016). A disposable power source in resource-limited environments: A paper-based biobattery generating electricity from wastewater. *Biosensors and Bioelectronics*, *85*, 190-197..

42 Liu, H., & Crooks, R. M. (2011). Three-dimensional paper microfluidic devices assembled using the principles of origami. *Journal of the American Chemical Society*, *133*(44), 17564-17566.

43 Liu, H., & Crooks, R. M. (2012). based electrochemical sensing platform with integral battery and electrochromic read-out. *Analytical chemistry*, *84*(5), 2528-2532..

44 Hasanzadeh, M., & Shadjou, N. (2016). Electrochemical and photoelectrochemical nano-immunesensing using origami paper based method. *Materials Science and Engineering: C*, *61*, 979-1001..

45 Cho, J. H., Keung, M. D., Verellen, N., Lagae, L., Moshchalkov, V., Van Dorpe, P., & Gracias, D. H. (2011). Nanoscale origami for 3D optics. Small, 7(14), 1943-1948.

46 Miyashita, S., Guitron, S., Yoshida, K., Li, S., Damian, D. D., Rus, D., (2016). IEEE International Conference on Robotics and Automation (IRCA).

47 Lee, D. J., LG Display Co Ltd, (2013). United States patent US9326375B2.

48 Roudaut, A., Karnik, A., Löchtefeld, M., & Subramanian, S. (2013, April). Morphees: toward high" shape resolution" in self-actuated flexible mobile devices. In *Proceedings of the SIGCHI Conference on Human Factors in Computing Systems* (pp. 593-602).

49 Zirbel, S. A., Lang, R. J., Thomson, M. W., Sigel, D. A., Walkemeyer, P. E., Trease, B. P., ... & Howell, L. L. (2013). Accommodating thickness in origami-based deployable arrays. *Journal of Mechanical Design*, *135*(11).

50 Liu, Y., Genzer, J., & Dickey, M. D. (2016). "2D or not 2D": Shape-programming polymer sheets. *Progress in Polymer Science*, *52*, 79-106.

51 Akinwande, D., Brennan, C. J., Bunch, J. S., Egberts, P., Felts, J. R., Gao, H., ... & Zhu, Y. (2017). A review on mechanics and mechanical properties of 2D materials—Graphene and beyond. *Extreme Mechanics Letters*, *13*, 42-77.

52 Lauff, C., Simpson, T. W., Frecker, M., Ounaies, Z., Ahmed, S., von Lockette, P., ... & Lien, J. M. (2014, January). Differentiating bending from folding in origami engineering

using active materials. In *ASME 2014 international design engineering technical conferences and computers and information in engineering conference*. American Society of Mechanical Engineers Digital Collection..

53 Peraza-Hernandez, E. A., Hartl, D. J., Malak Jr, R. J., & Lagoudas, D. C. (2014). Origami-inspired active structures: a synthesis and review. *Smart Materials and Structures*, *23*(9), 094001.

54 Hernandez, E. A. P., Hu, S., Kung, H. W., Hartl, D., & Akleman, E. (2013). Towards building smart self-folding structures. *Computers & Graphics*, *37*(6), 730-742.

55 Cerda, E., Chaieb, S., Melo, F., & Mahadevan, L. (1999). Conical dislocations in crumpling. *Nature*, *401*(6748), 46-49.

56 Komura, S., Tamura, K., & Kato, T. (2005). Buckling of spherical shells adhering onto a rigid substrate. *The European Physical Journal E*, *18*(3), 343-358.

57 Landau, L. D., & Lifshitz, E. M. (1986). *Theory of elasticity* (Vol. 7, No. 3). New York: Pergamon Press, Oxford.

58 Cerda, E., & Mahadevan, L. (2005). Confined developable elastic surfaces: cylinders, cones and the Elastica. *Proceedings of the Royal Society A: Mathematical, Physical and Engineering Sciences*, *461*(2055), 671-700.

59 Witten, T. A. (2007). Stress focusing in elastic sheets. *Reviews of Modern Physics*, *79*(2), 643.

60 Croll, A. B., Twohig, T., & Elder, T. (2019). The compressive strength of crumpled matter. *Nature communications*, *10*(1), 1-8.

61 Sahni, V., Blackledge, T. A., & Dhinojwala, A. (2010). Viscoelastic solids explain spider web stickiness. *Nature Communications*, *1*(1), 1-4.

62 Brely, L., Bosia, F., & Pugno, N. M. (2015). Numerical implementation of multiple peeling theory and its application to spider web anchorages. *Interface focus*, *5*(1), 20140051.

63 Shirtcliffe, N. J., McHale, G., & Newton, M. I. (2012). Wet adhesion and adhesive locomotion of snails on anti-adhesive non-wetting surfaces. *PLoS One*, *7*(5), e36983..

64 Poh, B. T., & Yong, A. T. (2008). Effect of molecular weight of rubber on tack and peel strength of SMR L-based pressure-sensitive adhesives using gum rosin and petroresin as tackifiers. *Journal of Macromolecular Science, Part A*, *46*(1), 97-103..

65 Dirks, J. H., & Federle, W. (2011). Fluid-based adhesion in insects–principles and challenges. *Soft Matter*, *7*(23), 11047-11053.

66 Autumn, K., Liang, Y. A., Hsieh, S. T., Zesch, W., Chan, W. P., Kenny, T. W., ... & Full, R. J. (2000). Adhesive force of a single gecko foot-hair. *Nature*, *405*(6787), 681-685.

67 Autumn, K., & Gravish, N. (2008). Gecko adhesion: evolutionary nanotechnology. *Philosophical Transactions of the Royal Society A: Mathematical, Physical and Engineering Sciences*, *366*(1870), 1575-1590.

68 Bartlett, M. D., Croll, A. B., King, D. R., Paret, B. M., Irschick, D. J., & Crosby, A. J. (2012). Looking beyond fibrillar features to scale gecko-like adhesion. *Advanced Materials*, *24*(8), 1078-1083..

69 Ben Amar, M., & Pomeau, Y. (1997). Crumpled paper. *Proceedings of the Royal Society of London. Series A: Mathematical, Physical and Engineering Sciences*, *453*(1959), 729-755..

70 Resch, R. D., (1965). United States patent US3201894.

71 Lv, C., Krishnaraju, D., Konjevod, G., Yu, H., & Jiang, H. (2014). Origami based mechanical metamaterials. *Scientific reports*, *4*(1), 1-6..

72 Maugis, D., & Barquins, M. (1980). Fracture mechanics and adherence of viscoelastic solids. *In Adhesion and adsorption of polymers* (pp. 203-277). Springer, Boston, MA.

73 Kendall, K. (1971). The adhesion and surface energy of elastic solids. *Journal of Physics D: Applied Physics*, *4*(8), 1186.

74 Kendall, K. (1975). Thin-film peeling-the elastic term. *Journal of Physics D: Applied Physics*, *8*(13), 1449..

75 Johnson, K. L., Kendall, K., & Roberts, A. (1971). Surface energy and the contact of elastic solids. *Proceedings of the royal society of London. A. mathematical and physical sciences*, *324*(1558), 301-313..

76 Shull, K. R. (2002). Contact mechanics and the adhesion of soft solids. *Materials Science and Engineering: R: Reports*, *36*(1), 1-45.

77 Elder, T. M. (2018). Bending and Force Recovery in Polymer Films and Microgel Formation.

78 T. Elder, D. Rozairo, A. B. Croll, Macromolecules 52:2, 690. 2019.

79 Elder, T., Rozairo, D., & Croll, A. B. (2019). Origami inspired mechanics: measuring modulus and force recovery with bent polymer films. *Macromolecules*, *52*(2), 690-699.

80 Singer, C., Holmgard, E. J., Hall, A. R., (1954). A History of Technology, Oxford University Press, New York.

81 Cai, J., Ren, Z., Ding, Y., Deng, X., Xu, Y., & Feng, J. (2017). Deployment simulation of foldable origami membrane structures. *Aerospace Science and Technology*, *67*, 343-353.

82 Chiche, A., Stafford, C. M., & Cabral, J. T. (2008). Complex micropatterning of periodic structures on elastomeric surfaces. *Soft Matter*, *4*(12), 2360-2364..

83 Schneider, F., Fellner, T., Wilde, J., & Wallrabe, U. (2008). Mechanical properties of silicones for MEMS. *Journal of Micromechanics and Microengineering*, *18*(6), 065008.

84 Baker, I. (2018). *Fifty materials that make the world*. Springer.

85 Staudinger, H., Brunner, M., Frey, K., Garbsch, P., Signer, R., & Wehrli, S. (1929). Über hochpolymere Verbindungen, 14. Mitteilung: Über das Polystyrol, ein Modell des Kautschuks. *Berichte der deutschen chemischen Gesellschaft (A and B Series)*, *62*(1), 241-263.

86 Boedeker Plastics, Inc., Shiner, Texas, USA, Retrieved December 12, 2017, www.boedeker.com.

87 Dialectric Corporation, Retrieved December 12, 2017, http://www.dielectriccorp.com/downloads/thermoplastics/lexan.pdf.

88 Gurmessa, B. J., & Croll, A. B. (2013). Onset of plasticity in thin polystyrene films. *Physical review letters*, *110*(7), 074301.

89 Elder, T., Twohig, T., Singh, H., & Croll, A. B. (2020). Adhesion of a tape loop. *Soft Matter*, *16*(47), 10611-10619.

90 Ye, X., Cai, D., Ruan, X., & Cai, A. (2018). Research on the selective adhesion characteristics of polydimethylsiloxane layer. *AIP Advances*, *8*(9), 095004.

91 Bico, J., Reyssat, É., & Roman, B. (2018). Elastocapillarity: when surface tension deforms elastic solids. *Annual Review of Fluid Mechanics*, *50*, 629-659.

92 Wagner, T. J., & Vella, D. (2013). The 'sticky elastica': delamination blisters beyond small deformations. *Soft Matter*, *9*(4), 1025-1030.

93 Majidi, C. (2007). Remarks on formulating an adhesion problem using Euler's elastica (draft). *Mechanics Research Communications*, *34*(1), 85-90.

94 Fuller, K. N. G., & Tabor, D. (1975). The effect of surface roughness on the adhesion of elastic solids. *Proceedings of the Royal Society of London. A. Mathematical and Physical Sciences*, *345*(1642), 327-342.

95 Prieto-López, L. O., & Williams, J. A. (2016). Switchable adhesion surfaces with enhanced performance against rough counterfaces. *Biomimetics*, *1*(1), 2.

96 Palasantzas, G. (2003). Adhesion of elastic films on mound rough surfaces. *Surface science*, *529*(3), 527-532.

97 Wolff, J. O., & Gorb, S. N. (2013). Radial arrangement of Janus-like setae permits friction control in spiders. *Scientific reports*, *3*(1), 1-7.

98 Frost, K. F., Gorb, S. N., & Wolff, J. O. (2018). Adhesion and friction in hunting spiders: The effect of contact splitting on their attachment ability. *Zoologischer Anzeiger*, *273*, 231-239.

99 Kamperman, M., Kroner, E., del Campo, A., McMeeking, R. M., & Arzt, E. (2010). Functional adhesive surfaces with "gecko" effect: The concept of contact splitting. *Advanced Engineering Materials*, *12*(5), 335-348.

100 Croll, A. B., Hosseini, N., & Bartlett, M. D. (2019). Switchable adhesives for multifunctional interfaces. *Advanced Materials Technologies*, *4*(8), 1900193.

101 Peressadko, A. G., & Gorb, S. N. (2004). Surface profile and friction force generated by insects. In *First international industrial conference Bionik 2004* (pp. 257-261). VDI Verlag.

102 Arzt, E., Gorb, S., & Spolenak, R. (2003). From micro to nano contacts in biological attachment devices. *Proceedings of the National Academy of Sciences*, *100*(19), 10603-10606.

103 Varenberg, M., Pugno, N. M., & Gorb, S. N. (2010). Spatulate structures in biological fibrillar adhesion. *Soft Matter*, *6*(14), 3269-3272.

104 Gorb, S. N. (2005). Uncovering insect stickiness: structure and properties of hairy attachment devices. *American Entomologist*, *51*(1), 31-35.

105 Niederegger, S., Gorb, S. N., & Vötsch, W. (2001). Fly walking: a compromise between attachment and motion. *Biona Report*, *15*, 327-330.

106 Gorb, S. (2001). *Attachment devices of insect cuticle*. Springer Science & Business Media.

107 Wolff, J. O., & Gorb, S. N. (2012). Comparative morphology of pretarsal scopulae in eleven spider families. *Arthropod structure & development*, *41*(5), 419-433.

108 Niederegger, S., & Gorb, S. (2003). Tarsal movements in flies during leg attachment and detachment on a smooth substrate. *Journal of Insect Physiology*, *49*(6), 611-620.